

Parallaxes, Proper Motions, and Near-Infrared Photometry for 173 L and T Dwarfs From The US Naval Observatory Infrared Astrometry Program

FREDERICK J. VRBA,¹ ADAM C. SCHNEIDER ,² JEFFREY A. MUNN ,¹ ARNE A. HENDEN ,¹ CHRISTAIN B. LUGINBUHL,³ CONARD C. DAHN,¹ HARRY H. GUETTER,¹ BLAISE J. CANZIAN,⁴ TRUDY M. TILLEMAN,² SCOTT E. DAHM ,⁵ STEPHEN J. WILLIAMS,² JUSTICE E. BRUURSEMA,¹ J. DAVY KIRKPATRICK ,⁶ AND ADAM J. BURGASSER ⁷

¹ United States Naval Observatory, Flagstaff Station, 10391 West Naval Observatory Rd., Flagstaff, AZ 86005, USA (retired)

² United States Naval Observatory, Flagstaff Station, 10391 West Naval Observatory Rd., Flagstaff, AZ 86005, USA

³ Flagstaff Dark Skies Coalition, P.O. Box 1892, 86002, Flagstaff, AZ, USA

⁴ L-3 Communications/Brashear, 615 Epsilon Drive, Pittsburgh, PA 15238-2807, USA

⁵ Gemini Observatory/NSF's NOIRLab, 950 N. Cherry Avenue, Tucson, AZ 85719, USA

⁶ California Institute of Technology (IPAC), 1200 E. California Blvd., Pasadena, CA 91125, USA

⁷ Center for Astrophysics and Space Science, University of California San Diego, La Jolla, CA 92093, USA

ABSTRACT

We present near-infrared parallax and proper motion astrometry for 74 L-dwarfs and 99 T-dwarfs, as single objects or in binary systems, obtained with the ASTROCAM astrometric imager on the USNO, Flagstaff Station 1.55-m telescope over two observing periods. For all 173 objects the median number of observational epochs was 62 with a median time frame of 5.25 years, resulting in median uncertainties of $\sigma(\pi_{abs}) = 1.51$ mas, $\sigma(\mu_{abs}) = 1.02$ mas yr⁻¹, and $\sigma(V_{tan}) = 1.01$ km s⁻¹. Our observations provide the first parallax/proper motion results for 16 objects and the highest precision parallaxes/proper motions for an additional 116 objects. A serendipitous overlap of 40 objects with Gaia DR3 astrometry allows direct comparison and confirmation of our results, along with an investigation on the effects of resolved binarity on astrometric results. We also provide a uniform set of J -, H -, K_S -band photometry in the UKIRT/MKO system, most of it being from new observations. We use these results to examine objects included in this study of special-interest populations, consisting of binaries, wide companions, young objects, subdwarfs, and brown dwarf spectral standards.

Keywords: astrometry — color-magnitude diagrams — stars:distances — stars: late-type — stars: low-mass, brown dwarfs

1. INTRODUCTION

Beginning shortly after the early discoveries of significant numbers of brown dwarfs from the Two Micron All Sky Survey (2MASS; Skrutskie et al. 2006) and the Sloan Digital Sky Survey (SDSS; York et al. 2000) many efforts have been made to obtain high-quality parallaxes and proper motions, as these are essential to understanding fundamental astrophysical properties such as luminosities, effective temperatures, and surface gravities, along with galactic questions such as space densities and velocities. Several larger-scale, facilities-based surveys include USNO (Vrba et al. 2004; Dahn et al. 2017), CFHT (Dupuy & Liu 2012; Liu et al. 2016; Sanghi et al. 2023), UKIRT (Marocco et al. 2010; Best et al. 2021), Palomar (Kirkpatrick et al. 2019), Spitzer (Dupuy & Kraus 2013; Martin et al. 2018; Kirkpatrick et al. 2019, 2021), NTT (Smart et al. 2013; Marocco et al. 2013),

CTIO (Faherty et al. 2012), ESO 2.2m (Smart et al. 2018), VLT (Sahlmann et al. 2014), and SOFI (Tinney et al. 2003), along with numerous single- or few-object studies. More recently, the Gaia satellite (Gaia Collaboration et al. 2016, 2023) has provided parallaxes and proper motions of unprecedented quality, but generally for the hotter and/or nearer brown dwarfs.

In this paper we provide the final results of the USNO infrared astrometry program which ran in two epochs between late-2000 to mid-2019. In Section 2 we give a brief history of the USNO parallax and proper motion programs, including early work on brown dwarfs at optical wavelengths. Section 3 presents background on the USNO infrared astrometry program from which results are presented in this paper. In Section 4 we present detailed descriptions of the observational choices, frame processing and quality control, and astrometric consid-

erations and reductions. Section 5 describes our methods for making corrections from relative to absolute parallax and proper motion values and our rationale for choosing these methods. In Section 6 we describe the sample for which we present results in this work along with selected spectral-typing references, which served as primary selection criteria for inclusion in our program. Section 7 gives details of the observations for each object, such as the number of epochs and durations of observations. Section 8 presents the astrometric results including relative and absolute parallax and proper motion determinations and resultant tangential velocities, along with a discussion of the distributions of these values. Section 9 gives a brief discussion of internal systematics while Section 10 gives an extended comparison of results presented here with those of Gaia. New and adopted *JHK* photometry is presented in Section 11 for use in the astrophysical analyses in subsequent Sections. In Section 12 we present the fundamental near-infrared color vs. absolute magnitude and spectral type vs. absolute magnitude diagrams we use for analysis. Section 13 contains discussions of objects included in this study which are members of populations of interest including binaries, wide companions, young objects, subdwarfs, and brown dwarf spectral standards. Finally, in Section 14 we summarize some of the main results of this work.

2. BACKGROUND OF ASTROMETRY AT USNO, FLAGSTAFF STATION

We give here a brief history of ground-based astrometry at the United States Naval Observatory (USNO), Flagstaff Station (NOFS), which began with the commissioning of the 61-inch (1.55-m) telescope in 1963 (Strand 1964). This telescope has a “folded-Newtonian” optical design employing a parabolic primary mirror and a flat secondary mirror. At a focal ratio of $f/7$ and a focal length of nearly 50 feet providing a focal plane scale of 13.55 arcsec/mm, it is a physically large telescope for its modest aperture. With a large secondary mirror providing an un-vignetted ≈ 1 deg field of view, the effective open aperture of the telescope is only about 1.25 m. However, at the cost of a large telescope with limited aperture, this optical design provides a uniquely stable astrometric instrument. Both the primary and secondary mirrors are kept fixed and focus is provided by a motor-driven tailpiece instrument mount. Because of this, the focal plane plate scale and point spread function (PSF) are independent of focus. In addition, the telescope has been essentially dedicated to long-term astrometric observations providing many nights of data with few instrument changes or modifications to the telescope itself. NOFS is a generally good observing site

with approximately 70 percent of the nights usable and median seeing of $1.^{\prime\prime}0$ full-width half-max (FWHM) at zenith, $1.^{\prime\prime}3$ FWHM overall, and $0.^{\prime\prime}6$ in the best conditions (Harris & Vrba 1992). Together, these circumstances provide the ability for exceptional ground-based long-term astrometric programs.

Between 1964 and 1994 the 1.55-m was used to obtain parallaxes and proper motions for more than 1000 objects using evolving technologies of photographic plates. The results presented in a long series of publications (c.f. Dahn et al. 1988) were informed by numerous proper motion surveys by Eggen, Giclas, Greenstein, Luyten, and others (c.f. Luyten 1976), also using small aperture telescopes and photographic technology. Despite the aperture limitations, these combined works helped define the bottom of the stellar main and sub-dwarf sequences almost down to the hydrogen-burning limit.

With the advent of charge-coupled device (CCD) technology USNO began experimenting with CCD astrometric observations in the mid-1980s, evolving into a full program by the early 1990s (see Monet et al. 1992). Digital technology allowed for improved parallax accuracies from characteristically 3 mas down to well below 1 mas given a suitable reference frame and target brightness. This program was initially informed for target selection by the same photographic proper motion surveys mentioned above. However, with the advent of the optical Sloan Digital Sky Survey (SDSS; York et al. 2000) and the near-infrared Two Micron All Sky Survey (2MASS; Skrutskie et al. 2006), by 2000 target selection for the USNO program was now being informed by much deeper color-color and approximate color-magnitude studies from these surveys. This allowed the USNO CCD program to extend the low-mass sequence well below the hydrogen burning limit to objects as cool/low-mass as early T spectral types for a few nearby objects. This program continued until 2017 when it was terminated due to the first data release (DR1) from the European Space Agency’s astrometric Gaia satellite (Gaia Collaboration et al. 2016), which provides much higher accuracy parallaxes and proper motions than the USNO CCD program and to similar magnitude limits. The final results for this program were given in Dahn et al. (2017) which also gives a good retrospective of the program.

Despite Gaia’s outstanding performance, it has limitations in obtaining astrometry for cool objects due to the optical wavelengths at which it operates (Gaia Collaboration et al. 2016). In practice, Gaia reaches few objects cooler than mid-L spectral types due to the general space density of brown dwarfs (e.g., Theissen 2018). Thus, the USNO infrared astrometry program, which

was initiated as an extension of the above programs, can still provide important results which are beyond the reach of Gaia.

3. THE USNO INFRARED ASTROMETRY PROGRAM

Much of the early history, instrumentation, observation, and reduction details of this program have already been given in [Vrba et al. \(2004\)](#), which presented some preliminary astrometric results. Thus, while we give an updated history of the program, we refer the reader to [Vrba et al. \(2004\)](#) for many details and we will emphasize changes to observations and reductions since that time.

Although by the early-1990s the astrometric characteristics of CCD arrays were well known, this was not yet the case for the rapidly-evolving complementary metal-oxide semiconductor (CMOS) array technology, which is necessary for the higher backgrounds encountered even at near infrared wavelengths. Due to this, USNO initiated a test program with a camera built at UCLA and delivered in 1995 using a Rockwell 256² HgCdHe (NICMOS2) as the detector ([Vrba et al. 2000](#)). Testing over several years with this camera, which was not astrometrically optimized, on the 1.55-m was sufficiently encouraging, both in terms of immediate astrometry and long term stability to lead USNO to the development of an astrometrically optimized near-infrared camera with a larger field of view.

In the mid-1990s USNO joined with National Optical Astronomical Observatory (NOAO, now NOIRLab) to develop a 1024² InSb array (dubbed ALADDIN) at Santa Barbara Research Corporation (currently part of RTX Corporation). At the time this was the largest CMOS array and most complex integrated chip ([Fowler et al. 1996](#)). In parallel, USNO joined with the Naval Research Laboratory to design an astrometric camera around the ALADDIN array optimized for use on the 1.55-m telescope. The camera (ASTROCAM) was final-designed and manufactured by Mauna Kea Infrared (MKI; [Fischer et al. 2003](#)). ASTROCAM eliminates refractive optics, other than the entrance window and filters, by the use of an Offner 1:1 re-imaging/apodization system. The ALADDIN array's $\approx 27 \mu\text{m}$ pixels thus give a scale of $0''.3654/\text{pixel}$ providing nearly-ideal sampling for the site's characteristic 1.0-1.1" seeing. ASTROCAM together with the 1.55-m telescope's optical design provide an exceptional combination for near-infrared ground-based astrometry, albeit with a limited field of view (FOV) of approximately $6''.2 \times 6''.2$. See [Vrba et al. \(2004\)](#) for more details regarding the ALADDIN array and ASTROCAM instrument development.

ASTROCAM was delivered to NOFS with an engineering-grade array for test observing and characterization in August 1999. In April 2000 a science-grade array was installed and tested prior to the beginning of long-term astrometric observations in August 2000 reported in this work.

4. OBSERVATIONS AND DATA REDUCTION

In this section we briefly discuss the observations and data processing, quality control, and reductions relevant to the astrometric results presented in this work.

4.1. Series 1 and Series 2 Observations

Observations were carried out between 2000 and 2017 but with a major interruption resulting in two series of observations as described here.

Series 1: Science astrometric observations commenced on UT 2000 September 09 with 40 initial objects on the program. [Vrba et al. \(2004\)](#) reported preliminary results for these objects on very short time baselines of between roughly $\Delta t \approx 1.3$ to 2.0 years, sufficient to give some of the earliest parallax and proper motion results for substellar objects. During this time ASTROCAM was scheduled for observations approximately 14 nights out of each lunar cycle on the 1.55-m telescope with about 65% of the nights of suitable quality. The number of objects on the program was slowly increased from the original 40 to 65 until the end of Series 1 on UT 2006 June 14 when ASTROCAM was largely destroyed due to an explosion of its LN₂ pre-charge canister from an uncontrolled warm-up. The latter was the result of a forced evacuation of the site due to a nearby wild fire. Of the 65 objects at Series 1 termination, 13 had insufficient data for even preliminary results. The remaining 52 objects had a median time baseline of $\Delta t = 5.25$ years with a median number of observational epochs of 59.5.

After the ASTROCAM explosion an engineering evaluation study was carried out at MKI to determine if ASTROCAM could be sensibly repaired or if a new camera should be built. Amazingly, the original ALADDIN array suffered only minor damage with fewer than 50 pixels becoming non-functional. In addition, the entrance window and the filters *J* and *H* used for this astrometry were not damaged. It was ultimately decided to rebuild ASTROCAM despite most of the structural mechanics needing replacement and a new and optically improved Offner re-imaging system installed. Between separate contracting for evaluation and actual ASTROCAM rebuild several years passed until the astrometry program could be re-started.

Series 2: Astrometric observations were recommenced on UT 2011 May 07 with 50 target objects, including the

13 objects from Series 1 which were incomplete. During the early part of Series 2 nights were evenly split with the optical program each lunar cycle. However, as Gaia astrometric results became available, the optical program was slowly eliminated, such that during the last several years of operation the ASTROCAM program used essentially all nights on the 1.55-m. During this period about 70% of the nights were of suitable quality. These circumstances allowed the program to increase to roughly 140 objects. The final observations were obtained UT 2019 June 24 due to changing USNO mission requirements and failing ASTROCAM electronics. There are a total of 121 objects in Series 2 which had reasonably complete astrometric results with a median time baseline of $\Delta t = 5.27$ years and a median number of observational epochs of 64. Both of these numbers are serendipitously similar to those of Series 1.

Series 1 and Series 2 combine for a total of 173 objects, the results for which we present in this paper, with total median $\Delta t = 5.25$ years and median observational epochs per target of 62. We note that with both Series being terminated in an uncoordinated manner we have included a few objects, the observations for which were not completed and hence have large error bars, but which we felt still had sufficient value to present.

4.2. Observational Procedures

After the first year of Series 1, during which an observer was required to make target decisions, observations were largely automated. At the beginning of each night biases and dome flats were obtained manually for each filter to be used that night. As a safety precaution it was necessary to start the automated observing manually, after which the program ran until shortly before dawn and closed telescope operations automatically. The program was not a strict queue, but made decisions based on several inputs. First was input from a weather station giving readings on wind, humidity, precipitation, and particulates each of which could terminate observations and close the telescope beyond preset limits. If it was found difficult to find a guide star after several attempts it would assume either clouds or pointing issues and close the telescope. Due to the relatively long exposure times needed, observations were also terminated if seeing degraded to above $2''.5$. The software also recognized the position of the Moon and twilight sky brightnesses. Due to safety concerns the software was not allowed to restart observations without human intervention.

The software captured the program observational history during the previous month and prioritized objects with no or few observations during that period. For each

target field, filters and exposure times as a function of seeing had been previously determined (see below). All dithered sets of exposures were started such that the central time of the set would be within ± 15 minutes of time from the meridian to minimize differential color refraction. The optical guide camera position was preset to acquire the same guide star for each re-visit and, once guiding, assured that the reference frame would be positioned to better than one pixel, keeping with the differential nature of the astrometry. As has been the policy for all 1.55-m astrometry, it is felt that keeping the reference frame position constant and allowing the target to move via proper motion is optimal. Once the guide star was acquired and properly centered a quick exposure was obtained to measure the seeing and set the exposure time. From previous testing it was determined that three $10''$ dithers, in either N-S or E-W directions, were sufficient to prevent PSF overlap and determine background, thus minimizing telescope overhead time; the dither direction being a function of the reference frame stellar positional distribution.

4.3. Filter and Initial Reference Frame Selection

All observations were carried out in either J - or H -band, giving the highest signal-to-noise when combining the spectra of target objects, minimizing sky/telescope backgrounds, and having the best possible reference frame. Test observations were carried out for each target field in both J - and H -band to determine the optimum filter to use. As could be expected *a priori* from the spectra of L- and T-dwarfs at these wavelengths, J -band observations would typically be optimum for T-dwarfs, while H -band observations would be optimum for L-dwarfs. In actuality, 68/74 (92%) of L-dwarfs (or L-dwarf dominated binaries) were observed in H -band and 6/74 (8%) in J -band, while 81/99 (82%) of T-dwarfs were observed in J -band and 18/99 (18%) in H -band. The exceptions were typically for objects with unusual blue or red spectra and a general bias toward J -band due to somewhat lesser telescope and sky glow backgrounds and typically higher signal for the stellar reference frame.

The ALADDIN array of 1024^2 pixels and with 1:1 re-imaging provides a rather small FOV of approximately $6''.2 \times 6''.2$. However, even at this FOV, employing reference stars as near the target object as possible maximizes isoplanarity and astrometric repeatability. Since our target L- and T-dwarfs were already faint for a 1.55-m telescope, few reference frame stars were selected fainter than the target objects. Very bright reference frame stars, although usable with very short exposure times and many internal co-adds at the expense of higher

net read noise, are systematically nearby thus stretching the reference frame depth and associated mean error when conversion to absolute parallax (see §5 below). In practice, the initial reference frame stars chosen were typically within 1-2 magnitudes and as near as possible to the target objects. Optimistically, 10 to 30 initial reference frame stars were chosen although the final reference frames would be reduced in numbers due to optimization and inclusion in Gaia Data Release 3 (DR3) (Gaia Collaboration et al. 2023) for converting to absolute parallax and proper motions, as explained in §5.

4.4. Exposure Time Determinations

Based on significant testing data the goal was to have a minimum 3000-5000 ADU level of the central pixel of the target object image for each dither. An initial integration time, based on nominal 1''.0 seeing, was determined at the time of the filter selection test observations. Since integration time scales as the square of the seeing in order to keep a constant central pixel value, a series of integration times as a function of seeing for each object was developed and used by the automated observing program. While the integration times were calculated up to the seeing limit of 2''.5, in practice few observations were obtained at seeing $>2''.0$ due to long total integration times. Integration times for each dither were based on the product of a fundamental exposure time and the number of coadds employed to ensure that neither the target object nor any reference frame star would be saturated even at the best seeings. Exposure times ranged from 5 to 60 seconds with the number of coadds determined by the seeing, but ensuring a minimum total integration time of 5 minutes for each of the specified 3 dithers.

4.5. Data Processing and Quality Control

Data processing is the same as described in Vrba et al. (2004), which we briefly summarize here. Biases obtained each night were only used as a test of camera electronics and were not part of data frame processing. Dome flats for each night and each filter used were obtained by differencing three sets of illuminated and unilluminated flat screen images in order to remove any thermal signature of the flat screen. The resultant difference frames were median-combined and normalized to form a single flat-field image for each filter. All flat field and program frames were linearized, pixel by pixel, in a process described in Luginbuhl et al. (1998). After flat-fielding, each set of dithered target observations was run through a min/max pixel value filter to form a background frame which was subtracted from each frame of the dithered set to form a final frame.

Each night's data were processed as above by a program that also allowed inspection of each data frame as a first step in quality control. Frames could be removed from further consideration by issues such as trailed images, weak images, images with PSFs larger than 2''.5, significant meteor/aircraft trails, or any data wherein all three dithered images in a set were not completed. Only a small fraction of the frames were rejected at this step since the automated observing program performed well, but it did remove data that would have been problematic in later analyses. However, the general philosophy at this point was to not discard frames until detailed scrutiny, as described below.

For the first few nights of observations of a new object on the program, processed frames were inspected carefully to ensure that the initial setup was correct and that observations were being carried out correctly. After that, preliminary astrometric reductions were carried out after every season of observing to ensure that observations had continued correctly and that new issues had not arisen, such as a slightly different bad pixel set after a scheduled ASTROCAM thermal cycle impinging on the target or the reference frame set. This served as the second level of quality control and, equally important, this allowed evaluation of the parallax and proper motion accuracies as more data were being obtained.

Final astrometry for a given field (described in the next section) was completed after all observations had been collected. At this point, close attention was given as to what frames would be kept in the solution. Frames that were removed were predominantly affected by poorer seeing and weak signal due to clouds that had come in during the long dithered triplet exposures (20–60 minutes) or if any crucial reference frame star was affected by a bad pixel. Of the total of more than 36,000 science frames taken during both Series, 16% were not used in the final astrometry in Series 1 and 17% were rejected in Series 2. We note that these are very similar rejection rates to those of the *H*-band and *K*-band USNO-led UKIRT Hemisphere Survey (UHS) being carried out with the UKIRT telescope (Dye et al. 2018; Schneider et al. 2025). While this work and the UHS surveys have different goals and observational quality criteria, ground-based, near-infrared surveys will be affected by changing atmospheric conditions and significant quality control is needed to ensure optimal results.

4.6. Astrometric Reductions

The image centroiding technique used in this work for ASTROCAM data was developed by D. Monet in the early 1980s and has been used for all narrow-field CCD astrometry at USNO since that time and thus has a

proven record of reliability (Monet & Dahn 1983). Effectively, it is a 2-dimensional Gaussian fit to the PSF and is discussed further in Dahn et al. (2017). The software we use for determining parallax and proper motion, modified for the specifics of ASTROCAM, are again those developed for and used by the USNO CCD astrometry program and are thus well-tested. Monet et al. (1992) discusses the philosophy of the reductions in some detail, but we point out some major points here. Dithered frames for an object observation set are treated as individual frames and are not combined in any way. Each frame has unit weight and each reference star within that frame has unit weight. Ultimately, only linear frame constants are employed due to the nature of the images produced by the 1.55-m telescope and ASTROCAM. Frame scale and rotation are allowed as free parameters. In practice frame scale is effectively a constant due to the nature of the telescope and ASTROCAM, while rotation is solved for due to the slight misalignment of the telescope polar axis.

The data set for an object is solved for proper motion and parallax independently in right ascension (α) and declination (δ), relative to the reference frame, by a three-step iteration of least-squares fits to the data. This gives the α and δ components of the proper motion directly. The parallaxes in α and δ are corrected for the parallax factor in each component and combined by their weighted averages. Due to the relatively low inclination of the Earth's orbit, the errors in the α determination always have much smaller statistical errors than those derived from the δ determination such that the α solutions are the dominant component. For 6 of our 173 target objects, through a combination of the object position in the sky and the distribution of observational epochs, the resultant parallax in δ was indeterminate and thus not included in the solution. These objects are indicated in Table 3 below.

Once an initial solution for a field has been determined a detailed examination of global frame errors and individual stellar errors as a function of frame number is initiated. The global frame errors point to frames which were strongly affected by poor seeing, clouds, or trailed images that had not been previously removed. The deletion of frames at this level accounts for nearly all of the 16% and 17% depreciation rate for Series 1 and 2, respectively, described in §4.5 above.

4.7. Reference Frame Determination

Once a nearly-final data frame set is established a nearly-final set of reference frame stars is determined. During the initial set-up phase for each field, other than checking for resolved binarity or extended PSFs, po-

tential reference frame stars were liberally included as they might prove to be useful and could later be removed at the stage described here. In fact, most of the fainter potential reference frame stars and even some brighter stars which are farther from the target object and shaded by closer useful stars at the same position angle degraded the solutions and were removed. In addition, a few potential reference frame stars were removed due to a variety of reasons, such as routinely landing on a bad pixel in one of the dithers. Since we give unit weight to each star and we require an identical reference for every image frame used in the processing, for each case a decision was made as to whether removing the star from all frames or deleting the frame in question provided the optimal results. We note that these kinds of decisions are a luxury of having a nearly-dedicated telescope producing many epochs/frames of data. There is also one other very minor deletion of potential reference frame stars which is described in §5.

The final median number of reference frame stars employed was 11 for both Series 1 and 2 with a high of 26 and a low, for one object, of 3. The relatively small number of stars used in the reference frames is directly due to the small $6.2' \times 6.2'$ FOV of ASTROCAM. However, this gives a tight reference frame and, with Gaia DR3 results available, ensures an accurate correction to absolute parallaxes and proper motions as described in the next section.

5. CORRECTION FROM RELATIVE TO ABSOLUTE PARALLAXES AND PROPER MOTIONS

The Gaia DR3 catalog (Gaia Collaboration et al. 2023) provides both absolute parallax and proper motion data for stars of the general magnitude range used in the reference frames for this work described above. This allows a straightforward method for correcting the parallaxes and proper motions we directly determine relative to the in-field reference frames to absolute values. For parallax corrections we use the unweighted mean value of the Gaia DR3 results for the reference frame stars with an uncertainty calculated as the unweighted standard deviation of the mean values. The corrections are added to our relative parallaxes to determine absolute parallaxes with the absolute parallax uncertainties calculated as the relative parallax errors added in quadrature to the relative to absolute parallax correction errors.

While USNO has traditionally published only relative proper motion values, we also provide absolute proper motion values. This is similar to the parallax corrections, as we use the unweighted mean Gaia DR3 proper

motion of the reference frame stars for each field added to the relative proper motions we determine. The correction uncertainties are taken as the mean of Gaia DR3 proper motion errors for each reference frame field. The absolute proper motion uncertainties are calculated as the relative proper motion errors added in quadrature to the relative to absolute proper motion correction errors. For proper motions the corrections and associated uncertainties are determined for α and δ components independently.

There are two reasons why the correction to absolute values may have an affect on the final reference frame employed. First, a small fraction of the desired reference frame stars did not have Gaia DR3 parallaxes and proper motions. Rather than opting for an alternative method of estimating the distances to those stars, we chose to eliminate them in order to have a purely Gaia-based system of reference frame data. The second reason is that we wanted to have a minimal spread in the reference frame distances. Thus, a few closer stars were eliminated to minimize the uncertainty in the correction to absolute parallax, as described above. The mean distance of the reference frames is about 1 kpc and will be discussed in more detail below.

6. OBJECTS ON PROGRAM

The selection of objects to be put on the near-IR astrometry program evolved considerably over time. All of the Series 1 objects were chosen on the basis of early discoveries from follow-up spectroscopic observations of either 2MASS or SDSS objects: e.g. [Burgasser et al. \(1999\)](#), [Kirkpatrick et al. \(1999\)](#), [Geballe et al. \(2002\)](#). Initially objects were chosen based on discoveries available and thus did not represent systematic choices. In addition, several binaries were included based on apparent brightnesses which were not yet recognized as such by the evolving spectroscopic understanding of brown dwarfs. Nonetheless, such objects were subsequently left

on the program. Later in Series 1, objects were selected based on such criteria as the importance of the L-T transition, subdwarf nature, etc.

By the time Series 2 was initiated the understanding of brown dwarf physics was considerably advanced. In addition to 2MASS and SDSS, many objects were added based on initial discoveries from the Wide-field Infrared Survey Explorer (WISE) ([Wright et al. 2010](#)) such as those from ([Kirkpatrick et al. 2011](#)) and from other surveys such as Pan-STARRS ([Chambers et al. 2016](#)) and UKIDSS ([Lawrence et al. 2007](#)). A better understanding of brown dwarf ages allowed for the selection of objects more astrophysically interesting, such as potentially young objects and low-metallicity subdwarfs. The program was also tasked with additional practical questions such as testing faintness limits and pushing the limits of astrometric accuracy, both of which influenced target selections.

Ultimately, a total of 74 L-dwarfs and 99 T-dwarfs were sufficiently observed to produce meaningful results. Of these, numerous targets have special properties such as being in known or suspected binary systems, having a wide companion, having unusual colors or peculiar spectra, are subdwarfs, or objects with metallicity or association indications of youth. These objects will be discussed individually in §13. Serendipitously, 40 objects also have Gaia DR3 astrometric results which we employ below in §10 for checks on astrometric accuracy and systematic errors.

Table 1 presents background information for all 173 single objects or binary pairs. Column (1) gives their CatWISE 2020 identifications ([Marocco et al. 2021](#)), which we use consistently throughout this paper. Columns (2) and (3) give their discovery names and discovery references, respectively. Columns (4) and (5) give optical spectral typing and associated references, while columns (6) and (7) give infrared spectral typing and associated references.

Table 1. Target Sample and Optical and Infrared Wavelength Spectral Types

Name (CatWISE)	Discovery Name	Ref. (1)	SpT (opt) (2)	Ref. (5)	SpT (IR) (6)	Ref. (7)
J000013.51+255419.7	SDSS J000013.54+255418.6	1	T5	1	T4.5	56
J000849.71–173925.0	WISEPC J000849.76–173922.6	2	T6	2
J001502.52+295928.7	2MASS J00150206+2959323	3	L7	3	L7.5 pec (blue)	3
J003030.38–145033.8	2MASSW J0030300–145033	4	L7	4	L6 FLD-G	57
J003259.67+141037.2	SDSSp J003259.36+141036.6	5	L9	58

Table 1 *continued*

Table 1 (*continued*)

Name (CatWISE)	Discovery Name	Ref. (1)	SpT (opt) (2)	Ref. (5)	SpT (IR) (6)	Ref. (7)
J003452.12+052307.3	2MASS J00345157+0523050	6	T6.5	49
J004121.65+354712.5	2MASS J00412179+3547133	6	sdL0.5	59	sdL?	6
J004521.80+163444.0	2MASSW J0045214+163445	7	L2 β	60	L2 VL-G	61
J004928.58+044101.0	CFBDS J004928+044058	8	L9	2
J005911.15-011401.4	CFBDS J005910.90-011401.3	9	T8.5	62
J010332.40+193536.5	2MASSI J0103320+193536	4	L6	4	L6 pec (red)	63
J010753.11+004157.7	SDSSp J010752.34+004156.1	10	L7.5	64	L7 pec (red)	63
J011912.41+240331.7	SDSS J011912.22+240331.6	11	T2	11
J013836.61-032222.8	WISEPC J013836.59-032221.2	2	T3	2
J015011.41+382723.7	WISEPA J015010.86+382724.3	2	T0	2
J015142.59+124428.7	SDSSp J015141.69+124429.6	5	T1	5	T1	49
J020625.45+264023.3	WISEPA J020625.26+264023.6	2	L8 (red)	57
J020743.00+000056.1	SDSSp J020742.83+000056.2	5	T4.5	5
J023618.06+004852.1	SDSSp J023617.93+004855.0	5	L9	65	L6.5	5
J024313.38-245332.8	2MASSI J0243137-245329	12	T5.5	56	T6	12
J025116.11-035315.7	2MASS J0251149-035246	13	L3	16	L1	13
J025409.54+022358.7	WISEPC J025409.45+022359.1	14	T8	66
J030533.66+395434.6	WISEPA J030533.54+395434.4	2	T6	2
J031100.13+164815.6	2MASSW J0310599+164816	4	L8	4	L9.5	58
J031326.13+780744.6	WISEPA J031325.96+780744.2	2	T9	67
J032553.05+042539.6	SDSS J032553.17+042540.1	11	T5.5	11
J032842.66+230204.1	2MASSI J0328426+230205	4	L8	4	L9.5	5
J035523.53+113336.7	2MASS J03552337+1133437	15	L5 γ	60	L3-L6 γ	63
J040709.03+151455.0	2MASS J04070885+1514565	6	T5	49
J041054.46+141130.8	WISEPA J041054.48+141131.6	2	T6	2
J041522.17-093457.1	2MASSI J0415195-093506	12	T8	68	T8	12
J042348.22-041402.0	SDSSp J042348.57-041403.5	5,10	L7.5	16	L7.5+T2	69
J043900.87-235310.7	2MASSI J0439010-235308	16	L6	70	L4.5	58
J044853.70-193543.6	WISEPA J044853.29-193548.5	2	sdT5	82
J050021.02+033044.8	2MASS J05002100+0330501	15	L4	71
J051317.27+060812.3	WISEPA J051317.28+060814.7	2	T6.5	2
J051609.20-044553.3	2MASS J05160945-0445499	17	T6	49
J052536.18+673951.5	WISEPA J052536.33+673952.3	2	T6 pec	2
J053312.61+824617.2	2MASS J05325346+8246465	18	esdL7	72	esdL8	90
J053952.16-005856.5	SDSSp J053951.99-005902.0	19	L5	19	L5 (blue)	58
J054231.20-162827.6	WISEPA J054231.26-162829.1	2	T6.5	2
J055919.85-140454.8	2MASSI J0559191-140448	20	T5	56	T4.5	49
J060206.71+404355.4	2MASS J06020638+4043588	21	T4.5	21
J060738.42+242951.2	WISEP J060738.65+242953.4	22	L8	73	L9	74
J061407.41+391233.2	WISEPA J061407.49+391236.4	2	T6	2
J062542.19+564625.4	WISEPA J062542.21+564625.5	2	T6	2
J062720.06-111429.6	WISEPA J062720.07-111428.8	2	T6	2

Table 1 *continued*

Table 1 (*continued*)

Name (CatWISE)	Discovery Name	Ref. (1)	SpT (opt) (2)	Ref. (5)	SpT (IR) (6)	Ref. (7)
J064626.92+793454.5	HD 46588 B	23	L9	75
J065609.75+420532.8	WISEPA J065609.60+420531.0	2	T3	2
J070036.80+315718.2	2MASS J07003664+3157266	24	L3.5	24	L3+L6.5	76
J072226.89–054027.5	UGPS J072227.51–054031.2	25	T9	62
J072719.22+170950.1	2MASSI J0727182+171001	12	T8	68	T7	12
J074200.88+205515.7	SDSS J074201.41+205520.5	1	T5	1
J075547.93+221212.8	2MASSI J0755480+221218	12	T6	68	T5	49
J075840.07+324718.8	SDSS J075840.33+324723.4	1	T3	56	T2	1
J081957.98–033529.3	WISEPA J081958.05–033529.0	2	T4	56	T4	2
J082131.64+144317.8	WISE J0821+1443	26	T5.5	2
J082518.97+211546.1	2MASSI J0825196+211552	4	L7	77	L7 pec (red)	63
J083006.91+482838.3	SDSSp J083008.12+482847.4	5	L8	78	L9.5	58
J083541.88–081918.0	2MASSI 0835425–081923	27	L5	56	L4 pec (red)	63
J083717.18–000020.8	SDSS J083717.21–000018.0	28	T0	78	T1	55
J085035.75+105715.3	2MASSs J0850359+105716	29	L6	29	L6.5+L8.5	76
J085757.60+570844.6	SDSSp J085758.45+570851.4	5	L8	78	L8–L9 pec (red)	63
J085833.72+325628.6	SDSS J085834.42+325627.7	11	T1 pec (red)	79
J090023.73+253934.1	SDSS J090023.68+253934.3	30	L7	77
J090900.31+652525.8	SDSS J090900.73+652527.2	11	T1.5	11
J091534.04+042204.8	2MASS J09153413+0422045	15	L7+L7	15	L6+L6	80
J092615.40+584717.6	SDSSp J092615.38+584720.9	5	T5	56	T4+T5.5	81
J092933.34+342951.3	2MASSW J0929336+342952	4	L8	4	L7.5	1
J093735.98+293120.8	2MASSI J0937347+293142	12	T7 pec (red)	68	sdT6	90
J093936.13–244844.3	2MASS J09393548–2448279	31	T8	56	d/sdT8	90
J094908.49–154548.3	2MASS J09490860–1545485	31	T2	49
J095105.35+355800.1	2MASSW J0951054+355801	4	L6	4	L6	57
J101014.45–040650.0	2MASS 1010148+040649	16	L6	16	L6	3
J101905.55+652954.5	WISEPA J101905.63+652954.2	2	T7	2	T6	2
J102109.51–030421.1	SDSSp J102109.69–030420.1	28	T3.5	78	T1+T5.5	69
J103931.32+325623.7	SDSS J103931.35+325625.5	11	T1	11
J104307.42+222523.3	2MASSI 1043075+222523	32	L8	32	L8 pec	63
J104335.10+121310.8	SDSS J104335.08+121314.1	11	L9	3
J104751.75+212414.7	2MASSI J1047539+212423	33	T7	68	T6.5	12
J104828.96+091940.9	SDSS J104829.21+091937.8	11	T2.5	11
J110611.58+275414.1	2MASS J11061197+2754225	21	T2.5	21
J111009.77+011608.7	SDSSp J111010.01+011613.1	5	T5.5	1
J111447.51–261830.0	2MASS J11145133–2618235	31	T8	56	T7.5	31
J111812.22–085615.0	2MASS J11181292–0856106	3	L6	3	L6 pec (blue)	3
J112254.33+255020.2	WISEPC J112254.73+255021.5	2	T6	2
J115553.43+055956.6	SDSS J115553.86+055957.5	4	L6	77	L7 pec	63
J115821.40+043446.3	SDSS J115820.75+043501.7	30	sdL7	3	d/sdL8	90
J120746.66+024426.8	SDSS J120747.17+024424.8	34	L8	34	T0	1
J121709.86–031111.8	2MASSW J1217111–031113	33	T7	68	T7.5	12

Table 1 *continued*

Table 1 (*continued*)

Name (CatWISE)	Discovery Name	Ref. (opt)	SpT	Ref. (IR)	SpT	Ref.
(1)	(2)	(3)	(4)	(5)	(6)	(7)
J121757.13+162635.1	WISEPC J121756.91+162640.2	2	T8.5+Y0	83
J122554.84–273958.5	2MASSW J1225543–273947	33	T6	68	T5.5+T8	76
J123146.34+084717.1	2MASS J12314753+0847331	6	T6	56	T5.5	49
J123737.03+652607.2	2MASSW J1237392+652615	33	T7	68	T6.5	12
J125011.59+392542.6	SDSS J125011.65+392553.9	11	T4	11
J125453.41–012245.6	SDSS 125453.90–012247.4	28	T2	68	T2	5
J131141.74+362925.2	SDSS J131142.11+362923.9	30	L5 pec (blue)	2
J132003.78+603425.8	WISEPC J132004.16+603426.2	2	T6.5	2
J132233.51–234015.3	WISEPA J132233.66–234017.1	2	T8	2
J132407.64+190625.5	PSO J201.0320+19.1072	35	T3.5	35
J132434.67+635827.1	2MASS J13243559+6358284	21	T2.5:	41	T2:pec (red)	21
J132605.25+120010.1	ULAS J132605.18+120009.9	36	T6 pec	36
J132629.56–003833.2	SDSSp J132629.82–0003831.5	19	L8?	19	L7	58
J133553.35+113003.7	ULAS J133553.45+113005.2	37	T8.5	62
J134645.89–003152.2	2MASSW J1346464–003150	33	T6.5	49
J134807.08+660327.2	WISEPC J134806.99+660327.8	2	L9	2
J140255.70+080053.4	SDSS J140255.66+080055.2	11	T2 pec	84
J140753.30+124110.7	2MASS J14075361+1241099	38	L3	77	L4	58
J143517.22–004612.9	SDSS J143517.20–004612.9	34	L0	34
J143535.75–004348.6	SDSS J143535.72–004347.0	34	L3	34	L2.5	1
J143945.64+304218.7	SDSS J143945.86+304220.6	11	T2.5	11
J144600.78+002450.9	SDSSp J144600.60+002452.0	5	L6	34	L5	85
J145714.66+581509.7	WISEPC J145715.03+581510.2	2	T8	2	T7	2
J150319.71+252528.3	2MASS J15031961+2525196	27	T6	68	T5	49
J150648.79+702741.0	WISEPC J150649.97+702736.0	2	T6	56	T6	2
J150653.09+132105.8	2MASSW J1506544+132106	39	L3	39	L3	3
J151114.38+060739.4	SDSS J151114.66+060742.9	11	L5+T5	81
J151459.41+484803.4	2MASS J1515008+484742	13	L6	32	L6	13
J152040.10+354615.7	SDSS J152039.82+354619.8	11	L7.5	69
J152322.78+301453.4	2MASSW J152322.6+301456	40	L8	4	L8	58
J152613.76+204334.8	2MASSI J1526140+204341	4	L7	4	L7	6
J154614.94+493158.6	2MASS 15461461+4932114	41	T3	69
J155301.80+153239.5	2MASSI J1553+1532	12	T6.5+T7.5	76
J161705.76+180713.9	WISEPC J161705.75+180714.0	42	T8	2	T8	42
J162413.95+002915.6	SDSS 1624+00	43	T6	68	T6	12
J162541.25+152810.0	PSO J246.4222+15.4698	35	T4.5	35
J162618.23+392523.4	2MASS J16262034+3925190	44	usdL4	59	sdL4	86
J162725.60+325522.8	WISEPA J162725.64+325524.1	45	T6	2
J162918.64+033534.8	PSO J247.3273+03.5932	35	T3	56	T2	35
J163229.48+190439.6	2MASSW J1632291+190441	29	L8	29	L8	3
J164715.47+563209.4	WISEPA J164715.59+563208.2	2	L7	56	L9 pec (red)	2
J165311.00+444421.2	WISEPA J165311.05+444423.0	45	T8	2	T8	2

Table 1 *continued*

Table 1 (*continued*)

Name (CatWISE)	Discovery Name	Ref. (1)	SpT (opt) (2)	Ref. (5)	SpT (IR) (6)	Ref. (7)
J171145.73+223204.2	2MASSI J1711457+223204	4	L6.5	4	L9	69
J172811.54+394859.0	2MASSW J1728114+394859	4	L7	4	L5+L6.5	87
J174124.05+255312.0	WISEPC J174124.25+255319.5	14	T9	2	T9	2
J175023.78+422238.6	SDSS J175024.01+422237.8	1	T1.5	69
J175033.14+175905.4	SDSSp J175032.96+175903.9	5	T4	56	T3	69
J175609.98+281516.4	2MASS J17561080+2815238	3	sdL1	3	L1 pec (blue)	3
J175805.45+463318.2	SDSS J175805.46+463311.9	1	T6.5	49
J180026.66+013450.9	WISEP J180026.60+013453.1	46	L7.5	88	L7.5	46
J181210.89+272142.8	WISEPC J181210.85+272144.3	42	T8.5:	42
J182128.39+141357.2	2MASS J18212815+1414010	47	L4.5	47	L5	47
J183058.60+454258.2	WISEPA J183058.57+454257.9	3	L9	2
J184108.67+311728.6	2MASSW J1841086+311727	4	L4 pec	4
J185215.87+353714.9	WISEPA J185215.78+353716.3	3	T7	2
J190106.23+471820.5	2MASS J19010601+4718136	6	T5	6
J190624.72+450805.2	WISEPA J190624.75+450808.2	2	T6	2
J190648.66+401105.9	WISEP J190648.47+401106.8	48	L1	48
J195246.34+723957.9	WISEPA J195246.66+724000.8	2	T4	2
J200250.59-052154.2	2MASSI 2002507-052152	32	L5 β	89	L5-L7 γ	63
J204749.62-071821.6	SDSS J204749.61-071818.3	1	L7.5	69
J210115.58+175656.0	2MASSW J2101154+175658	4	L7.5	4	L7+L8	76
J212414.06+010003.8	SDSS J212413.89+010000.3	1	T5	49
J212702.63+761756.8	2MASS J21265916+7617440	3	L7	3	T0 pec	3
J213927.29+022024.7	2MASS J21392676+0220226	49	T2	56	T1.5	49
J215432.82+594211.3	2MASS J21543318+5942187	21	T5.5	69
J221354.65+091139.0	WISEPC J221354.69+091139.4	2	T7	2
J222444.39-015908.2	2MASSW J2224438-015852	4	L4.5	4	L3	57
J222622.96+044001.1	WISEPC J222623.05+044003.9	2	T8	2
J223937.67+161716.8	WISEPC J223937.55+161716.2	2	T3	2
J224253.65+254256.2	2MASSJ22425317+2542573	50	L3	32	L2 pec	63
J224431.96+204339.1	2MASSW J2244316+204343	51	L6.5	51	L6-L8 γ	63
J225418.98+312353.0	2MASSI J2254188+312349	12	T5	56	T4	49
J225529.03-003436.4	SDSS J225529.09-003433.4	52	L0	77
J232123.84+135450.3	ULAS J232123.79+135454.8	53	T7.5	53
J232545.24+425143.9	2MASS J23254530+4251488	15	L8	32	L7	87
J232728.85-273056.4	WISEPC J232728.75-273056.5	2	L9	2
J233051.30-084455.9	CFBDS J233051.24-084454.6	54	T0	54
J233910.67+135212.9	2MASSI J2339101+135230	12	T5	49
J234026.68-074509.6	WISEPC J234026.62-074507.2	2	T7	2	T7	2
J234841.34-102843.2	WISEPC J234841.10-102844.4	2	T7	2
J235122.32+301054.1	2MASS J23512200+3010540	4	L5.5	4	L5	4
J235654.19-155322.9	2MASSI J2356547-155310	55	T5	49

Table 1 *continued*

Table 1 (*continued*)

Name	Discovery	Ref.	SpT	Ref.	SpT	Ref.
(CatWISE)	Name		(opt)		(IR)	
(1)	(2)	(3)	(4)	(5)	(6)	(7)

References—(1) Knapp et al. (2004); (2) Kirkpatrick et al. (2011); (3) Kirkpatrick et al. (2010); (4) Kirkpatrick et al. (2000); (5) Geballe et al. (2002); (6) Burgasser et al. (2004); (7) Salim et al. (2003); (8) Reylé et al. (2010); (9) Delorme et al. (2008); (10) Schneider et al. (2002); (11) Chiu et al. (2006); (12) Burgasser et al. (2002); (13) Wilson et al. (2003); (14) Scholz et al. (2011); (15) Reid et al. (2006); (16) Cruz et al. (2003); (17) Burgasser et al. (2003b); (18) Burgasser et al. (2003c); (19) Fan et al. (2000); (20) Burgasser et al. (2000); (21)Looper et al. (2007); (22) Castro & Gizis (2012); (23) Loutrel et al. (2011); (24) Thorstensen & Kirkpatrick (2003); (25) Lucas et al. (2010); (26) Aberasturi et al. (2011); (27) Burgasser et al. (2003d); (28) Leggett et al. (2000); (29) Kirkpatrick et al. (1999); (30) Zhang et al. (2009); (31) Tinney et al. (2005); (32) Cruz et al. (2007); (33) Burgasser et al. (1999); (34) Hawley et al. (2002); (35) Deacon et al. (2011); (36) Burningham et al. (2010); (37) Burningham et al. (2008); (38) Jameson et al. (2008); (39) Gizis et al. (2000); (40) McLean et al. (2000); (41) Metchev et al. (2008); (42) Burgasser et al. (2011b); (43) Strauss et al. (1999); (44) Burgasser (2004); (45) Gelino et al. (2011); (46) Gizis et al. (2011b); (47) Looper et al. (2008b); (48) Gizis et al. (2011a); (49) Burgasser et al. (2006a); (50) Gizis et al. (2003); (51) Dahn et al. (2002); (52) Fan et al. (2001); (53) Scholz (2010); (54) Albert et al. (2011); (55) McLean et al. (2001); (56) Pineda et al. (2016); (57) Liu et al. (2016); (58) Schneider et al. (2014); (59) Zhang et al. (2017b); (60) Cruz et al. (2009); (61) Allers & Liu (2013); (62) Cushing et al. (2011); (63) Gagné et al. (2015b); (64) Cruz et al. (2018); (65) Scholz et al. (2009); (66) Liu et al. (2011); (67) Leggett et al. (2019); (68) Burgasser et al. (2003e); (69) Burgasser et al. (2010); (70) Burgasser (2007); (71) Reid et al. (2008); (72) Zhang et al. (2013); (73) Castro et al. (2013); (74) Thompson et al. (2013); (75) Loutrel et al. (2011); (76) Dupuy & Liu (2012); (77) Schmidt et al. (2010); (78) Kirkpatrick et al. (2008); (79) Faherty et al. (2009); (80) Bardalez Gagliuffi et al. (2019); (81) Bardalez Gagliuffi et al. (2015); (82) Zhang et al. (2019); (83) Leggett et al. (2017); (84) Kellogg et al. (2015); (85) Marocco et al. (2015); (86) Burgasser et al. (2007); (87) Burgasser et al. (2011a); (88) Gizis et al. (2015); (89) Faherty et al. (2016); (90) Burgasser et al. (2025)

7. SUMMARY OF OBSERVATIONS

In this section we give an overview of observations for each object on the program which are summarized in Table 2. Column (1) again gives the CatWISE object name, while column (2) gives a shorthand summary of the optical and IR spectral typing for reference. Column (3) shows whether the object was observed during Series 1 (52 objects) or Series 2 (121 objects). Column (4) shows the filter used for the astrometric observations with totals of 87 objects observed in *J*-band and 86 objects observed in *H*-band. Column (5) shows the number of independent observation epochs observed with a range of 11 to 220 and median numbers of 59.5 and 64.0 for Series 1 and Series 2, respectively, and with an

overall median of 62 epochs. Column (6) gives the time duration of each set of observations from the first to the last epoch used in the final astrometric reductions with a range of 2.69 to 8.12 with an overall median value of 5.25 years. We note that even the shortest of these time durations encompasses observations during at least parts of four seasons, which USNO has traditionally seen as a minimum to completely separate parallax and proper motion. Column (7) provides the mean epochs of observation calculated from only those frames used in the final astrometric reductions. Column (8) gives the number of reference frame stars used in the final reductions with a median number of 11 for both Series 1 and 2. Column (9) shows whether Gaia DR3 astrometric values are available, which will be used in a consistency and reliability analysis in §10.

Table 2. Parallax and Proper Motion Object Observations and Reference Stars

Object Name	SpecT	Series	Filter	No. Epochs	ΔT (yrs)	Mean Epoch	No. Ref. Stars	In Gaia?
CatWISE	opt/IR							
(1)	(2)	(3)	(4)	(5)	(6)	(7)	(8)	(9)
J000013.51+255419.7	T5/T4.5	2	<i>J</i>	90	7.34	2014.7512	9	
J000849.71–173925.0	–/T6	2	<i>J</i>	66	7.36	2014.8949	7	
J001502.52+295928.7	L7/L7.5 pec (blue)	2	<i>H</i>	38	4.30	2017.2425	18	
J003030.38–145033.8	L7/L6 FLD-G	1	<i>H</i>	65	5.27	2003.5844	13	
J003259.67+141037.2	–/L9	1	<i>H</i>	60	5.10	2003.8004	14	

Table 2 *continued*

Table 2 (*continued*)

Object Name	SpecT	Series	Filter	No. Epochs	ΔT (yrs)	Mean Epoch	No. Ref. Stars	In Gaia?
CatWISE	opt/IR							
(1)	(2)	(3)	(4)	(5)	(6)	(7)	(8)	(9)
J003452.12+052307.3	−/T6.5	2	J	73	7.36	2014.9679	5	
J004121.65+354712.5	sdL0.5/sdL?	2	H	46	5.27	2016.3624	13	Gaia
J004521.80+163444.0	L2 β /L2 VL-G	2	H	39	5.27	2016.4792	8	Gaia
J004928.58+044101.0	−/L9	2	J	66	7.26	2015.0053	6	
J005911.15−011401.4	−/T8.5	2	J	11	3.16	2018.3110	9	
J010332.40+193536.5	L6/L6 pec (red)	2	H	73	4.33	2016.7854	13	
J010753.11+004157.7	L7.5/L7 pec (red)	1	H	90	4.95	2004.0956	7	
J011912.41+240331.7	−/T2	2	H	65	4.00	2017.2812	17	
J013836.61−032222.8	−/T3	2	H	71	3.21	2017.6562	9	
J015011.41+382723.7	−/T0	2	H	146	5.38	2016.1376	16	
J015142.59+124428.7	T1/T1	1	H	69	5.17	2003.7852	10	
J020625.45+264023.3	−/L8 (red)	2	H	156	5.42	2016.3538	11	
J020743.00+000056.1	−/T4.5	1	H	59	5.08	2003.9954	11	
J023618.06+004852.1	L9/L6.5	2	H	93	4.39	2017.0055	9	
J024313.38−245332.8	T5.5/T6	1	J	70	5.34	2003.6408	9	
J025116.11−035315.7	L3/L1	2	H	61	5.27	2016.0129	9	Gaia
J025409.54+022358.7	−/T8	2	J	131	7.33	2014.4005	11	
J030533.66+395434.6	−/T6	2	J	105	7.35	2014.4591	17	
J031100.13+164815.6	L8/L9.5	1	H	30	3.32	2004.0835	11	
J031326.13+780744.6	−/T9	2	J	35	3.98	2017.1154	15	
J032553.05+042539.6	−/T5.5	2	J	34	3.20	2017.4982	8	
J032842.66+230204.1	L8/L9.5	1	H	53	5.35	2003.4117	18	
J035523.53+113336.7	L5 γ /L3-L6 γ	2	H	95	6.05	2016.0492	13	Gaia
J040709.03+151455.0	−/T5	2	J	99	7.41	2015.1326	19	
J041054.46+141130.8	−/T6	2	J	104	7.40	2015.1590	13	
J041522.17−093457.1	T8/T8	1	J	62	5.34	2003.7253	7	
J042348.22−041402.0	L7.5/L7.5+T2	1	H	62	5.25	2003.9656	11	Gaia
J043900.87−235310.7	L6/L4.5	2	H	48	4.02	2016.9863	11	Gaia
J044853.70−193543.6	−/sdT5	2	H	59	4.33	2016.8059	19	
J050021.02+033044.8	L4/−	2	H	90	6.05	2015.4119	11	Gaia
J051317.27+060812.3	−/T6.5	2	J	149	7.40	2014.2212	15	
J051609.20−044553.3	−/T6	1	J	46	2.98	2004.9613	11	
J052536.18+673951.5	−/T6 pec	2	J	37	4.02	2017.2288	14	
J053312.61+824617.2	esdL7/esdL8	1	H	37	2.98	2004.8103	12	Gaia
J053952.16−005856.5	L5/L5(blue)	1	H	63	5.23	2003.8234	15	Gaia
J054231.20−162827.6	−/T6.5	2	J	28	3.26	2017.3767	22	
J055919.85−140454.8	T5/T4.5	1	J	95	5.34	2003.8918	13	Gaia
J060206.71+404355.4	−/T4.5	2	J	31	3.26	2017.5148	16	
J060738.42+242951.2	L8/L9	2	J	93	7.27	2014.5519	22	Gaia
J061407.41+391233.2	−/T6	2	J	85	7.30	2014.5799	20	
J062542.19+564625.4	−/T6	2	J	88	7.28	2014.2581	15	
J062720.06−111429.6	−/T6	2	J	28	3.22	2017.6912	13	

Table 2 *continued*

Table 2 (*continued*)

Object Name	SpecT	Series	Filter	No. Epochs	ΔT (yrs)	Mean Epoch	No. Ref. Stars	In Gaia?
CatWISE	opt/IR							
(1)	(2)	(3)	(4)	(5)	(6)	(7)	(8)	(9)
J064626.92+793454.5	-/L9	2	H	31	3.24	2017.7400	11	
J065609.75+420532.8	-/T3	2	J	116	7.34	2014.6467	11	
J070036.80+315718.2	L3.5/L3+L6.5	2	H	91	6.14	2015.5478	12	Gaia
J072226.89-054027.5	-/T9	2	J	43	4.20	2017.1137	19	
J072719.22+170950.1	T8/T7	1	J	95	5.33	2003.7811	11	
J074200.88+205515.7	-/T5	2	J	119	7.35	2014.7690	16	
J075547.93+221212.8	T6/T5	1	J	55	3.31	2004.4925	12	
J075840.07+324718.8	T3/T2	2	J	113	7.34	2014.7385	17	Gaia
J081957.98-033529.3	T4/T4	2	J	36	3.16	2017.7417	16	
J082131.64+144317.8	-/T5.5	2	J	99	7.37	2014.8615	16	
J082518.97+211546.1	L7/L7 pec (red)	1	H	54	5.25	2003.8967	15	Gaia
J083006.91+482838.3	L8/L9.5	1	H	52	5.26	2004.3483	11	Gaia
J083541.88-081918.0	L5/L4 pec (red)	2	H	87	6.18	2015.8820	12	Gaia
J083717.18-000020.8	T0/T1	1	J	39	4.95	2003.6761	12	
J085035.75+105715.3	L6/L6.5+L8.5	1	H	53	5.23	2003.8130	12	
J085757.60+570844.6	L8/L8-L9 pec (red)	2	H	70	6.19	2015.5105	11	Gaia
J085833.72+325628.6	-/T1 pec (red)	2	H	37	4.22	2017.0858	14	
J090023.73+253934.1	L7/-	2	H	29	4.05	2017.1831	12	
J090900.31+656525.8	-/T1.5	2	H	19	3.11	2017.9158	10	
J091534.04+042204.8	L7+L7/L6+L6	2	J	91	7.42	2014.6001	10	Gaia
J092615.40+584717.6	T5/T4+T5.5	1	J	33	3.23	2004.5633	13	
J092933.34+342951.3	L8/L7.5	2	H	33	3.16	2017.8105	11	
J093735.98+293120.8	T7 pec (red)/sdT6	1	J	44	5.28	2003.7034	8	
J093936.13-244844.3	T8/d/sdT8	2	J	92	7.36	2015.0471	15	
J094908.49-154548.3	-/T2	2	H	38	3.17	2017.7768	13	
J095105.35+355800.1	L6/L6	1	H	51	5.26	2003.6711	12	Gaia
J101014.45-040650.0	L6/L6	2	H	34	3.19	2017.8427	9	
J101905.55+652954.5	T7/T6	2	J	109	7.95	2014.7231	7	
J102109.51-030421.1	T3.5/T1+T5.5	1	J	59	5.29	2004.1753	10	
J103931.32+325623.7	-/T1	2	H	27	3.17	2017.7852	7	
J104307.42+222523.3	L8/L8 pec	2	H	21	3.16	2017.8359	8	
J104335.10+121310.8	-/L9	2	H	22	3.20	2017.5144	8	
J104751.75+212414.7	T7/T6.5	1	J	68	5.29	2003.5886	6	
J104828.96+091940.9	-/T2.5	2	H	21	3.20	2018.0375	10	
J110611.58+275414.1	-/T2.5	2	J	29	3.19	2017.9380	5	Gaia
J111009.77+011608.7	-/T5.5	1	J	43	3.38	2004.3237	9	
J111447.51-261830.0	T8/T7.5	2	J	89	7.31	2015.0406	19	
J111812.22-085615.0	L6/L6 pec (blue)	2	H	38	3.12	2018.1265	8	Gaia
J112254.33+255020.2	-/T6	2	J	110	7.95	2015.1655	7	
J115553.43+055956.6	L6/L7 pec	2	H	72	4.29	2017.0018	7	
J115821.40+043446.3	sdL7/d/sdL8	2	H	37	3.13	2018.0378	10	Gaia
J120746.66+024426.8	L8/T0	2	H	55	4.09	2017.5132	7	
J121709.86-031111.8	T7/T7.5	1	J	62	5.29	2003.8303	8	

Table 2 *continued*

Table 2 (*continued*)

Object Name	SpecT	Series	Filter	No. Epochs	ΔT (yrs)	Mean Epoch	No. Ref. Stars	In Gaia?
CatWISE	opt/IR							
(1)	(2)	(3)	(4)	(5)	(6)	(7)	(8)	(9)
J121757.13+162635.1	−/T8.5+Y0	2	<i>J</i>	17	3.10	2017.7509	11	
J122554.84−273958.5	T6/T5.5+T8	1	<i>J</i>	46	5.25	2003.6483	11	
J123146.34+084717.1	T6/T5.5	2	<i>J</i>	180	8.02	2014.3637	7	
J123737.03+652607.2	T7/T6.5	1	<i>J</i>	53	5.33	2003.9171	5	
J125011.59+392542.6	−/T4	2	<i>H</i>	36	3.27	2017.4639	9	
J125453.41−012245.6	T2/T2	1	<i>J</i>	50	5.26	2003.7879	8	
J131141.74+362925.2	−/L5 pec (blue)	2	<i>J</i>	65	7.98	2014.6520	9	Gaia
J132003.78+603425.8	−/T6.5	2	<i>J</i>	60	8.00	2014.4508	7	
J132233.51−234015.3	−/T8	2	<i>J</i>	63	7.87	2014.7101	8	
J132407.64+190625.5	−/T3.5	2	<i>J</i>	63	6.99	2015.3268	3	
J132434.67+635827.1	T2.5:/T2: pec(red)	2	<i>H</i>	30	3.22	2018.0138	8	
J132605.25+120010.1	−/T6 pec	2	<i>J</i>	14	3.15	2017.7938	13	
J132629.56−003833.2	L8?/L7	1	<i>H</i>	85	5.33	2004.0752	6	
J133553.35+113003.7	−/T8.5	2	<i>J</i>	16	3.15	2017.8629	12	
J134645.89−003152.2	−/T6.5	1	<i>J</i>	92	5.36	2004.3195	8	
J134807.08+660327.2	−/L9	2	<i>H</i>	82	5.29	2016.8284	10	
J140255.70+080053.4	−/T2 pec	2	<i>H</i>	67	4.10	2017.5111	10	
J140753.30+124110.7	L3/L4	2	<i>H</i>	151	6.29	2015.1740	9	Gaia
J143517.22−004612.9	L0/−	1	<i>H</i>	78	5.35	2004.0412	6	
J143535.75−004348.6	L3/L2.5	1	<i>H</i>	78	5.35	2004.0288	6	
J143945.64+304218.7	−/T2.5	2	<i>H</i>	76	4.31	2017.2131	11	
J144600.78+002450.9	L6/L5	1	<i>H</i>	69	5.33	2003.7094	10	
J145714.66+581509.7	T8/T7	2	<i>J</i>	133	8.05	2014.8997	11	
J150319.71+252528.3	T6/T5	1	<i>J</i>	49	3.30	2004.5020	8	Gaia
J150648.79+702741.0	T6/T6	2	<i>J</i>	122	8.05	2014.8189	6	Gaia
J150653.09+132105.8	L3/L3	2	<i>H</i>	89	6.27	2015.6727	16	Gaia
J151114.38+060739.4	−/L5+T5	2	<i>H</i>	38	3.98	2017.8066	11	
J151459.41+484803.4	L6/L6	2	<i>H</i>	39	3.98	2017.7328	7	Gaia
J152040.10+354615.7	−/L7.5	2	<i>H</i>	50	4.06	2017.7802	8	
J152322.78+301453.4	L8/L8	1	<i>H</i>	79	5.32	2003.5904	14	
J152613.76+204334.8	L7/L7	2	<i>H</i>	56	4.16	2017.4366	10	Gaia
J154614.94+493158.6	−/T3	2	<i>J</i>	202	8.13	2014.4620	11	
J155301.80+153239.5	−/T6.5+T7.5	1	<i>J</i>	42	3.31	2004.4192	9	
J161705.76+180713.9	T8/T8	2	<i>J</i>	40	4.03	2017.8027	10	
J162413.95+002915.6	T6/T6	1	<i>J</i>	55	5.25	2003.3333	9	
J162541.25+152810.0	−/T4.5	2	<i>J</i>	61	7.07	2015.6299	14	
J162618.23+392523.4	usdL4/sdL4	2	<i>H</i>	54	6.31	2016.3005	11	Gaia
J162725.60+325522.8	−/T6	2	<i>J</i>	84	8.05	2015.0827	9	
J162918.64+033534.8	T3/T2	2	<i>J</i>	55	7.11	2016.0868	15	
J163229.48+190439.6	L8/L8	1	<i>H</i>	59	5.25	2003.5659	16	
J164715.47+563209.4	L7/L9 pec (red)	2	<i>H</i>	53	5.00	2016.9886	10	
J165311.00+444421.2	T8/T8	2	<i>H</i>	44	4.04	2017.6767	10	

Table 2 *continued*

Table 2 (*continued*)

Object Name	SpecT	Series	Filter	No. Epochs	ΔT (yrs)	Mean Epoch	No. Ref. Stars	In Gaia?
CatWISE	opt/IR							
(1)	(2)	(3)	(4)	(5)	(6)	(7)	(8)	(9)
J171145.73+223204.2	L6.5/L9	1	<i>H</i>	84	5.18	2003.7680	17	
J172811.54+394859.0	L7/L5+L6.5	1	<i>H</i>	73	5.18	2003.6422	26	
J174124.05+255312.0	T9/T9	2	<i>J</i>	94	8.10	2015.4459	12	
J175023.78+422238.6	−/T1.5	2	<i>J</i>	80	8.12	2015.4009	12	
J175033.14+175905.4	T4/T3	1	<i>J</i>	71	5.04	2003.3001	25	
J175609.98+281516.4	sdL1/L1 pec (blue)	2	<i>H</i>	59	6.22	2016.3656	15	Gaia
J175805.45+463318.2	−/T6.5	2	<i>J</i>	71	8.13	2015.0107	13	
J180026.66+013450.9	L7.5/L7.5	2	<i>J</i>	64	7.90	2015.7498	13	Gaia
J181210.89+272142.8	−/T8.5:	2	<i>J</i>	19	4.67	2018.0987	19	
J182128.39+141357.2	L4.5/L5	2	<i>H</i>	86	6.18	2016.1783	14	Gaia
J183058.60+454258.2	−/L9	2	<i>H</i>	63	5.78	2016.9046	26	
J184108.67+311728.6	L4 pec/−	1	<i>H</i>	91	5.75	2003.4407	26	
J185215.87+353714.9	−/T7	2	<i>J</i>	99	8.04	2015.2472	15	
J190106.23+471820.5	−/T5	1	<i>J</i>	45	2.69	2004.9215	21	
J190624.72+450805.2	−/T6	2	<i>J</i>	90	8.11	2015.4566	13	
J190648.66+401105.9	−/L1	2	<i>J</i>	96	7.96	2015.2938	15	Gaia
J195246.34+723957.9	−/T4	2	<i>J</i>	220	8.05	2015.2340	13	
J200250.59−052154.2	L5β/L5-L7γ	2	<i>H</i>	113	4.72	2017.4839	25	Gaia
J204749.62−071821.6	−/L7.5	2	<i>H</i>	106	4.72	2017.5590	19	
J210115.58+175656.0	L7.5/L7+L8	1	<i>H</i>	119	5.76	2003.7206	17	
J212414.06+010003.8	−/T5	2	<i>J</i>	155	7.94	2014.6552	17	
J212702.63+761756.8	L7/T0 pec	2	<i>H</i>	69	4.68	2017.0680	20	Gaia
J213927.29+022024.7	T2/T1.5	2	<i>H</i>	51	3.82	2017.4431	10	
J215432.82+594211.3	−/T5.5	2	<i>J</i>	51	3.22	2017.3195	18	
J221354.65+091139.0	−/T7	2	<i>J</i>	161	7.38	2014.5447	8	
J222444.39−015908.2	L4.5/L3	1	<i>H</i>	118	5.19	2003.5661	5	Gaia
J222622.96+044001.1	−/T8	2	<i>J</i>	50	3.21	2017.2994	9	
J223937.67+161716.8	−/T3	2	<i>H</i>	56	3.20	2017.3175	9	
J224253.65+254256.2	L3/L2 pec	2	<i>H</i>	110	5.30	2015.6177	8	Gaia
J224431.96+204339.1	L6.5/L6-L8γ	1	<i>H</i>	52	3.17	2004.2541	19	
J225418.98+312353.0	T5/T4	1	<i>J</i>	33	3.01	2004.6663	15	
J225529.03−003436.4	L0/−	1	<i>H</i>	82	5.10	2003.2746	11	Gaia
J232123.84+135450.3	−/T7.5	2	<i>J</i>	31	3.14	2017.4049	11	
J232545.24+425143.9	L8/L7	2	<i>H</i>	22	3.19	2017.4585	16	Gaia
J232728.85−273056.4	−/L9	2	<i>H</i>	49	5.21	2016.3766	9	
J233051.30−084455.9	−/T0	2	<i>H</i>	29	3.20	2017.3785	8	
J233910.67+135212.9	−/T5	1	<i>J</i>	56	3.08	2004.7886	10	
J234026.68−074509.6	T7/T7	2	<i>J</i>	74	7.23	2014.3586	9	
J234841.34−102843.2	−/T7	2	<i>J</i>	74	7.29	2014.7906	7	
J235122.32+301054.1	L5.5/L5	2	<i>H</i>	31	3.19	2017.4205	13	
J235654.19−155322.9	−/T5	1	<i>J</i>	88	5.26	2003.3541	8	

8. ASTROMETRIC RESULTS

In this section we present our basic astrometric results along with brief discussions of these results and associated error distributions.

8.1. *Summary of Astrometric Results*

The main astrometric results of this work are presented in Table 3. Column (1) again presents the CatWISE object names. Column (2) gives the parallaxes relative to the final reference frame (π_{rel}) and associated uncertainties. Column (3) gives the absolute parallaxes (π_{abs}) after correction for the mean Gaia DR3 distances of the reference frame stars, as described above, along with associated uncertainties, which are calculated by the relative parallax uncertainties added in quadrature with those of the corrections to absolute parallax. Column (4) gives the relative proper motions in the Right Ascension coordinate ($\mu\alpha_{rel}$) and associated uncertainties. Column (5) gives the absolute proper motions in

Right Ascension ($\mu\alpha_{abs}$) after correction for the mean Gaia DR3 proper motions in Right Ascension of the reference frame stars, as described above, along with associated uncertainties, which are calculated by the relative proper motion errors in Right Ascension added in quadrature with those of the corrections to absolute proper motions in Right Ascension. Similarly, columns (6) and (7) give the relative and absolute proper motions in Declination ($\mu\delta_{rel}$ and $\mu\delta_{abs}$, respectively) and associated uncertainties. For convenience, columns (8) and (9) give the total absolute proper motions (μ_{abs}) and position angles (P.A.) of proper motion in degrees (in the usual sense of East of North), respectively, and associated uncertainties. Column (10) gives the tangential velocities (V_{tan}) based on the combined values of columns (3) and (8). The tangential velocity uncertainties are calculated by combining in quadrature the uncertainties imposed on V_{tan} by the independent uncertainties of π_{abs} and μ_{abs} . All listed uncertainties are 1σ values.

Table 3. Astrometric Results

Object Name	π_{rel}	π_{abs}	$\mu\alpha_{rel}$	$\mu\alpha_{abs}$	$\mu\delta_{rel}$	$\mu\delta_{abs}$	P.A.	V_{tan}
CatWISE	(mas)	(mas)	(mas yr $^{-1}$)	(mas yr $^{-1}$)	(mas yr $^{-1}$)	(mas yr $^{-1}$)	(deg)	(km s $^{-1}$)
(1)	(2)	(3)	(4)	(5)	(6)	(7)	(8)	(9)
J000013.54+255419.7	74.25 \pm 1.00	75.54 \pm 1.06	-51.94 \pm 0.26	-38.49 \pm 0.27	130.33 \pm 0.37	126.68 \pm 0.37	343.10 \pm 0.10	8.42 \pm 0.16
J000849.76-173925.0 ^a	36.57 \pm 3.91	37.64 \pm 3.92	-177.36 \pm 0.92	-166.64 \pm 0.93	-361.40 \pm 1.08	-370.53 \pm 1.08	406.28 \pm 1.43	204.22 \pm 0.10
J001502.52+295928.7	31.86 \pm 1.65	33.05 \pm 1.66	371.22 \pm 0.91	374.28 \pm 0.91	-211.74 \pm 1.05	-223.02 \pm 1.05	435.69 \pm 1.39	120.79 \pm 0.09
J003030.38-145033.8	34.14 \pm 1.75	35.64 \pm 1.78	244.20 \pm 0.58	252.36 \pm 0.59	-27.90 \pm 0.74	-41.70 \pm 0.74	255.78 \pm 0.95	99.38 \pm 0.11
J003259.67+141037.2	29.79 \pm 1.89	30.61 \pm 1.89	271.67 \pm 0.74	281.65 \pm 0.75	34.79 \pm 1.06	27.32 \pm 1.06	282.97 \pm 1.30	84.46 \pm 0.14
J003452.12+052307.3	115.47 \pm 1.22	116.34 \pm 1.28	670.32 \pm 0.31	666.59 \pm 0.33	183.50 \pm 0.35	172.57 \pm 0.36	688.57 \pm 0.49	75.49 \pm 0.04
J004121.65+354712.5 ^a	8.50 \pm 1.56	9.38 \pm 1.56	-113.74 \pm 0.54	-114.80 \pm 0.54	-54.77 \pm 1.18	-57.94 \pm 1.18	128.59 \pm 1.30	243.22 \pm 0.29
J004521.80+163444.0	64.00 \pm 1.34	65.17 \pm 1.36	357.93 \pm 0.43	358.96 \pm 0.46	-41.48 \pm 0.47	-48.85 \pm 0.49	362.27 \pm 0.67	97.75 \pm 0.06
J004928.58+044101.0	62.55 \pm 1.98	64.60 \pm 2.04	280.71 \pm 0.46	304.11 \pm 0.47	241.53 \pm 0.66	240.12 \pm 0.67	387.48 \pm 0.82	51.71 \pm 0.07
J005911.15-011401.4	114.02 \pm 19.05	115.10 \pm 19.05	895.09 \pm 16.03	907.82 \pm 16.03	39.24 \pm 13.80	14.38 \pm 13.80	907.93 \pm 21.15	89.09 \pm 0.68
J010332.40+193536.5	32.31 \pm 1.39	33.22 \pm 1.40	301.97 \pm 0.57	303.38 \pm 0.63	27.69 \pm 0.81	22.56 \pm 0.83	304.22 \pm 1.04	85.75 \pm 0.10
J010753.11+004157.7	64.78 \pm 1.72	66.52 \pm 1.75	633.41 \pm 0.65	644.50 \pm 0.67	104.36 \pm 0.89	97.42 \pm 0.90	651.82 \pm 1.12	81.40 \pm 0.05
J011912.41+240331.7	30.12 \pm 2.30	31.51 \pm 2.31	263.80 \pm 1.18	265.47 \pm 1.19	16.23 \pm 2.02	9.02 \pm 2.02	265.62 \pm 2.34	39.96 \pm 0.25
J013836.61-032222.8	35.71 \pm 1.66	37.47 \pm 1.69	94.26 \pm 1.06	106.29 \pm 1.10	-295.71 \pm 1.64	-306.74 \pm 1.65	324.63 \pm 1.98	160.89 \pm 0.17
J015011.41+382723.7	39.52 \pm 0.97	40.38 \pm 0.97	878.63 \pm 0.32	877.83 \pm 0.33	-119.42 \pm 0.39	-121.94 \pm 0.40	886.26 \pm 0.52	97.91 \pm 0.04
J015142.59+124428.7	41.54 \pm 1.14	42.98 \pm 1.23	747.33 \pm 0.46	750.42 \pm 0.57	-33.54 \pm 0.74	-42.42 \pm 0.79	751.62 \pm 0.97	93.24 \pm 0.04
J020625.45+264023.3	52.46 \pm 0.99	53.81 \pm 1.05	438.53 \pm 0.34	443.26 \pm 0.35	-38.98 \pm 0.45	-43.92 \pm 0.46	445.43 \pm 0.58	95.66 \pm 0.05
J020743.00+000056.1	33.97 \pm 2.88	35.48 \pm 2.89	149.89 \pm 1.31	163.21 \pm 1.32	-4.69 \pm 1.72	-23.07 \pm 1.73	164.83 \pm 2.18	98.05 \pm 0.41
J023618.06+004852.1	37.63 \pm 1.23	38.39 \pm 1.24	122.87 \pm 0.60	127.94 \pm 0.62	-162.87 \pm 0.70	-166.98 \pm 0.71	210.36 \pm 0.94	142.54 \pm 0.13
J024313.38-245332.8	86.46 \pm 1.62	89.07 \pm 1.72	-286.04 \pm 0.60	-281.34 \pm 0.62	-201.30 \pm 0.81	-201.55 \pm 0.83	346.08 \pm 1.04	234.38 \pm 0.09
J025116.11-035315.7	87.28 \pm 1.23	88.38 \pm 1.27	1101.84 \pm 0.45	1108.76 \pm 0.46	-1843.95 \pm 0.85	-1850.04 \pm 0.85	2156.85 \pm 0.97	149.07 \pm 0.03
J025409.54+022358.7	143.01 \pm 1.24	144.29 \pm 1.27	2565.50 \pm 0.37	2575.12 \pm 0.39	227.16 \pm 0.42	218.05 \pm 0.43	2584.34 \pm 0.58	85.16 \pm 0.03
J030533.66+395434.6	38.59 \pm 1.87	39.62 \pm 1.88	273.01 \pm 0.53	275.78 \pm 0.54	7.29 \pm 0.58	4.24 \pm 0.58	275.81 \pm 0.79	89.12 \pm 0.09
J031100.13+164815.6	34.93 \pm 1.72	35.89 \pm 1.73	239.31 \pm 0.95	244.11 \pm 0.96	12.87 \pm 1.43	4.59 \pm 1.44	244.15 \pm 1.73	88.92 \pm 0.20
J031326.23+780744.6	143.66 \pm 4.36	144.84 \pm 4.37	71.97 \pm 2.29	73.13 \pm 2.29	46.54 \pm 3.65	46.76 \pm 3.65	86.80 \pm 4.31	57.40 \pm 1.44
J032553.05+042539.6	40.04 \pm 2.08	41.81 \pm 2.12	-168.38 \pm 1.33	-167.30 \pm 1.33	-55.65 \pm 1.80	-63.85 \pm 1.80	179.07 \pm 2.24	249.11 \pm 0.36
J032842.66+230204.1	25.82 \pm 1.54	27.25 \pm 1.56	25.19 \pm 0.62	27.90 \pm 0.64	-61.87 \pm 0.91	-66.09 \pm 0.92	71.74 \pm 1.12	157.11 \pm 0.47
J03523.53+113336.7	108.89 \pm 0.61	109.82 \pm 0.62	215.02 \pm 0.23	220.88 \pm 0.24	-627.29 \pm 0.28	-630.37 \pm 0.28	667.95 \pm 0.37	160.69 \pm 0.04
J040709.03+151455.0	56.49 \pm 1.15	57.62 \pm 1.16	209.58 \pm 0.31	213.47 \pm 0.32	-118.72 \pm 0.34	-124.15 \pm 0.35	246.95 \pm 0.47	120.18 \pm 0.07
J041054.46+141130.8	24.76 \pm 2.48	26.00 \pm 2.49	-10.41 \pm 0.72	-8.56 \pm 0.73	-90.63 \pm 0.88	-95.94 \pm 0.88	96.32 \pm 1.14	185.10 \pm 0.34

Table 3 *continued*

Table 3 (*continued*)

Object Name	π_{rel}	π_{abs}	$\mu_{\alpha rel}$	$\mu_{\alpha abs}$	$\mu_{\delta rel}$	$\mu_{\delta abs}$	P.A.	V_{tan}	
CatWISE	(mas)	(mas)	(mas yr $^{-1}$)	(deg)	(km s $^{-1}$)				
(1)	(2)	(3)	(4)	(5)	(6)	(7)	(8)	(9)	
J041522.117-093457.1	174.47 ± 1.14	176.01 ± 1.20	2197.95 ± 0.51	2209.68 ± 0.52	528.63 ± 0.77	525.92 ± 0.77	2271.40 ± 0.93	76.61 ± 0.03	61.15 ± 0.42
J042348.22-041402.0	66.74 ± 0.69	67.73 ± 0.71	-326.66 ± 0.31	-322.31 ± 0.32	84.31 ± 0.47	86.19 ± 0.47	333.64 ± 0.57	284.97 ± 0.05	23.34 ± 0.24
J043900.87-235310.7	78.95 ± 1.19	79.86 ± 1.20	-113.58 ± 0.70	-113.55 ± 0.70	-152.27 ± 0.93	-154.30 ± 0.93	191.58 ± 1.16	216.35 ± 0.17	11.37 ± 0.18
J044853.70-193543.6	53.42 ± 5.17	54.18 ± 5.17	900.50 ± 2.83	904.86 ± 2.83	767.20 ± 3.37	763.76 ± 3.37	1184.10 ± 4.40	49.83 ± 0.11	103.61 ± 9.99
J050021.02+033044.8	75.24 ± 0.64	76.39 ± 0.67	8.77 ± 0.27	9.28 ± 0.27	-346.39 ± 0.37	-350.55 ± 0.37	350.67 ± 0.46	178.48 ± 0.04	21.76 ± 0.19
J051317.27+060812.3	69.65 ± 1.16	70.70 ± 1.17	-4.60 ± 0.39	-2.20 ± 0.39	-432.04 ± 0.41	-435.73 ± 0.41	435.74 ± 0.57	180.29 ± 0.05	29.20 ± 0.48
J051609.20-044553.3	47.94 ± 1.31	48.95 ± 1.31	-221.30 ± 0.89	-216.47 ± 0.89	-201.88 ± 1.37	-202.06 ± 1.37	296.12 ± 1.63	226.97 ± 0.16	28.68 ± 0.79
J052536.18+673951.5	38.84 ± 4.88	39.69 ± 4.88	-250.23 ± 3.00	-250.02 ± 3.01	-69.07 ± 3.92	-71.95 ± 3.92	260.17 ± 4.94	253.95 ± 0.54	31.08 ± 3.92
J053312.61+824617.2	37.69 ± 1.26	38.70 ± 1.27	2043.46 ± 0.81	2044.13 ± 0.81	-1649.47 ± 1.19	-1651.33 ± 1.19	2627.80 ± 1.44	128.93 ± 0.03	321.85 ± 10.57
J053952.16-005856.5	77.64 ± 0.66	78.15 ± 0.67	158.84 ± 0.27	161.69 ± 0.28	323.95 ± 0.50	322.19 ± 0.51	360.49 ± 0.58	26.65 ± 0.05	21.86 ± 0.19
J054231.20-162827.6	60.29 ± 2.42	61.52 ± 2.43	-216.64 ± 1.72	-214.35 ± 1.72	299.93 ± 2.45	299.99 ± 2.45	368.70 ± 2.99	324.45 ± 0.23	28.40 ± 1.14
J055919.85-140454.8	94.85 ± 0.58	95.75 ± 0.61	569.84 ± 0.24	570.54 ± 0.25	-339.78 ± 0.38	-340.10 ± 0.38	664.22 ± 0.45	120.80 ± 0.03	32.88 ± 0.21
J060206.71+404355.4 ^a	66.09 ± 1.47	66.82 ± 1.48	235.24 ± 1.04	235.99 ± 1.04	-216.02 ± 1.27	-221.49 ± 1.27	323.65 ± 1.64	133.18 ± 0.14	22.97 ± 0.52
J060738.42+242951.2 ^a	137.52 ± 0.51	138.16 ± 0.52	-473.77 ± 0.16	-473.41 ± 0.16	-314.78 ± 0.29	-317.54 ± 0.29	570.04 ± 0.33	236.15 ± 0.03	19.56 ± 0.08
J061407.41+391233.2	50.35 ± 1.42	50.83 ± 1.42	-190.82 ± 0.45	-189.99 ± 0.46	-500.76 ± 0.58	-503.47 ± 0.58	538.12 ± 0.74	200.67 ± 0.05	50.17 ± 1.40
J062542.19+564625.4	45.99 ± 1.72	46.76 ± 1.72	-51.72 ± 0.58	-49.75 ± 0.58	-18.13 ± 0.59	-22.02 ± 0.59	54.41 ± 0.83	246.13 ± 0.44	5.52 ± 0.22
J062720.06-111429.6	75.62 ± 1.89	76.43 ± 1.91	-14.05 ± 1.19	-13.33 ± 1.19	-335.32 ± 1.61	-336.82 ± 1.61	337.08 ± 2.00	182.27 ± 0.17	20.90 ± 0.53
J064626.92+793454.5	58.87 ± 1.76	60.16 ± 1.79	-108.10 ± 1.23	-107.85 ± 1.23	-600.78 ± 2.00	-605.11 ± 2.00	614.65 ± 2.35	190.11 ± 0.11	48.42 ± 1.45
J065609.75+420532.8	62.08 ± 0.77	63.18 ± 0.82	320.25 ± 0.23	322.16 ± 0.24	159.53 ± 0.34	154.35 ± 0.34	357.23 ± 0.42	64.40 ± 0.04	26.80 ± 0.35
J070036.80+315718.2	88.24 ± 0.70	89.01 ± 0.71	104.11 ± 0.27	104.72 ± 0.27	-548.90 ± 0.26	-553.38 ± 0.26	563.20 ± 0.37	169.28 ± 0.04	29.98 ± 0.24
J072226.89-054027.5	240.52 ± 2.64	240.99 ± 2.64	-898.42 ± 1.35	-899.41 ± 1.35	369.93 ± 2.29	369.00 ± 2.29	972.16 ± 2.66	292.31 ± 0.09	19.12 ± 0.22
J072719.22+170950.1	110.05 ± 0.83	110.90 ± 0.84	1044.58 ± 0.32	1043.41 ± 0.33	-764.27 ± 0.57	-767.37 ± 0.57	1295.21 ± 0.66	126.33 ± 0.03	55.36 ± 0.42
J074200.88+205515.7	56.01 ± 1.08	56.95 ± 1.10	-325.21 ± 0.31	-327.66 ± 0.32	-229.07 ± 0.37	-230.66 ± 0.37	400.71 ± 0.49	234.86 ± 0.05	33.35 ± 0.64
J075547.93+221212.8	65.50 ± 1.19	66.57 ± 1.20	-17.71 ± 0.58	-17.05 ± 0.59	-245.34 ± 0.89	-251.93 ± 0.89	252.51 ± 1.07	183.87 ± 0.13	17.98 ± 0.33
J075840.07+324718.8	90.56 ± 0.58	91.69 ± 0.62	-231.35 ± 0.19	-230.35 ± 0.20	-317.95 ± 0.20	-328.36 ± 0.20	401.10 ± 0.28	215.05 ± 0.04	20.74 ± 0.14
J081957.98-033529.3	69.76 ± 1.20	70.81 ± 1.21	-195.11 ± 0.89	-196.06 ± 0.89	-160.44 ± 1.30	-162.40 ± 1.30	254.58 ± 1.58	230.36 ± 0.18	17.04 ± 0.31
J082131.64+144317.8	44.08 ± 1.54	45.77 ± 1.58	-36.68 ± 0.49	-34.66 ± 0.50	-267.09 ± 0.53	-273.22 ± 0.53	275.41 ± 0.73	187.23 ± 0.08	28.52 ± 0.39
J082515.97+211546.1	89.22 ± 0.91	90.20 ± 0.92	-501.14 ± 0.34	-504.27 ± 0.35	-294.30 ± 0.45	-300.42 ± 0.45	586.98 ± 0.57	239.22 ± 0.03	30.85 ± 0.32
J083006.91+482838.3	78.68 ± 1.12	80.02 ± 1.14	-1006.97 ± 0.46	-1016.24 ± 0.46	-764.78 ± 0.47	-774.04 ± 0.47	1277.45 ± 0.66	232.70 ± 0.03	75.67 ± 1.08
J083541.88-081918.0	136.34 ± 0.77	137.93 ± 0.82	-525.84 ± 0.27	-532.35 ± 0.27	305.92 ± 0.31	302.02 ± 0.31	612.06 ± 0.41	299.57 ± 0.04	21.03 ± 0.13

Table 3 *continued*

Table 3 (continued)

Object Name	π_{rel}	π_{abs}	$\mu_{\alpha_{rel}}$	$\mu_{\alpha_{abs}}$	$\mu_{\delta_{rel}}$	$\mu_{\delta_{abs}}$	P.A.	V_{tan}
CatWISE	(mas)	(mas)	(mas yr $^{-1}$)	(deg)	(km s $^{-1}$)			
(1)	(2)	(3)	(4)	(5)	(6)	(7)	(8)	(9)
J083717.18-000020.8	29.51 \pm 4.07	30.43 \pm 4.07	-26.06 \pm 1.91	-30.99 \pm 1.91	-173.79 \pm 2.99	-174.52 \pm 2.99	177.25 \pm 3.55	190.07 \pm 0.57
J085035.75+105715.3	31.15 \pm 1.61	32.06 \pm 1.63	-147.63 \pm 0.60	-149.04 \pm 0.61	-11.19 \pm 0.72	-14.16 \pm 0.73	149.71 \pm 0.95	264.57 \pm 0.18
J085757.60+570844.6	69.88 \pm 0.89	70.93 \pm 0.91	-401.33 \pm 0.33	-403.84 \pm 0.34	-376.21 \pm 0.39	-386.44 \pm 0.39	558.95 \pm 0.52	226.26 \pm 0.04
J085833.72+325628.6	41.89 \pm 1.45	43.68 \pm 1.51	-627.88 \pm 0.73	-626.46 \pm 0.73	70.54 \pm 1.30	65.05 \pm 1.30	629.83 \pm 1.49	275.93 \pm 0.08
J090023.73+253934.1	29.08 \pm 1.72	30.22 \pm 1.73	52.85 \pm 0.93	48.87 \pm 0.93	-12.25 \pm 1.14	-19.93 \pm 1.14	52.78 \pm 1.47	112.19 \pm 0.80
J090900.31+652525.8	53.69 \pm 2.95	55.60 \pm 2.99	-212.15 \pm 2.00	-226.25 \pm 2.00	-108.66 \pm 2.21	-125.45 \pm 2.21	258.70 \pm 2.98	240.99 \pm 0.36
J091534.04+042204.8	54.58 \pm 1.18	55.74 \pm 1.21	-108.64 \pm 0.27	-112.27 \pm 0.28	29.94 \pm 0.30	25.89 \pm 0.31	115.22 \pm 0.42	282.99 \pm 0.10
J092615.40+584717.6	38.33 \pm 1.18	39.41 \pm 1.19	15.41 \pm 0.57	11.18 \pm 0.58	-209.82 \pm 0.78	-219.97 \pm 0.79	220.25 \pm 0.98	177.09 \pm 0.14
J092933.34+342951.3	31.65 \pm 2.19	33.57 \pm 2.23	-223.68 \pm 1.56	-227.50 \pm 1.56	-76.58 \pm 2.30	-90.99 \pm 2.30	245.02 \pm 2.78	248.20 \pm 0.34
J093735.98+293120.8	165.96 \pm 1.12	167.19 \pm 1.22	945.57 \pm 0.46	941.60 \pm 0.50	-1314.05 \pm 0.89	-1323.85 \pm 0.90	1624.56 \pm 1.03	144.58 \pm 0.03
J093936.13-244844.3	181.55 \pm 1.26	182.38 \pm 1.26	573.30 \pm 0.35	565.38 \pm 0.35	-1041.97 \pm 0.51	-1040.84 \pm 0.51	1184.48 \pm 0.62	151.49 \pm 0.03
J094908.49-154548.3 a	33.53 \pm 2.69	35.26 \pm 2.71	-108.39 \pm 1.42	-111.37 \pm 1.42	17.36 \pm 1.56	12.90 \pm 1.56	112.11 \pm 2.11	276.61 \pm 0.55
J095105.35+355800.1	27.91 \pm 1.85	28.88 \pm 1.86	-92.07 \pm 0.62	-98.68 \pm 0.63	-161.36 \pm 1.24	-169.64 \pm 1.24	196.25 \pm 1.39	210.19 \pm 0.22
J101014.45-040650.0	48.26 \pm 1.64	49.50 \pm 1.70	-311.79 \pm 0.97	-315.70 \pm 0.97	-12.52 \pm 1.25	-17.45 \pm 1.25	316.18 \pm 1.58	266.84 \pm 0.15
J101905.55+652954.5	42.01 \pm 1.38	43.29 \pm 1.43	-89.64 \pm 0.38	-88.38 \pm 0.38	120.21 \pm 0.61	113.24 \pm 0.61	143.65 \pm 0.72	322.03 \pm 0.14
J102109.51-030421.1	25.44 \pm 2.30	27.20 \pm 2.33	-162.98 \pm 0.76	-168.36 \pm 0.79	-57.26 \pm 0.97	-75.22 \pm 0.99	184.40 \pm 1.27	245.93 \pm 0.20
J103931.32+325623.7	28.35 \pm 2.04	30.30 \pm 2.13	-24.83 \pm 1.14	-40.77 \pm 1.14	-133.68 \pm 1.68	-150.62 \pm 1.68	156.04 \pm 2.03	195.15 \pm 0.43
J104307.42+222523.3	44.00 \pm 1.47	45.76 \pm 1.52	-124.93 \pm 0.79	-127.28 \pm 0.79	-4.36 \pm 1.66	-20.53 \pm 1.66	128.93 \pm 1.84	260.84 \pm 0.41
J104335.10+121310.8	61.21 \pm 1.92	63.12 \pm 1.97	23.34 \pm 0.66	12.70 \pm 0.67	-252.10 \pm 0.88	-257.55 \pm 0.88	257.86 \pm 1.11	177.18 \pm 0.12
J104751.75+212414.7	95.75 \pm 1.37	96.66 \pm 1.38	-1677.37 \pm 0.50	-1678.84 \pm 0.62	-490.75 \pm 0.74	-503.42 \pm 0.81	1752.69 \pm 1.02	253.31 \pm 0.03
J104828.96+091940.9	25.65 \pm 3.15	27.73 \pm 3.18	-270.15 \pm 1.91	-270.37 \pm 1.91	253.96 \pm 2.81	235.63 \pm 2.82	358.64 \pm 3.41	311.07 \pm 0.27
J110611.58+275414.1	48.18 \pm 1.20	49.64 \pm 1.24	-284.11 \pm 0.65	-280.16 \pm 0.65	-441.70 \pm 0.99	-450.17 \pm 0.99	530.23 \pm 1.18	211.90 \pm 0.07
J111009.77+011608.7	52.12 \pm 1.93	53.17 \pm 1.94	-212.23 \pm 1.03	-219.47 \pm 1.03	-279.80 \pm 1.12	-286.32 \pm 1.12	360.76 \pm 1.52	217.47 \pm 0.12
J111447.51-261830.0	184.28 \pm 1.80	185.61 \pm 1.81	-3011.91 \pm 0.46	-3023.73 \pm 0.46	-379.42 \pm 0.55	-380.18 \pm 0.55	3047.54 \pm 0.72	262.83 \pm 0.03
J111812.22-085615.0	45.51 \pm 2.21	46.98 \pm 2.26	-627.66 \pm 1.35	-630.17 \pm 1.36	-232.93 \pm 2.06	-242.14 \pm 2.06	675.09 \pm 2.47	248.98 \pm 0.11
J112254.33+255020.2	65.07 \pm 1.80	66.48 \pm 1.85	-981.13 \pm 0.49	-1005.61 \pm 0.52	-311.80 \pm 0.55	-320.38 \pm 0.58	1055.41 \pm 0.78	252.33 \pm 0.04
J115553.43+055956.6	50.56 \pm 1.54	51.59 \pm 1.56	-441.82 \pm 0.56	-448.45 \pm 0.57	-61.39 \pm 0.50	-70.54 \pm 0.50	453.96 \pm 0.76	261.06 \pm 0.05
J115821.40+043446.3	40.82 \pm 2.42	42.92 \pm 2.51	588.39 \pm 1.42	572.68 \pm 1.42	-908.47 \pm 1.79	-919.56 \pm 1.79	1083.31 \pm 2.28	148.09 \pm 0.07
J120746.66+024426.8	40.09 \pm 1.53	41.58 \pm 1.62	-490.45 \pm 0.65	-503.98 \pm 0.66	127.94 \pm 0.85	126.26 \pm 0.85	519.56 \pm 1.08	284.06 \pm 0.07
J121709.86-031111.8	100.39 \pm 1.58	102.13 \pm 1.61	-1054.76 \pm 0.58	-1063.98 \pm 0.69	75.94 \pm 1.12	68.01 \pm 1.15	1066.15 \pm 1.34	273.66 \pm 0.04
J121757.13+162635.1	107.41 \pm 8.33	109.65 \pm 8.35	779.79 \pm 3.49	772.22 \pm 3.49	-1230.65 \pm 6.05	-1238.74 \pm 6.05	1459.73 \pm 6.98	148.06 \pm 0.14
								63.10 \pm 4.84

Table 3 *continued*

Table 3 (continued)

Object Name	π_{rel}	π_{abs}	$\mu\alpha_{rel}$	$\mu\alpha_{abs}$	$\mu\delta_{rel}$	$\mu\delta_{abs}$	P.A.	V_{tan}
CatWISE	(mas)	(mas)	(mas yr $^{-1}$)	(deg)	(km s $^{-1}$)			
(1)	(2)	(3)	(4)	(5)	(6)	(7)	(8)	(9)
J122554.84-273958.5	71.94 ± 1.15	73.44 ± 1.19	383.51 ± 0.39	373.77 ± 0.40	-629.38 ± 0.96	-628.40 ± 0.96	731.16 ± 1.04	149.26 ± 0.04
J123146.34+084717.1	71.17 ± 1.08	72.75 ± 1.11	-1167.65 ± 0.31	-1177.88 ± 0.34	-1038.88 ± 0.34	-1043.90 ± 0.36	1573.89 ± 0.50	228.45 ± 0.03
J123737.03+652607.2	100.72 ± 1.49	101.63 ± 1.50	-989.60 ± 0.54	-995.72 ± 0.54	-530.93 ± 0.73	-537.70 ± 0.73	1131.63 ± 0.91	241.63 ± 0.03
J125011.59+392542.6	36.36 ± 2.92	37.61 ± 2.94	-38.42 ± 1.65	-43.57 ± 1.65	-817.66 ± 2.30	-827.59 ± 2.30	828.74 ± 2.83	183.01 ± 0.10
J125453.41-012245.6	74.01 ± 0.89	74.94 ± 0.94	-480.73 ± 0.32	-491.93 ± 0.33	123.42 ± 0.46	114.04 ± 0.46	504.98 ± 0.57	283.05 ± 0.03
J131141.74+362925.2	26.61 ± 1.19	27.59 ± 1.21	-348.81 ± 0.34	-354.94 ± 0.34	96.73 ± 0.46	84.66 ± 0.46	364.90 ± 0.57	283.42 ± 0.06
J132003.78+603425.8	62.70 ± 2.00	64.47 ± 2.04	-550.23 ± 0.56	-554.82 ± 0.57	-51.53 ± 0.84	-55.09 ± 0.84	557.55 ± 1.02	264.33 ± 0.06
J132233.51-234015.3	75.08 ± 3.65	76.63 ± 3.66	-346.43 ± 0.93	-356.88 ± 0.93	388.95 ± 0.99	381.25 ± 0.99	522.22 ± 1.36	316.89 ± 0.09
J132407.64+190625.5	31.34 ± 1.91	32.51 ± 1.93	-109.13 ± 0.55	-117.61 ± 0.55	-89.54 ± 0.62	-96.90 ± 0.62	152.39 ± 0.83	230.51 ± 0.16
J132434.67+635827.1	80.69 ± 1.35	82.95 ± 1.47	-358.47 ± 0.68	-372.77 ± 0.68	-62.69 ± 1.45	-65.80 ± 1.45	378.53 ± 1.60	259.99 ± 0.13
J132605.25+120010.1	26.36 ± 14.56	27.61 ± 14.56	80.78 ± 5.78	71.40 ± 5.78	-23.88 ± 8.67	-31.22 ± 8.67	77.93 ± 10.42	113.62 ± 3.82
J132629.56-003833.2	45.74 ± 1.56	46.51 ± 1.58	-228.86 ± 0.57	-233.65 ± 0.59	-101.04 ± 0.76	-108.18 ± 0.76	257.48 ± 0.96	245.16 ± 0.11
J133553.35+113003.7	80.63 ± 9.39	82.34 ± 9.40	-172.82 ± 3.61	-191.06 ± 3.61	-188.34 ± 5.33	-197.55 ± 5.33	274.83 ± 6.44	224.04 ± 0.72
J134645.89-003152.2	74.47 ± 1.27	75.78 ± 1.28	-497.70 ± 0.45	-508.12 ± 0.47	-118.04 ± 1.35	-117.99 ± 1.35	521.64 ± 1.43	256.93 ± 0.08
J134807.08+660327.2	42.62 ± 1.72	43.49 ± 1.73	108.57 ± 0.57	104.16 ± 0.57	-230.30 ± 0.72	-236.30 ± 0.72	258.24 ± 0.92	156.21 ± 0.10
J140255.70+080053.4	18.06 ± 3.17	19.65 ± 3.19	78.62 ± 1.56	60.14 ± 1.57	-147.49 ± 1.76	-148.26 ± 1.76	159.99 ± 2.36	157.92 ± 0.42
J140753.30+124110.7	34.54 ± 0.93	35.50 ± 0.96	-331.73 ± 0.33	-337.18 ± 0.34	65.62 ± 0.36	56.40 ± 0.36	341.86 ± 0.50	279.50 ± 0.05
J143517.22-004612.9	11.62 ± 1.77	12.17 ± 1.77	23.79 ± 0.60	16.65 ± 0.61	12.45 ± 0.84	3.75 ± 0.84	17.07 ± 1.04	77.31 ± 1.74
J143535.75-004348.6	15.37 ± 2.33	16.21 ± 2.33	30.92 ± 0.83	28.50 ± 0.85	-95.58 ± 0.95	-99.35 ± 0.97	103.36 ± 1.29	163.99 ± 0.36
J143945.64+304218.7	21.42 ± 2.37	22.68 ± 2.38	-243.79 ± 0.93	-251.08 ± 0.93	-138.43 ± 1.50	-140.16 ± 1.50	287.55 ± 1.76	240.83 ± 0.18
J144600.78+002450.9	38.49 ± 1.15	40.26 ± 1.19	179.80 ± 0.39	182.54 ± 0.41	-54.66 ± 0.77	-66.22 ± 0.78	194.18 ± 0.88	109.94 ± 0.13
J145714.66+581509.7	52.63 ± 1.83	54.34 ± 1.86	-497.82 ± 0.43	-503.54 ± 0.44	-61.92 ± 0.61	-63.72 ± 0.62	507.56 ± 0.76	262.79 ± 0.05
J150319.71+252528.3	155.74 ± 0.78	156.59 ± 0.79	99.62 ± 0.41	88.72 ± 0.41	560.72 ± 0.53	558.09 ± 0.54	565.10 ± 0.68	9.03 ± 0.03
J150648.79+702741.0	192.92 ± 0.47	194.02 ± 0.53	-1196.00 ± 0.11	-1197.05 ± 0.11	1045.90 ± 0.19	1039.26 ± 0.19	1585.24 ± 0.22	310.96 ± 0.03
J150653.09+132105.8	84.64 ± 0.85	86.02 ± 0.88	-1063.61 ± 0.25	-1071.92 ± 0.27	-8.35 ± 0.31	-15.78 ± 0.33	1072.04 ± 0.43	269.16 ± 0.03
J151114.38+060739.4	30.24 ± 1.83	31.41 ± 1.84	-300.47 ± 0.95	-303.60 ± 0.95	-237.04 ± 1.33	-243.92 ± 1.33	389.45 ± 1.63	231.22 ± 0.12
J151459.41+484803.4	100.84 ± 3.50	102.28 ± 3.52	-971.43 ± 1.92	-982.68 ± 1.92	1487.90 ± 2.77	1487.36 ± 2.77	1782.67 ± 3.37	326.55 ± 0.06
J152040.10+354615.7	66.04 ± 2.19	67.41 ± 2.21	335.36 ± 0.97	321.63 ± 0.97	-383.21 ± 1.50	-387.17 ± 1.50	503.34 ± 1.79	140.28 ± 0.10
J152322.78+301453.4	54.38 ± 1.10	55.36 ± 1.11	141.21 ± 0.37	133.30 ± 0.37	-178.99 ± 0.64	-182.35 ± 0.64	225.88 ± 0.74	143.83 ± 0.09
J152613.76+204334.8	45.58 ± 1.18	46.91 ± 1.20	-201.04 ± 0.54	-218.06 ± 0.54	-355.78 ± 0.61	-360.55 ± 0.61	421.36 ± 0.81	211.17 ± 0.07
J154614.94+493158.6	43.84 ± 1.00	45.03 ± 1.02	172.71 ± 0.25	165.24 ± 0.25	-659.73 ± 0.31	-668.10 ± 0.31	688.23 ± 0.40	166.11 ± 0.04

Table 3 continued

Table 3 (continued)

Object Name	π_{rel}	π_{abs}	$\mu\alpha_{rel}$	$\mu\alpha_{abs}$	$\mu\delta_{rel}$	$\mu\delta_{abs}$	P.A.	V_{tan}
CatWISE	(mas)	(mas)	(mas yr $^{-1}$)	(deg)	(km s $^{-1}$)			
(1)	(2)	(3)	(4)	(5)	(6)	(7)	(8)	(9)
J155301.89+153239.5	71.95 ± 1.08	73.61 ± 1.20	-369.69 ± 0.54	-383.97 ± 0.54	151.48 ± 0.80	153.47 ± 0.80	413.50 ± 0.97	291.79 ± 0.07
J161705.76+180713.9	79.79 ± 6.18	81.16 ± 6.20	96.75 ± 2.96	94.35 ± 2.96	-31.06 ± 4.18	-37.13 ± 4.18	101.39 ± 5.12	111.48 ± 1.44
J162413.95+002915.6	89.64 ± 0.96	90.51 ± 0.98	-372.32 ± 0.39	-376.64 ± 0.39	-11.20 ± 0.60	-10.76 ± 0.60	376.79 ± 0.72	268.36 ± 0.06
J162541.25+152810.0	36.50 ± 3.04	37.72 ± 3.05	-218.70 ± 0.70	-224.94 ± 0.70	-225.84 ± 0.96	-232.74 ± 0.96	323.68 ± 1.19	224.02 ± 0.11
J162618.23+392523.4	30.14 ± 1.19	31.41 ± 1.21	-1371.07 ± 0.30	-1372.26 ± 0.30	237.81 ± 0.35	232.58 ± 0.35	1391.83 ± 0.46	279.62 ± 0.03
J162725.60+325522.8	54.11 ± 1.50	55.30 ± 1.51	-83.46 ± 0.31	-89.34 ± 0.31	-341.84 ± 0.43	-347.15 ± 0.44	358.46 ± 0.54	194.43 ± 0.05
J162918.64+033534.8	80.21 ± 1.20	81.31 ± 1.21	234.85 ± 0.28	233.99 ± 0.29	-142.73 ± 0.39	-150.24 ± 0.39	278.07 ± 0.49	122.70 ± 0.06
J163229.48+190439.6	60.45 ± 1.19	61.41 ± 1.20	292.48 ± 0.47	292.16 ± 0.48	-55.13 ± 0.64	-57.28 ± 0.65	297.72 ± 0.81	101.09 ± 0.08
J164715.47+563209.4	43.11 ± 1.47	43.85 ± 1.48	-171.03 ± 0.53	-174.13 ± 0.53	246.54 ± 0.76	244.43 ± 0.76	300.11 ± 0.93	324.53 ± 0.09
J165311.00+444421.2	81.82 ± 5.59	82.81 ± 5.59	-74.90 ± 2.69	-79.99 ± 2.70	-385.69 ± 3.67	-391.79 ± 3.68	399.87 ± 4.56	191.54 ± 0.33
J171145.73+223204.2	29.18 ± 1.61	29.96 ± 1.62	22.80 ± 0.58	18.49 ± 0.58	0.34 ± 0.84	-7.06 ± 0.84	19.79 ± 1.02	110.90 ± 1.47
J172811.54+394859.0	37.38 ± 1.27	38.25 ± 1.28	35.53 ± 0.45	31.47 ± 0.46	-20.67 ± 1.00	-23.35 ± 1.01	39.19 ± 1.11	126.57 ± 0.81
J174124.05+255312.0	216.17 ± 1.66	216.93 ± 1.67	-507.61 ± 0.34	-512.24 ± 0.34	-1473.37 ± 0.52	-1478.82 ± 0.52	1565.02 ± 0.62	199.11 ± 0.03
J175023.78+422238.6	31.25 ± 1.57	32.43 ± 1.58	-44.53 ± 0.33	-44.66 ± 0.33	73.70 ± 0.39	68.81 ± 0.39	82.03 ± 0.51	327.02 ± 0.18
J175033.14+175905.4	37.67 ± 1.77	38.58 ± 1.78	180.63 ± 0.81	179.88 ± 0.81	95.47 ± 1.20	90.62 ± 1.20	201.42 ± 1.45	63.26 ± 0.21
J175609.98+281516.4	30.02 ± 1.06	30.86 ± 1.07	-610.19 ± 0.30	-613.01 ± 0.30	-406.79 ± 0.34	-414.32 ± 0.34	739.89 ± 0.45	235.95 ± 0.04
J175805.45+463318.2	70.49 ± 1.34	71.25 ± 1.35	-15.13 ± 0.25	-17.20 ± 0.26	581.49 ± 0.35	578.06 ± 0.36	578.32 ± 0.44	358.30 ± 0.04
J180026.66+013450.9	127.53 ± 0.96	128.01 ± 0.96	186.58 ± 0.22	184.39 ± 0.23	-379.51 ± 0.23	-385.79 ± 0.24	427.59 ± 0.33	154.45 ± 0.04
J181210.89+272142.8	52.54 ± 14.29	53.12 ± 14.29	151.63 ± 8.19	150.84 ± 8.19	-304.92 ± 10.28	-309.77 ± 10.28	344.54 ± 13.14	154.04 ± 1.10
J182128.39+141357.2	108.39 ± 0.73	109.38 ± 0.77	229.31 ± 0.22	228.22 ± 0.22	-239.04 ± 0.22	-246.46 ± 0.22	335.90 ± 0.31	137.20 ± 0.04
J183058.60+454258.2	33.23 ± 1.85	34.22 ± 1.86	92.24 ± 0.68	91.04 ± 0.68	136.04 ± 1.41	133.88 ± 1.41	161.90 ± 1.57	34.22 ± 0.28
J184108.67+311728.6	23.18 ± 0.76	23.99 ± 0.77	54.13 ± 0.34	51.32 ± 0.35	35.96 ± 0.85	33.55 ± 0.85	61.31 ± 0.92	56.83 ± 0.43
J185215.87+353714.9	68.85 ± 1.26	69.81 ± 1.27	252.34 ± 0.28	252.82 ± 0.28	-287.34 ± 0.46	-292.00 ± 0.46	386.24 ± 0.54	139.11 ± 0.05
J190106.23+471820.5	56.38 ± 1.04	57.15 ± 1.04	121.38 ± 0.91	119.68 ± 0.91	411.57 ± 1.33	406.74 ± 1.33	423.98 ± 1.61	16.40 ± 0.11
J190624.72+450805.2	61.75 ± 1.03	62.30 ± 1.03	-21.51 ± 0.26	-25.46 ± 0.26	-350.73 ± 0.38	-351.65 ± 0.38	352.57 ± 0.46	184.14 ± 0.05
J190648.66+401105.9	58.75 ± 0.51	59.50 ± 0.53	439.13 ± 0.14	438.13 ± 0.14	-175.73 ± 0.15	-179.51 ± 0.15	473.48 ± 0.21	112.28 ± 0.03
J195246.34+723957.9	71.19 ± 0.51	72.14 ± 0.53	-293.82 ± 0.14	-293.85 ± 0.15	-355.93 ± 0.20	-353.64 ± 0.21	459.79 ± 0.26	219.72 ± 0.03
J200250.59-052154.2	55.64 ± 0.62	56.44 ± 0.64	-110.27 ± 0.38	-111.12 ± 0.38	-111.74 ± 0.46	-117.68 ± 0.46	161.85 ± 0.60	223.36 ± 0.11
J204749.62-071821.6	41.89 ± 1.83	43.00 ± 1.84	20.23 ± 1.11	26.97 ± 1.11	-232.62 ± 1.16	-241.44 ± 1.16	242.94 ± 1.61	173.63 ± 0.20
J210115.58+175656.0	30.33 ± 1.31	31.17 ± 1.32	142.39 ± 0.51	139.23 ± 0.51	-151.59 ± 0.68	-158.37 ± 0.68	210.87 ± 0.85	138.68 ± 0.12
J212414.06+010003.8	49.60 ± 1.03	50.72 ± 1.05	180.95 ± 0.27	183.45 ± 0.29	271.23 ± 0.31	263.75 ± 0.33	321.28 ± 0.44	34.82 ± 0.05

Table 3 continued

Table 3 (continued)

Object Name	π_{rel}	π_{abs}	$\mu\alpha_{rel}$	$\mu\alpha_{abs}$	$\mu\delta_{rel}$	$\mu\delta_{abs}$	P.A.	V_{tan}
CatWISE	(mas)	(mas)	(mas yr $^{-1}$)	(deg)	(km s $^{-1}$)			
(1)	(2)	(3)	(4)	(5)	(6)	(7)	(8)	(9)
J212702.63+761756.8	60.36 ± 0.77	61.22 ± 0.78	758.33 ± 0.38	754.99 ± 0.39	822.08 ± 0.61	819.71 ± 0.61	1114.42 ± 0.72	42.65 ± 0.04
J213927.29+022024.7	94.44 ± 1.08	95.68 ± 1.10	482.71 ± 0.64	485.33 ± 0.64	124.12 ± 0.81	122.84 ± 0.81	500.63 ± 1.03	75.80 ± 0.07
J215432.82+594211.3	65.80 ± 1.81	66.25 ± 1.81	-161.72 ± 1.00	-164.30 ± 1.00	-463.09 ± 1.24	-466.33 ± 1.24	494.43 ± 1.59	199.41 ± 0.09
J221354.65+091139.0	50.26 ± 1.85	51.07 ± 1.85	-121.50 ± 0.47	-117.87 ± 0.47	-28.63 ± 0.50	-36.08 ± 0.50	123.27 ± 0.69	252.98 ± 0.16
J222444.39-015908.2	85.16 ± 0.66	85.97 ± 0.73	468.60 ± 0.24	468.59 ± 0.24	-867.60 ± 0.45	-873.53 ± 0.45	991.28 ± 0.51	151.79 ± 0.03
J222622.96+044001.1	49.56 ± 3.98	51.09 ± 4.00	-276.23 ± 2.03	-268.56 ± 2.03	-459.19 ± 2.27	-462.10 ± 2.27	534.47 ± 3.05	210.16 ± 0.16
J223937.67+161716.8	40.81 ± 1.68	41.59 ± 1.69	390.83 ± 0.96	390.98 ± 0.96	231.14 ± 0.99	224.72 ± 0.99	450.96 ± 1.38	60.11 ± 0.09
J224253.65+254256.2	46.11 ± 0.83	47.24 ± 0.90	385.17 ± 0.24	380.96 ± 0.25	-55.02 ± 0.28	-64.60 ± 0.28	386.40 ± 0.38	99.62 ± 0.04
J224431.96+204339.1	57.41 ± 1.42	58.31 ± 1.42	224.23 ± 0.74	226.45 ± 0.75	-229.64 ± 1.27	-234.59 ± 1.27	326.06 ± 1.47	136.01 ± 0.13
J225418.98+312353.0	65.85 ± 1.18	66.77 ± 1.19	57.60 ± 0.73	57.26 ± 0.73	189.61 ± 1.16	185.53 ± 1.16	194.17 ± 1.37	17.15 ± 0.20
J225529.03-003436.4	14.71 ± 1.11	15.80 ± 1.16	-36.04 ± 0.41	-28.14 ± 0.44	-175.86 ± 0.72	-177.82 ± 0.73	180.03 ± 0.85	188.99 ± 0.14
J232123.85+135450.3 ^a	84.09 ± 3.29	85.20 ± 3.30	68.13 ± 1.58	68.47 ± 1.58	-562.21 ± 2.41	-568.81 ± 2.41	572.92 ± 2.88	173.14 ± 0.15
J232345.24+425143.9	65.31 ± 1.41	66.12 ± 1.42	-41.96 ± 0.84	-43.27 ± 0.84	-286.19 ± 1.03	-289.85 ± 1.03	293.06 ± 1.33	188.49 ± 0.13
J232728.85-273056.4	50.14 ± 3.41	51.32 ± 3.43	284.42 ± 1.20	290.72 ± 1.21	67.29 ± 1.43	61.63 ± 1.44	297.18 ± 1.88	78.03 ± 0.19
J233051.30-084455.9	31.24 ± 7.66	32.95 ± 7.67	92.87 ± 2.14	106.60 ± 2.14	-137.79 ± 2.73	-146.44 ± 2.73	181.13 ± 3.47	143.95 ± 0.60
J233910.67+135212.9	57.65 ± 1.69	58.75 ± 1.70	365.13 ± 1.00	370.91 ± 1.00	-974.34 ± 2.00	-984.24 ± 2.00	1051.81 ± 2.24	159.35 ± 0.06
J234026.68-074509.6	45.64 ± 2.42	47.65 ± 2.45	151.83 ± 0.62	164.03 ± 0.62	-249.81 ± 0.66	-254.81 ± 0.66	303.04 ± 0.91	147.23 ± 0.09
J234841.34-102843.2	58.63 ± 2.81	59.93 ± 2.83	624.85 ± 0.66	623.94 ± 0.66	156.61 ± 0.72	146.78 ± 0.72	640.97 ± 0.98	76.76 ± 0.05
J235122.32+301054.1	40.79 ± 2.06	41.83 ± 2.07	251.99 ± 1.26	254.86 ± 1.27	13.29 ± 1.48	6.89 ± 1.48	254.95 ± 1.95	88.45 ± 0.22
J235654.19-155322.9	66.97 ± 1.35	68.28 ± 1.37	-430.71 ± 0.43	-423.54 ± 0.43	-603.30 ± 0.68	-612.03 ± 0.68	744.29 ± 0.80	214.68 ± 0.03

^a π measured in α only due to small π factor in δ

8.2. Astrometric Results Discussion

Table 4 presents median values of the parallax results for Series 1 (52 objects), Series 2 (121 objects), and combined Series 1+2. Column (2) gives the median relative parallaxes and median relative parallax uncertainties. We note that the median uncertainty for Series 2 is larger than for Series 1, despite similar numbers of frames and ΔT , which is likely due to the selection of somewhat more difficult objects due to programmatic decisions as described in §6. Column (3) gives the median parallax values for the reference frames, and hence the median corrections from relative to absolute parallax, along with the median reference frame distances in parsecs in parentheses. Column (4) gives the program object median absolute parallaxes, median absolute parallax uncertainties, and, parenthetically, the median program object distances. A typical reference frame is at a distance of 900 parsecs, compared to a typical program object distance of 18 parsecs; roughly a factor of 50. This distance ratio is sufficient to cause only a small increase in uncertainty in the conversion to absolute parallax.

Table 4. Summary: Object and Reference Frame Parallaxes and Distances.

Series	π_{rel} (mas)	$\pi_{rel} \rightarrow \pi_{abs}$ (mas/pc)	π_{abs} (mas/pc)
(1)	(2)	(3)	(4)
Series 1	56.75 ± 1.27 (1020 pc)	0.98	57.73 ± 1.28 (17.32 pc)
Series 2	54.15 ± 1.57 (862 pc)	1.16	55.31 ± 1.62 (18.08 pc)
Series 1+2	54.49 ± 1.47 (909 pc)	1.10	55.59 ± 1.51 (17.99 pc)

Figure 1 expands on the absolute parallax results showing the distribution of absolute parallaxes, the distribution of absolute uncertainties, and their associated median values. The distance distribution, peaking at about 30 parsecs, is less physical and more a product of the relatively small number of brown dwarfs known at the time within 10 parsecs and our desire to observe astrophysically interesting objects. The distribution of absolute parallax uncertainties, while having a median value of 1.51 mas, shows a tail of larger errors both due to selection of interesting, but faint, objects and the fact that both Series 1 and Series 2 observations had un-

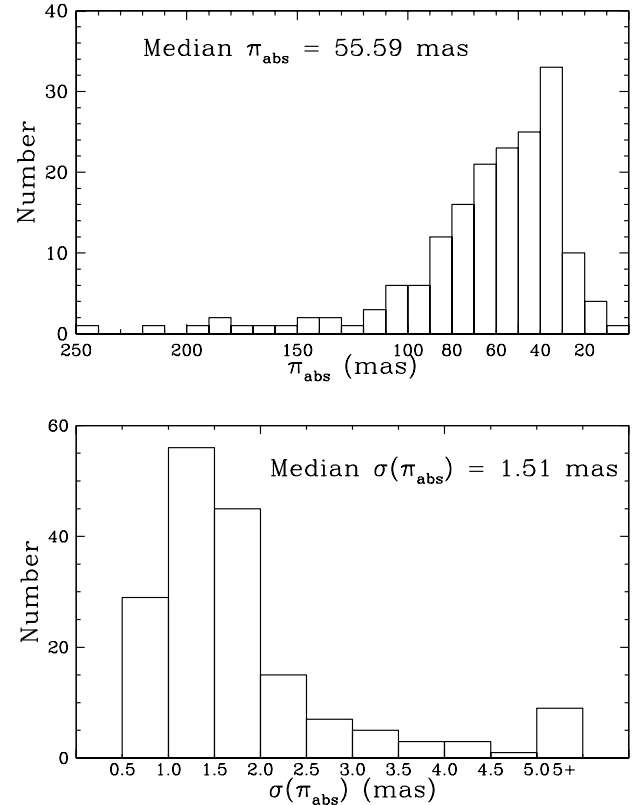


Figure 1. Distributions of π_{abs} and $\sigma(\pi_{abs})$ along with median values for the combined Series 1 and Series 2 results.

planned, abrupt endings leaving some objects without coverage we would otherwise have provided. Nonetheless, to our knowledge, our results provide the first published parallaxes for 16 objects and the highest precision parallaxes available for an additional 106 objects, along with concomitant proper motions.

Figure 2 shows similar diagrams for absolute total proper motion values, the distribution of absolute uncertainties, and their associated median values. As with Figure 1, the distribution of absolute proper motion uncertainties, with a median value of 1.02 mas yr^{-1} , has a long tail toward larger uncertainties for similar reasons.

The panels in Figure 3 show the distribution of tangential velocities and tangential velocity uncertainties, along with mean values for both, based on the absolute parallax and absolute proper motion determinations. The red lines depict the tangential velocities of the eight verified subdwarfs included in this study (J0041+35, J0448-19, J0533+82, J0937+29, J0939-24, J1158+04, J1626+39, J1756+28), reflecting their large range in tangential velocities. See §13.4 for brief reviews of the certain and likely subdwarfs included in

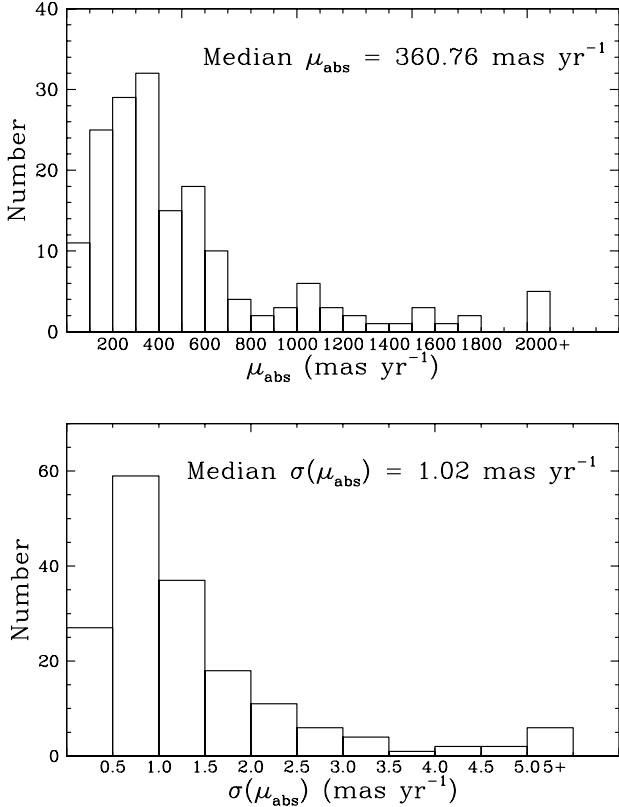


Figure 2. Distributions of μ_{abs} and $\sigma(\mu_{\text{abs}})$ along with median values for combined Series 1 and Series 2 results.

this study. As described above, the tangential velocity uncertainties are based on a combination of absolute parallax and absolute proper motion uncertainties and thus have a tail toward larger values. Nonetheless, the median tangential velocity uncertainty is about 1 km s^{-1} , with a plurality having uncertainties of $<0.5 \text{ km s}^{-1}$. We will re-visit the validity of the uncertainties presented in Table 3 and in this section in the comparison with Gaia astrometric results below.

9. SYSTEMATIC INTERNAL ANALYSIS

While every effort has been made to properly calculate parallaxes and proper motions in this study, an internal consistency evaluation is still of value. In our previous study (Vrba et al. 2004), with fewer observations and a time baseline of no more than $\Delta T = 2.0$ years, the data were insufficient to base determinations of parallaxes on more than the parallactic factor in Right Ascension and, hence, were deemed “preliminary”. A general rule of thumb for USNO narrow-field astrometry has long been to consider any result as “preliminary” unless based on a minimum time baseline of $\Delta T \geq 3$ years (i.e., a minimum of 4 observing seasons) in order to properly sep-

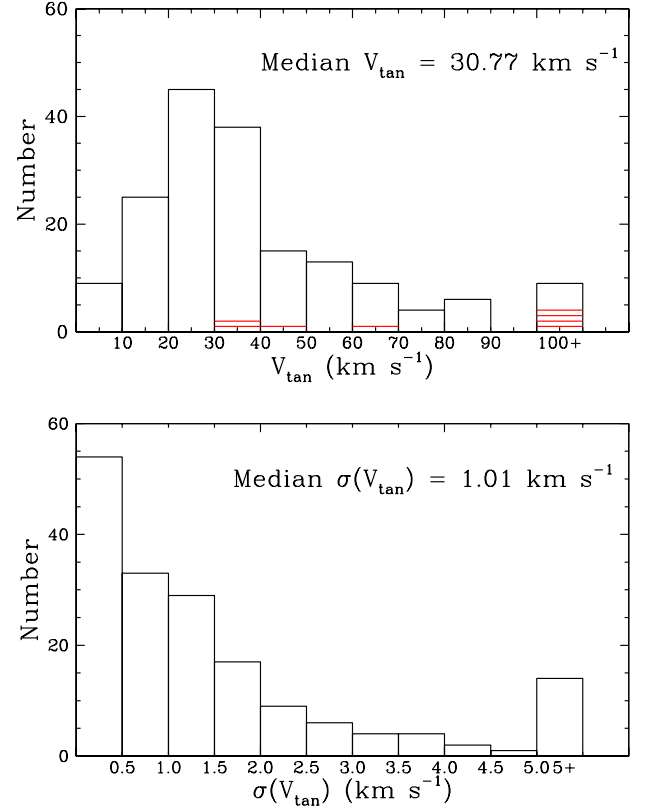


Figure 3. Distributions of V_{tan} and $\sigma(V_{\text{tan}})$ along with median values. The red lines correspond to the V_{tan} velocities of the eight verified subdwarfs in this study.

arate parallax and proper motions. The current study has sufficient data to allow combined weighted means of parallaxes determined independently in Right Ascension and Declination, as described in §4.6, except for six objects with indeterminate Declination solutions. For the remaining 167 objects, in Figure 4 we plot the relative parallax solutions in Right Ascension versus those in Declination, with blue and red points representing Series 1 and Series 2 results, respectively. Error bars in both coordinates are plotted, however, only those in Declination are easily seen. A weighted fit to the data is shown with a slope of 0.997 ± 0.005 , indicating no systematic differences in the Right Ascension and Declination solutions and justifying the combined results presented in Column (2) of Table 3.

10. COMPARISON WITH GAIA ASTROMETRIC RESULTS

The European Space Agency’s Gaia satellite mission (Gaia Collaboration et al. 2016) has provided astrometry at optical wavelengths with unprecedented accuracy. The International Astronomical Union has recognized

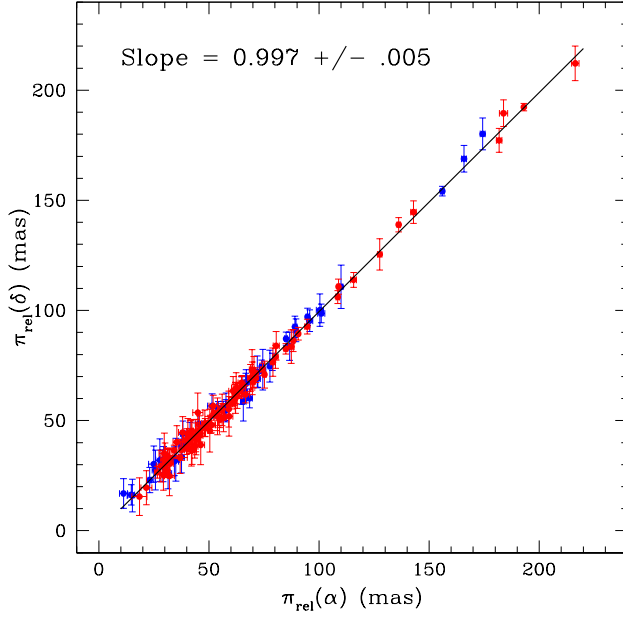


Figure 4. Comparison of relative parallaxes determined in the α and δ directions independently. Blue points display Series 1 data while red points display Series 2 data.

Gaia products as the optical realization of the International Celestial Reference Frame 3 (ICRF3) via Resolution B3 at its XXXIst General Assembly. The latest data update from Gaia is Data Release 3 (DR3) (Gaia Collaboration et al. 2023), providing both parallax and proper motion values. There are 40 objects serendipitously in common between this study and Gaia DR3. In this section we compare our parallax and proper motion results with those of the Gaia/ICRF standard values.

10.1. Parallax Comparison

We compare our π_{abs} values from Column 3 of Table 3 of this study to the values presented in Gaia DR3. Figure 5 plots our values against those of Gaia. The best-fit straight line, weighted by $(\sigma(\pi_{abs} \text{ USNO}))^{-2}$, has a slope of 1.006 ± 0.004 . Error bars for both the USNO and Gaia results are shown in this figure, although typically too small to be apparent at this scale.

In Figure 6 we plot the differences in π_{abs} in the sense of (USNO-Gaia) versus Gaia π_{abs} . The error bars shown are the USNO and Gaia errors combined in quadrature. The solid red line shows the net difference between the two sets of results of -0.024 ± 0.183 mas, weighted by the inverse squared sum of the errors. We note that there is only one object with $\Delta\pi_{abs}$ at the $\approx 3\sigma$ level (J042348.22–041402.0 – see discussion of this object in Section 10.2), which can be expected for 40 sets of measures with a normal error distribution.

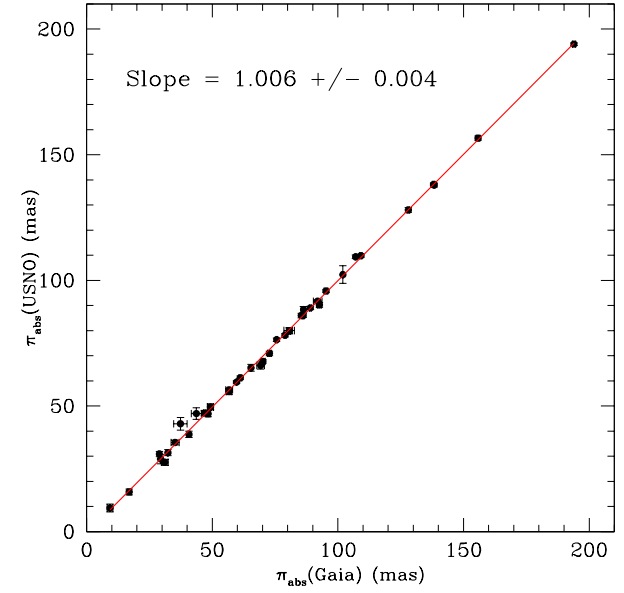


Figure 5. A plot of USNO versus Gaia π_{abs} values for the 40 objects in common. Error bars for both sets of data are plotted along with the solid red line being the best fit to the data weighted by $(\sigma(\pi_{abs} \text{ USNO}))^{-2}$, and a resulting slope of 1.006.

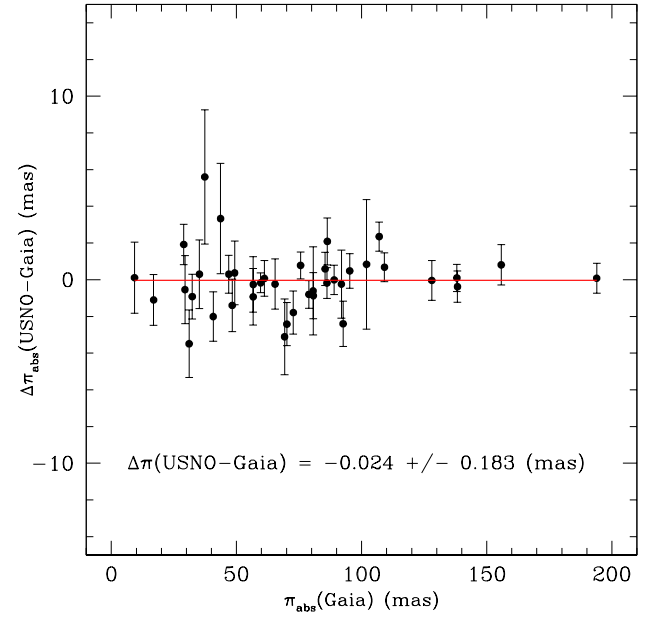


Figure 6. The differences in USNO minus Gaia π_{abs} values plotted versus Gaia π_{abs} for the 40 objects in common. The error bars displayed are the USNO and Gaia errors combined in quadrature. The solid red line shows the net difference between the two sets of results of -0.024 ± 0.183 mas, weighted by the inverse squared sum of the errors.

Based on the results shown in Figures 5 and 6 we find no significant offsets or systematic differences as a function of object distances, including conversions to absolute parallax, between the π_{abs} values determined in this work and those from Gaia DR3.

10.2. Proper Motion Comparison

The comparison of USNO and Gaia proper motion determinations is a bit more complicated due to Gaia's enhanced resolution of closely separated binaries, which did not appear to be an issue in the comparison of parallaxes in the previous section. In Figure 7, we plot the USNO-Gaia differences in absolute proper motions in α (blue) and δ (red) versus the absolute Gaia proper motion in α and δ . Clearly, there are a number of outlying data points in this figure. In Table 5 we list the USNO-Gaia differences (U-G) in μ_{abs} in both α and δ ,

along with total errors added in quadrature, in columns (2) and (3), respectively, for the 40 objects in common. We also list the Gaia DR3 values in columns (4) and (5), respectively, for the Renormalized Unit Weight Error (RUWE) and Image Parameter Determination (gofha) (IPD), which we take to be independent indicators of binarity for values significantly above RUWE > 1.4 and IPD > 0.1 (Fabricius et al. 2021). Objects for which their RUWE or IPD values exceed these limits are noted with a tablenote in Table 5, along with J151459.41+484803.4 as discussed below. See Castro-Ginard et al. (2024) for a discussion of Gaia-based discovery of otherwise unresolved binaries based on RUWE values. Column (6) provides comments on potentially relevant properties such as binarity, high proper motions, or unusual spectral types.

Table 5. Comparison of USNO and Gaia Proper Motions and Gaia DR3 Indicators of Binarity

Object Name CatWISE	$\Delta\mu(\alpha)(U - G)$	$\Delta\mu(\delta)(U - G)$	RUWE	IPD	Comments				
	(mas yr $^{-1}$)	(mas yr $^{-1}$)							
	(1)	(2)	(3)	(4)	(5)				
J004121.65+354712.5	+3.69 \pm 1.09	-0.97 \pm 1.51	1.147	0.0470	Subdwarf				
J004521.80+163444.0	-0.11 \pm 0.50	-0.94 \pm 0.51	0.925	0.0159					
J025116.11-035315.7	-3.90 \pm 0.49	+3.82 \pm 0.87	1.178	0.0152	Large μ (2. $''$ 1 yr $^{-1}$)				
J035523.53+113336.7	-2.30 \pm 0.64	+0.93 \pm 0.46	1.210	0.0182					
J042348.22-041402.0 ^a	+17.65 \pm 1.01	+14.87 \pm 0.86	1.573	0.1940	0. $''$ 16 binary (HST)				
J043900.87-235310.7	-0.33 \pm 0.74	-1.44 \pm 1.00	1.166	0.0071					
J050021.02+033044.8	-2.00 \pm 0.42	+1.34 \pm 0.45	1.009	0.0084					
J053312.61+824617.2	+5.34 \pm 0.98	+11.63 \pm 1.28	1.119	0.0145	Subdwarf, Large μ (2. $''$ 6 yr $^{-1}$)				
J053952.16-005856.5	-0.41 \pm 0.44	-0.04 \pm 0.59	1.176	0.0406					
J055919.85-140454.8	-0.80 \pm 0.67	-1.93 \pm 0.78	1.303	0.0256					
J060738.42+242951.2	-0.54 \pm 0.54	+0.92 \pm 0.47	1.128	0.0023					
J070036.80+315718.2 ^a	+18.02 \pm 0.46	-3.67 \pm 0.40	1.995	0.1370	0. $''$ 2 binary (HST)				
J075840.07+324718.8 ^a	-5.91 \pm 2.88	+3.17 \pm 1.83	1.137	0.1210	Spectral binary				
J082518.97+211546.1	+0.18 \pm 0.97	+2.25 \pm 0.82	1.111	0.0188					
J083006.91+482838.3	+0.33 \pm 2.23	+0.93 \pm 1.04	1.090	0.0161					
J083541.88-081918.0	+2.46 \pm 0.35	+0.37 \pm 0.39	1.418	0.0237					
J085757.60+570844.6	-0.84 \pm 0.84	+1.18 \pm 0.72	1.244	0.0265					
J091534.04+042204.8	+0.91 \pm 1.04	+4.61 \pm 0.94	1.048	0.0653	0. $''$ 73 binary (HST)				
J095105.35+355800.1	+2.22 \pm 0.63	+1.94 \pm 1.24	1.289	0.0360					
J110611.58+275414.1 ^a	-9.35 \pm 1.40	+1.68 \pm 1.57	1.733	0.0116	Over-luminous, spectral binary				
J111812.22-085615.0	-2.99 \pm 2.80	+21.21 \pm 2.58	1.104	0.1510	Unusually blue				
J115821.40+043446.3	+2.28 \pm 2.88	+3.63 \pm 2.45	1.225	0.0173	Subdwarf				
J131141.74+362925.2	+1.53 \pm 0.87	-2.60 \pm 1.05	1.156	0.0116	Spectral binary				
J140753.30+124110.7	+0.19 \pm 1.47	+3.03 \pm 1.70	1.225	0.0217					
J150319.71+252528.3	+1.31 \pm 0.73	+0.31 \pm 0.88	1.274	0.0184					
J150648.79+702741.0	-2.87 \pm 0.73	-2.93 \pm 0.86	1.311	0.0182					
J150653.09+132105.8	-0.85 \pm 0.35	-3.98 \pm 0.39	0.979	0.0251					
J151459.41+484803.4 ^a	-44.64 \pm 1.93	+22.73 \pm 2.78	1.203	0.0289	Large μ (1. $''$ 8 yr $^{-1}$)				
J152613.76+204334.8	+3.42 \pm 1.08	-1.38 \pm 0.93	1.018	0.0160					

Table 5 *continued*

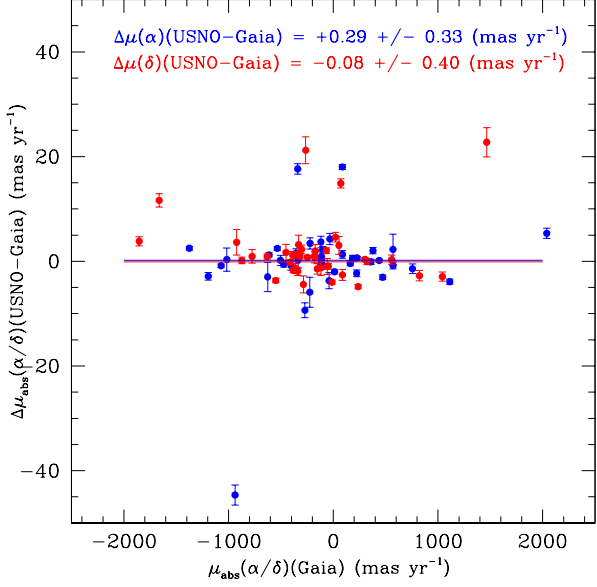


Figure 7. The USNO-Gaia differences in absolute proper motions ($\Delta\mu_{abs}$) in α (blue) and δ (red) versus the absolute Gaia proper motion in α/δ for the 40 objects in common. The error bars displayed are the USNO and Gaia errors combined in quadrature. The several outlying data points are for five objects with resolved or nearly-resolved binarity likely affecting the Gaia results, as discussed in §10.2. For the remaining 35 objects the blue and red lines show the mean differences in $\Delta\mu_{abs}$ in α and δ , respectively, of $+0.29 \pm 0.33$ mas yr^{-1} and -0.08 ± 0.40 mas yr^{-1} .

Table 5 (continued)

Object Name	$\Delta\mu(\alpha)(U - G)$	$\Delta\mu(\delta)(U - G)$	RUWE	IPD	Comments
CatWISE	(mas yr^{-1})	(mas yr^{-1})			
(1)	(2)	(3)	(4)	(5)	(6)
J162618.23+392523.4	$+2.50 \pm 0.34$	-4.84 ± 0.40	1.088	0.0045	Subdwarf, Large μ ($1.^{\circ}4 \text{ yr}^{-1}$)
J175609.98+281516.4	$+1.22 \pm 0.39$	-0.22 ± 0.46	1.162	0.0160	Subdwarf
J180026.66+013450.9	$+0.66 \pm 0.58$	-1.68 ± 0.50	1.183	0.0252	
J182128.39+141357.2	$+0.65 \pm 0.28$	$+0.77 \pm 0.30$	1.156	0.0105	
J190648.66+401105.9	-0.16 ± 0.18	$+0.20 \pm 0.20$	1.121	0.0073	
J200250.59-052154.2	$+0.32 \pm 1.87$	-1.24 ± 1.47	1.197	0.0336	
J212702.63+761756.8	-1.42 ± 0.93	-2.75 ± 1.01	1.465	0.0468	Spectral binary
J222444.39-015908.2	-3.05 ± 0.44	$+0.15 \pm 0.62$	1.023	0.1000	Astrometric binary candidate
J224253.65+254256.2	$+2.04 \pm 0.58$	$+2.03 \pm 0.56$	1.190	0.0466	
J225529.03-003436.4	$+4.27 \pm 1.06$	$+0.74 \pm 1.00$	1.039	0.1140	
J232545.24+425143.9	-3.71 ± 1.54	-4.42 ± 1.59	1.225	0.0110	

^a Objects which have indications of potential Gaia-resolved binarity as discussed in §10.2. See also §10.2 for definitions of (U-G), RUWE, and IPD.

From Table 5 we note that the objects with increased values of either RUWE or IPD have significantly dif-

ferent μ_{abs} in either α or δ between this study and Gaia DR3, and most have some independent indication of binarity. J042348.22-041402.0, with a RUWE value of 1.573 and IPD value of 0.1940, is a resolved

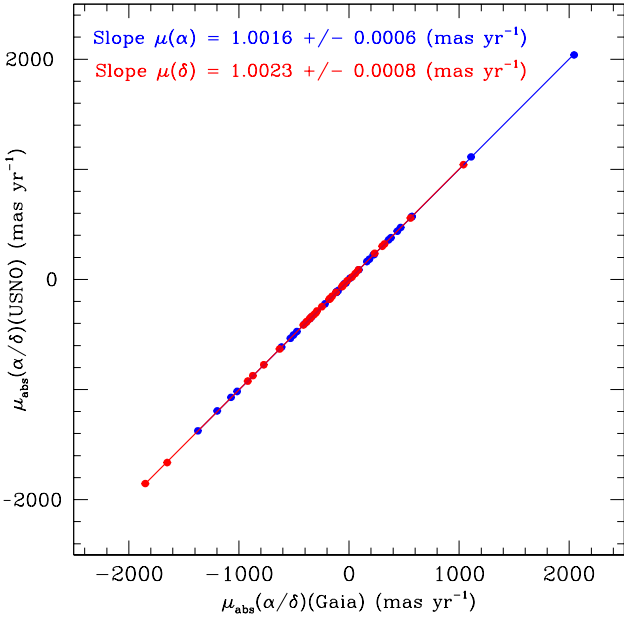


Figure 8. We plot the Gaia versus USNO values of μ_{abs} in α (blue) and δ (red), respectively, for the 35 not affected by likely binarity, as discussed in §10.2. The blue and red lines represent the best fits to the α and δ data with slopes of 1.0016 ± 0.0006 and 1.0023 ± 0.0008 , respectively.

binary with a separation of $0.^{\prime\prime}16$ found using Hubble Space Telescope (HST) imaging (Burgasser et al. 2005b). J070036.80+315718.2, with RUWE = 1.995 and IPD = 0.137, is another HST resolved $0.^{\prime\prime}2$ binary (Reid et al. 2006). J075840.07+324718.8 has a RUWE indicative of a single object (1.137), but an IPD value indicative of binarity (0.121). This object has been identified as a spectral binary candidate (Burgasser et al. 2010; Bardalez Gagliuffi et al. 2015), but is unresolved in high-resolution imaging (Radigan et al. 2013). J110611.58+275414.1 has a high RUWE value (1.733), has been noted as over-luminous (Manjavacas et al. 2013), shows radial velocity variations (Hsu et al. 2021), and is considered as strong spectral binary candidate in Burgasser et al. (2010), though unresolved (Looper et al. 2008a; Bardalez Gagliuffi et al. 2015). We remove these objects from our comparison of USNO and Gaia results along with the blue L dwarf J111812.22–085615.0 due to its high value of IPD (0.151). We also remove the high proper motion object J151459.41+484803.4 which, while having large proper motion discrepancies between USNO and Gaia in both α and δ , has no previous indications of binarity but is noted as a blue L dwarf contaminant in Bardalez Gagliuffi et al. (2014) with stable radial velocity measurements (Wilson et al. 2003). We note, however, that

Dahn et al. (2017) also find proper motion values for this object that are significantly discrepant with both this study and Gaia, while all three studies show consistent parallax results. Thus, a high-accuracy proper motion for J151459.41+484803.4 is indeterminate at this time. We leave in the mix J091534.04+042204.8, an HST resolved $0.^{\prime\prime}73$ binary (Reid et al. 2006) we take to have a wide enough separation so as to not affect Gaia proper motion astrometry.

For the five objects discussed above with significantly discrepant USNO and Gaia values of proper motion we cannot say with certainty which set of values are more reliable. However, we do note that the projected spatial separations are all well within the typical USNO PSFs, there were no issues found with the USNO data reductions for these objects, and that the data time baselines were considerably longer for the USNO data than for those of Gaia. The latter point is also relevant for considering the somewhat enhanced differences in USNO and Gaia proper motion values for high proper motion objects in Table 5.

For the remaining 35 objects in common with Gaia we return to Figure 7 where the blue and red lines show the mean differences in $\Delta\mu_{abs}$ in α and δ , respectively, of $+0.29 \pm 0.33$ mas yr^{-1} and -0.08 ± 0.40 mas yr^{-1} . In Figure 8 we plot the Gaia versus USNO values of μ_{abs} in α (blue) and δ (red), respectively. The blue and red lines represent the best fits to the α and δ data with slopes of 1.0016 ± 0.0006 and 1.0023 ± 0.0008 , respectively. We conclude that the proper motion values determined in this study do not differ systematically from those of Gaia DR3 for those objects not affected by resolved or nearly-resolved binarity.

11. NEW UKIRT AND ADOPTED MKO JHK PHOTOMETRY

For the following science sections we found it optimal to obtain or utilize J , H , and K_s photometry based on as uniform of a system as possible. We chose the UKIRT (MKO) photometry system (Simons & Tokunaga 2002; Hodgkin et al. 2009) due to its widespread use and USNO involvement in the UKIRT Hemisphere Survey project (UHS) (Dye et al. 2018; Schneider et al. 2025). While we obtained considerable new photometry for Series 2 objects using WFCAM (Casali et al. 2007) at UKIRT, we also employ previously published data from other sources, most of it obtained with WFCAM. Table 6 presents the collected J , H , and K_s photometry used in this study. Column (1) gives the CatWISE name while columns (2),(3), and (4) give the J , H , and K_s photometry and associated uncertainties based on photon statistics, respectively. Column (5)

gives the source of the photometry, which needs some clarification. In order of $J/H/K_s$, numbers show the number of independent new observations obtained in this study to give the photometry listed for the object and represent a large majority of the entries. These targeted UKIRT/WFCAM observations employed exposure times customized for the object and were run through the usual WFCAM photometric pipeline (Dye et al. 2018). Otherwise, letters represent the source of the photometry. Specifically, U represents data from the on-going UHS survey data (Dye et al. 2018; Schneider et al. 2025). Most of the other data were also taken with the WFCAM instrument on UKIRT, the primary

exceptions being data from the 2MASS (Skrutskie et al. 2006) and VISTA (McMahon et al. 2013; Sutherland et al. 2015) surveys, which use very similar filter systems. A full explanation of column (5) symbols is given in the footnotes to Table 6. Thus, for the purposes of this work, all photometry in Table 6 is on the same photometric system.

For completeness sake, we also present in Appendix A additional J , H , and K_s photometry obtained using the USNO 1.55-m telescope and ASTROCAM in the CIT photometric system, based on the standards of Guetter et al. (2003), primarily for Series 1 objects, however, this photometry is not used in this study.

Table 6. New UKIRT and Adopted JHK_s Photometry.

Name (CatWISE)	J (mag) (1)	H (mag) (2)	K_s (mag) (3)	Source ($J/H/K_s$: No. Obs./other) (4)	(5)
J000013.51+255419.7	14.864 \pm 0.003	14.817 \pm 0.005	14.970 \pm 0.007	2/2/2	
J000849.71–173925.0	16.872 \pm 0.010	17.168 \pm 0.013	17.304 \pm 0.020	1/1/1	
J001502.52+295928.7	16.165 \pm 0.009	15.209 \pm 0.006	14.535 \pm 0.006	1/1/1	
J003030.38–145033.8	16.471 \pm 0.010	15.362 \pm 0.006	14.490 \pm 0.009	6/6/5	
J003259.67+141037.2	16.645 \pm 0.016	15.689 \pm 0.011	15.002 \pm 0.013	L/L/L	
J003452.12+052307.3	15.202 \pm 0.005	15.575 \pm 0.008	16.093 \pm 0.023	1/1/1	
J004121.65+354712.5	16.072 \pm 0.008	15.509 \pm 0.008	15.126 \pm 0.011	1/1/1	
J004521.80+163444.0	12.969 \pm 0.001	12.077 \pm 0.001	11.348 \pm 0.001	1/1/1	
J004928.58+044101.0	15.819 \pm 0.007	14.836 \pm 0.005	14.203 \pm 0.004	1/1/2	
J005911.15–011401.4	18.084 \pm 0.026	18.415 \pm 0.038	19.197 \pm 0.243	1/2/2	
J010332.40+193536.5	16.145 \pm 0.009	14.989 \pm 0.005	14.120 \pm 0.005	1/1/1	
J010753.11+004157.7	15.751 \pm 0.006	14.593 \pm 0.004	13.670 \pm 0.003	1/1/1	
J011912.41+240331.7	16.987 \pm 0.014	16.497 \pm 0.015	16.262 \pm 0.018	1/1/1	
J013836.61–032222.8	16.168 \pm 0.009	15.668 \pm 0.009	15.329 \pm 0.010	1/1/1	
J015011.41+382723.7	15.958 \pm 0.008	15.069 \pm 0.005	14.545 \pm 0.006	1/1/1	
J015142.59+124428.7	16.387 \pm 0.006	15.610 \pm 0.011	15.297 \pm 0.007	3/3/2	
J020625.45+264023.3	16.487 \pm 0.008	15.304 \pm 0.005	14.423 \pm 0.006	2/2/2	
J020743.00+000056.1	16.730 \pm 0.013	16.805 \pm 0.039	16.721 \pm 0.051	L/L/L	
J023618.06+004852.1	16.052 \pm 0.006	15.176 \pm 0.004	14.608 \pm 0.009	2/2/2	
J024313.38–245332.8	15.156 \pm 0.021	15.379 \pm 0.021	15.335 \pm 0.026	3/3/1	
J025116.11–035315.7	12.929 \pm 0.006	12.304 \pm 0.001	11.718 \pm 0.004	4/4/3	
J025409.54+022358.7	15.940 \pm 0.006	16.308 \pm 0.008	16.638 \pm 0.025	2/2/2	
J030533.66+395434.6	16.794 \pm 0.013	17.121 \pm 0.014	17.291 \pm 0.022	2/2/2	
J031100.13+164815.6	15.964 \pm 0.011	14.974 \pm 0.007	14.226 \pm 0.008	U/U/U	
J031326.13+780744.6	17.65 \pm 0.07	17.63 \pm 0.06	...	K/K/-	
J032553.05+042539.6	16.017 \pm 0.005	16.240 \pm 0.014	16.519 \pm 0.023	3/3/3	
J032842.66+230204.1	16.506 \pm 0.014	15.577 \pm 0.014	14.945 \pm 0.006	G/G/G	
J035523.53+113336.7	13.980 \pm 0.006	12.658 \pm 0.002	11.553 \pm 0.005	4/4/4	

Table 6 *continued*

Table 6 (*continued*)

Name (CatWISE)	<i>J</i> (mag)	<i>H</i> (mag)	<i>K_S</i> (mag)	Source (<i>J/H/K_S</i> : No. Obs./other)
(1)	(2)	(3)	(4)	(5)
J040709.03+151455.0	15.684 \pm 0.012	15.820 \pm 0.014	15.885 \pm 0.011	2/2/2
J041054.46+141130.8	17.084 \pm 0.008	17.391 \pm 0.011	17.461 \pm 0.021	3/3/3
J041522.17-093457.1	15.341 \pm 0.005	15.725 \pm 0.010	15.931 \pm 0.017	1/1/1
J042348.22-041402.0	14.306 \pm 0.046	13.551 \pm 0.018	13.011 \pm 0.017	2/2/2
J043900.87-235310.7	14.588 \pm 0.003	13.664 \pm 0.002	13.015 \pm 0.002	1/1/1
J044853.70-193543.6	16.628 \pm 0.011	16.965 \pm 0.017	17.661 \pm 0.033	1/1/1
J050021.02+033044.8	13.665 \pm 0.014	12.789 \pm 0.001	12.131 \pm 0.001	2/1/1
J051317.27+060812.3	15.887 \pm 0.005	16.237 \pm 0.018	16.213 \pm 0.028	2/2/2
J051609.20-044553.3	15.545 \pm 0.008	15.773 \pm 0.011	15.787 \pm 0.020	G/G/G
J052536.18+673951.5	17.49 \pm 0.04	17.87 \pm 0.05	18.357 \pm 0.077	K/K/B
J053312.61+824617.2	15.179 \pm 0.059	14.904 \pm 0.092	14.918 \pm 0.146	M/M/M
J053952.16-005856.5	13.926 \pm 0.002	13.119 \pm 0.001	12.560 \pm 0.001	1/1/1
J054231.20-162827.6	16.329 \pm 0.009	16.669 \pm 0.017	17.018 \pm 0.019	1/1/1
J055919.85-140454.8	13.653 \pm 0.002	13.706 \pm 0.002	13.783 \pm 0.003	1/1/1
J060206.71+404355.4	15.312 \pm 0.006	15.403 \pm 0.021	15.539 \pm 0.007	1/1/1
J060738.42+242951.2	14.076 \pm 0.002	13.117 \pm 0.001	12.454 \pm 0.001	1/1/1
J061407.41+391233.2	16.418 \pm 0.009	16.771 \pm 0.019	17.402 \pm 0.018	3/3/2
J062542.19+564625.4	16.766 \pm 0.008	17.042 \pm 0.014	17.103 \pm 0.020	3/3/3
J062720.06-111429.6	15.271 \pm 0.003	15.551 \pm 0.021	15.619 \pm 0.008	2/2/2
J064626.92+793454.5	16.261 \pm 0.093	15.080 \pm 0.074	14.602 \pm 0.090	M/M/M
J065609.75+420532.8	15.280 \pm 0.003	14.879 \pm 0.010	14.892 \pm 0.017	2/2/2
J070036.80+315718.2	12.931 \pm 0.086	12.062 \pm 0.074	11.405 \pm 0.082	2/2/2
J072226.89-054027.5	16.570 \pm 0.007	16.872 \pm 0.011	16.919 \pm 0.020	2/2/2
J072719.22+170950.1	15.210 \pm 0.006	15.632 \pm 0.014	15.628 \pm 0.023	U/U/U
J074200.88+205515.7	15.806 \pm 0.006	16.011 \pm 0.008	16.188 \pm 0.009	3/3/3
J075547.93+221212.8	15.479 \pm 0.004	15.777 \pm 0.012	15.891 \pm 0.023	L/L/L
J075840.07+324718.8	14.863 \pm 0.085	14.270 \pm 0.070	13.946 \pm 0.072	2/2/2
J081957.98-033529.3	14.810 \pm 0.003	14.614 \pm 0.003	14.763 \pm 0.005	1/1/1
J082131.64+144317.8	16.428 \pm 0.009	16.661 \pm 0.011	16.790 \pm 0.016	1/1/1
J082518.97+211546.1	15.014 \pm 0.005	13.81 \pm 0.03	12.982 \pm 0.003	U/T/U
J083006.91+482838.3	15.315 \pm 0.005	14.412 \pm 0.003	13.745 \pm 0.003	1/1/1
J083541.88-081918.0	13.075 \pm 0.001	12.021 \pm 0.001	11.203 \pm 0.001	1/1/1
J083717.18-000020.8	16.949 \pm 0.015	16.290 \pm 0.018	15.925 \pm 0.024	L/L/L
J085035.75+105715.3	16.355 \pm 0.014	15.361 \pm 0.010	14.466 \pm 0.010	U/U/U
J085757.60+570844.6	15.111 \pm 0.003	14.038 \pm 0.002	13.231 \pm 0.002	1/1/1
J085833.72+325628.6	16.515 \pm 0.112	15.606 \pm 0.083	14.898 \pm 0.070	2/2/2
J090023.73+253934.1	16.281 \pm 0.006	15.527 \pm 0.005	14.951 \pm 0.006	2/2/2
J090900.31+652525.8	15.81 \pm 0.03	15.32 \pm 0.03	15.19 \pm 0.03	C/C/C
J091534.04+042204.8	14.532 \pm 0.003	13.643 \pm 0.002	12.911 \pm 0.002	1/1/1
J092615.40+584717.6	15.512 \pm 0.004	15.500 \pm 0.005	15.592 \pm 0.008	2/2/2
J092933.34+342951.3	16.750 \pm 0.012	15.680 \pm 0.007	14.844 \pm 0.008	1/1/1
J093735.98+293120.8	14.304 \pm 0.004	14.710 \pm 0.006	15.415 \pm 0.016	U/U/U

Table 6 *continued*

Table 6 (*continued*)

Name (CatWISE)	<i>J</i> (mag)	<i>H</i> (mag)	<i>K_S</i> (mag)	Source (<i>J/H/K_S</i> : No. Obs./other)
(1)	(2)	(3)	(4)	(5)
J093936.13–244844.3	15.685 ± 0.004	16.104 ± 0.009	17.058 ± 0.030	3/3/1
J094908.49–154548.3	15.970 ± 0.101	15.366 ± 0.095	15.368 ± 0.082	2/2/2
J095105.35+355800.1	17.056 ± 0.026	15.982 ± 0.024	15.073 ± 0.014	U/U/U
J101014.45–040650.0	15.416 ± 0.005	14.436 ± 0.004	13.694 ± 0.002	4/4/4
J101905.55+652954.5	16.341 ± 0.055	16.584 ± 0.115	16.502 ± 0.180	B/B/B
J102109.51–030421.1	15.966 ± 0.011	15.664 ± 0.015	15.388 ± 0.020	L/L/L
J103931.32+325623.7	16.153 ± 0.008	15.477 ± 0.006	15.087 ± 0.009	1/1/1
J104307.42+222523.3	15.867 ± 0.006	14.806 ± 0.010	14.030 ± 0.005	6/6/6
J104335.10+121310.8	15.891 ± 0.009	14.907 ± 0.006	14.261 ± 0.006	1/1/1
J104751.75+212414.7	15.444 ± 0.004	15.842 ± 0.013	16.256 ± 0.018	2/2/2
J104828.96+091940.9	16.449 ± 0.010	15.958 ± 0.008	15.850 ± 0.014	2/2/2
J110611.58+275414.1	14.593 ± 0.004	14.107 ± 0.003	13.846 ± 0.004	1/1/1
J111009.77+011608.7	16.161 ± 0.008	16.197 ± 0.021	16.051 ± 0.032	L/L/L
J111447.51–261830.0	15.952 ± 0.006	16.262 ± 0.011	16.949 ± 0.023	1/1/1
J111812.22–085615.0	15.557 ± 0.006	14.841 ± 0.005	14.314 ± 0.006	1/1/1
J112254.33+255020.2	16.346 ± 0.021	16.704 ± 0.017	16.855 ± 0.022	2/1/1
J115553.43+055956.6	15.727 ± 0.007	14.817 ± 0.004	14.142 ± 0.005	1/1/1
J115821.40+043446.3	15.459 ± 0.007	14.875 ± 0.005	14.493 ± 0.006	1/1/1
J120746.66+024426.8	15.428 ± 0.006	14.711 ± 0.005	14.239 ± 0.006	1/1/1
J121709.86–031111.8	15.575 ± 0.020	16.043 ± 0.033	15.963 ± 0.014	3/3/3
J121757.13+162635.1	17.741 ± 0.017	18.131 ± 0.025	19.025 ± 0.094	1/1/2
J122554.84–273958.5	14.88 ± 0.03	15.17 ± 0.03	15.28 ± 0.03	T/T/T
J123146.34+084717.1	15.165 ± 0.006	15.391 ± 0.008	15.542 ± 0.016	1/1/1
J123737.03+652607.2	15.56 ± 0.10	15.94 ± 0.10	16.40 ± 0.10	D/D/D
J125011.59+392542.6	16.089 ± 0.011	16.043 ± 0.013	16.114 ± 0.018	1/1/1
J125453.41–012245.6	14.667 ± 0.003	14.136 ± 0.003	13.886 ± 0.005	L/L/L
J131141.74+362925.2	15.414 ± 0.016	14.664 ± 0.003	14.152 ± 0.018	2/2/2
J132003.78+603425.8	16.228 ± 0.092	16.738 ± 0.149	16.475 ± 0.213	B/B/B
J132233.51–234015.3	16.857 ± 0.020	17.229 ± 0.024	17.833 ± 0.057	1/1/1
J132407.64+190625.5	15.633 ± 0.009	15.450 ± 0.009	15.615 ± 0.016	1/1/1
J132434.67+635827.1	15.435 ± 0.067	14.677 ± 0.060	14.082 ± 0.060	B/B/B
J132605.25+120010.1	17.501 ± 0.020	17.659 ± 0.019	17.758 ± 0.035	1/1/1
J132629.56–003833.2	16.199 ± 0.010	15.111 ± 0.007	14.171 ± 0.006	L/L/L
J133553.35+113003.7	17.932 ± 0.029	18.281 ± 0.039	18.333 ± 0.041	1/1/2
J134645.89–003152.2	15.655 ± 0.006	15.973 ± 0.011	15.961 ± 0.021	L/L/L
J134807.08+660327.2	16.870 ± 0.191	16.007 ± 0.152	15.252 ± 0.152	B/B/B
J140255.70+080053.4	16.832 ± 0.014	16.204 ± 0.021	15.706 ± 0.020	L/L/L
J140753.30+124110.7	15.352 ± 0.005	14.375 ± 0.003	13.669 ± 0.004	1/1/1
J143517.22–004612.9	16.362 ± 0.014	15.787 ± 0.016	15.336 ± 0.018	L/L/L
J143535.75–004348.6	16.449 ± 0.014	15.687 ± 0.014	15.133 ± 0.015	L/L/L
J143945.64+304218.7	16.983 ± 0.007	16.551 ± 0.013	16.417 ± 0.011	2/2/1
J144600.78+002450.9	15.580 ± 0.007	14.657 ± 0.005	13.921 ± 0.005	L/L/L
J145714.66+581509.7	16.786 ± 0.011	17.245 ± 0.052	17.425 ± 0.026	2/2/1

Table 6 *continued*

Table 6 (*continued*)

Name (CatWISE)	<i>J</i> (mag)	<i>H</i> (mag)	<i>K_S</i> (mag)	Source (<i>J/H/K_S</i> : No. Obs./other)
(1)	(2)	(3)	(4)	(5)
J150319.71+252528.3	13.621 \pm 0.002	13.90 \pm 0.03	14.072 \pm 0.007	U/P/U
J150648.79+702741.0	13.54 \pm 0.01	13.91 \pm 0.04	13.826 \pm 0.068	K/K/M
J150653.09+132105.8	13.220 \pm 0.001	12.408 \pm 0.001	11.758 \pm 0.001	1/1/1
J151114.38+060739.4	15.908 \pm 0.006	15.178 \pm 0.005	14.513 \pm 0.005	1/1/1
J151459.41+484803.4	14.000 \pm 0.002	13.134 \pm 0.001	12.564 \pm 0.001	1/1/1
J152040.10+354615.7	15.520 \pm 0.005	14.622 \pm 0.003	14.116 \pm 0.004	1/1/1
J152322.78+301453.4	16.080 \pm 0.011	15.090 \pm 0.009	14.350 \pm 0.009	U/U/U
J152613.76+204334.8	15.399 \pm 0.004	14.553 \pm 0.003	13.924 \pm 0.003	1/1/1
J154614.94+493158.6	15.688 \pm 0.006	15.290 \pm 0.004	15.251 \pm 0.011	2/2/2
J155301.80+153239.5	15.410 \pm 0.007	15.830 \pm 0.012	15.936 \pm 0.032	U/U/U
J161705.76+180713.9	17.617 \pm 0.012	17.900 \pm 0.021	17.954 \pm 0.036	2/1/1
J162413.95+002915.6	15.186 \pm 0.006	15.532 \pm 0.015	15.699 \pm 0.022	U/U/U
J162541.25+152810.0	16.722 \pm 0.014	16.961 \pm 0.019	17.163 \pm 0.030	1/1/1
J162618.23+392523.4	14.395 \pm 0.002	14.463 \pm 0.010	14.468 \pm 0.012	2/2/2
J162725.60+325522.8	16.253 \pm 0.010	16.601 \pm 0.014	17.049 \pm 0.022	1/1/1
J162918.64+033534.8	15.072 \pm 0.023	14.494 \pm 0.027	14.214 \pm 0.038	2/2/2
J163229.48+190439.6	15.854 \pm 0.008	14.828 \pm 0.008	13.97 \pm 0.05	2/2/T
J164715.47+563209.4	16.478 \pm 0.010	15.409 \pm 0.008	14.548 \pm 0.006	1/1/1
J165311.00+444421.2	17.046 \pm 0.008	17.458 \pm 0.015	17.741 \pm 0.032	2/2/1
J171145.73+223204.2	16.679 \pm 0.019	16.00 \pm 0.03	15.25 \pm 0.03	U/C/C
J172811.54+394859.0	15.777 \pm 0.009	14.730 \pm 0.006	13.886 \pm 0.006	U/U/U
J174124.05+255312.0	16.113 \pm 0.008	16.503 \pm 0.010	16.691 \pm 0.014	1/1/1
J175023.78+422238.6	16.187 \pm 0.008	15.599 \pm 0.007	15.342 \pm 0.009	1/1/1
J175033.14+175905.4	16.173 \pm 0.011	15.944 \pm 0.015	15.978 \pm 0.034	U/U/U
J175609.98+281516.4	14.600 \pm 0.004	14.180 \pm 0.005	13.767 \pm 0.006	U/U/U
J175805.45+463318.2	15.913 \pm 0.007	16.248 \pm 0.014	16.160 \pm 0.017	1/1/1
J180026.66+013450.9	14.191 \pm 0.002	13.180 \pm 0.001	12.418 \pm 0.001	1/1/1
J181210.89+272142.8	18.169 \pm 0.041	18.567 \pm 0.073	18.578 \pm 0.144	1/1/2
J182128.39+141357.2	13.311 \pm 0.008	12.402 \pm 0.006	11.637 \pm 0.003	2/2/2
J183058.60+454258.2	17.208 \pm 0.013	16.270 \pm 0.011	15.605 \pm 0.011	1/1/1
J184108.67+311728.6	15.952 \pm 0.010	15.088 \pm 0.009	14.312 \pm 0.009	U/U/U
J185215.87+353714.9	16.369 \pm 0.006	16.761 \pm 0.013	16.689 \pm 0.011	2/2/2
J190106.23+471820.5	15.526 \pm 0.007	15.664 \pm 0.050	15.924 \pm 0.033	U/S/U
J190624.72+450805.2	16.026 \pm 0.006	16.336 \pm 0.008	16.647 \pm 0.015	1/1/1
J190648.66+401105.9	12.986 \pm 0.001	12.308 \pm 0.001	11.792 \pm 0.001	1/1/1
J195246.34+723957.9	15.086 \pm 0.045	14.728 \pm 0.077	14.650 \pm 0.078	K/K/K
J200250.59-052154.2	15.272 \pm 0.006	14.274 \pm 0.004	13.466 \pm 0.003	1/1/1
J204749.62-071821.6	16.836 \pm 0.020	15.900 \pm 0.013	15.370 \pm 0.014	1/1/1
J210115.58+175656.0	16.867 \pm 0.021	15.781 \pm 0.017	14.897 \pm 0.013	U/U/U
J212414.06+010003.8	15.880 \pm 0.009	16.013 \pm 0.014	16.160 \pm 0.028	1/1/1
J212702.63+761756.8	14.336 \pm 0.032	13.586 \pm 0.038	13.160 \pm 0.039	M/M/M
J213927.29+022024.7	14.858 \pm 0.005	14.192 \pm 0.004	13.662 \pm 0.004	1/1/1

Table 6 *continued*

Table 6 (*continued*)

Name (CatWISE)	<i>J</i> (mag) (1)	<i>H</i> (mag) (2)	<i>K_S</i> (mag) (3)	Source (<i>J/H/K_S</i> : No. Obs./other) (4)	(5)
J215432.82+594211.3	15.421 \pm 0.010	15.675 \pm 0.008	15.761 \pm 0.016	2/2/1	
J221354.65+091139.0	16.844 \pm 0.015	17.126 \pm 0.021	17.326 \pm 0.029	1/1/1	
J222444.39–015908.2	13.982 \pm 0.002	12.884 \pm 0.001	12.066 \pm 0.005	2/2/2	
J222622.96+044001.1	16.962 \pm 0.015	17.324 \pm 0.025	17.467 \pm 0.035	1/1/1	
J223937.67+161716.8	15.985 \pm 0.009	15.536 \pm 0.009	15.380 \pm 0.013	1/1/1	
J224253.65+254256.2	14.719 \pm 0.004	13.767 \pm 0.002	13.044 \pm 0.002	1/1/1	
J224431.96+204339.1	16.401 \pm 0.016	15.051 \pm 0.008	13.827 \pm 0.006	U/U/U	
J225418.98+312353.0	15.000 \pm 0.005	14.925 \pm 0.007	15.051 \pm 0.013	U/U/U	
J225529.03–003436.4	15.504 \pm 0.004	14.836 \pm 0.006	14.312 \pm 0.006	V/L/L	
J232123.84+135450.3	16.704 \pm 0.015	17.109 \pm 0.021	17.073 \pm 0.026	1/1/1	
J232545.24+425143.9	15.446 \pm 0.005	14.457 \pm 0.004	13.767 \pm 0.004	1/1/1	
J232728.85–273056.4	16.470 \pm 0.010	15.502 \pm 0.007	14.881 \pm 0.007	1/1/1	
J233051.30–084455.9	17.304 \pm 0.015	16.274 \pm 0.010	15.553 \pm 0.009	1/1/1	
J233910.67+135212.9	15.882 \pm 0.007	16.028 \pm 0.012	16.171 \pm 0.013	1/1/1	
J234026.68–074509.6	16.046 \pm 0.007	16.447 \pm 0.011	16.695 \pm 0.019	1/1/1	
J234841.34–102843.2	16.597 \pm 0.023	17.065 \pm 0.014	17.085 \pm 0.017	2/2/1	
J235122.32+301054.1	15.791 \pm 0.007	14.754 \pm 0.004	14.009 \pm 0.004	1/1/1	
J235654.19–155322.9	15.529 \pm 0.013	15.731 \pm 0.007	15.770 \pm 0.012	3/3/2	

NOTE—

#/#/#: This paper. Number of observations. See text.
 L: UKIDSS Large Area Survey
 G: UKIDSS Galactic Clusters Survey
 M: 2 Micron All Sky Survey (2MASS)
 V: VISTA Hemisphere Survey
 U: UKIRT Hemisphere Survey
 S: UltracoolSheet – “Unpublished work/analysis done specifically for the UltracoolSheet version 2.0 release in 2024”
 K: Kirkpatrick et al. (2011)
 B: Best et al. (2021)
 T: Leggett et al. (2002)
 C: Chiu et al. (2006)
 P: Knapp et al. (2004)
 A: Liu et al. (2016)
 D: Leggett et al. (2010)
 R: Strauss et al. (1999)

12. COLORS AND ABSOLUTE MAGNITUDES

In Figure 9 we show the absolute magnitudes in *J*- and *K*-bands as a function of spectral type for all objects in this study. The absolute magnitudes are based on the astrometry from Table 3 and infrared photometry given in Table 6. Near-infrared spectral types from Table 1 are used for both panels except in cases where no near-infrared spectral type exists, then optical types are used. In Figure 10 we show the absolute *J*-band magnitudes of this sample as a function of their *J* – *K* colors with spectral types encoded by color, again using the data in Tables 1, 3, 6 as described above. For both Figures all photometric error bars are shown, while spectral types

are assumed to be known to one spectral subclass or better and are not specifically shown.

Rather than presenting numerous color-absolute magnitude and color-color diagrams, we have opted to use the three basic diagrams shown in Figures 9 and 10 which are sufficient to demonstrate the points we make about various brown dwarf populations in the next Section. These diagrams will be re-visited, in turn, as we discuss each of the populations of interest.

13. NOTES ON VARIOUS POPULATIONS

In this section we discuss objects in this study which are or may be members of populations of special interest. These include binaries, wide companions, young objects, subdwarfs, and spectral standards. While we give some background for each object considered and

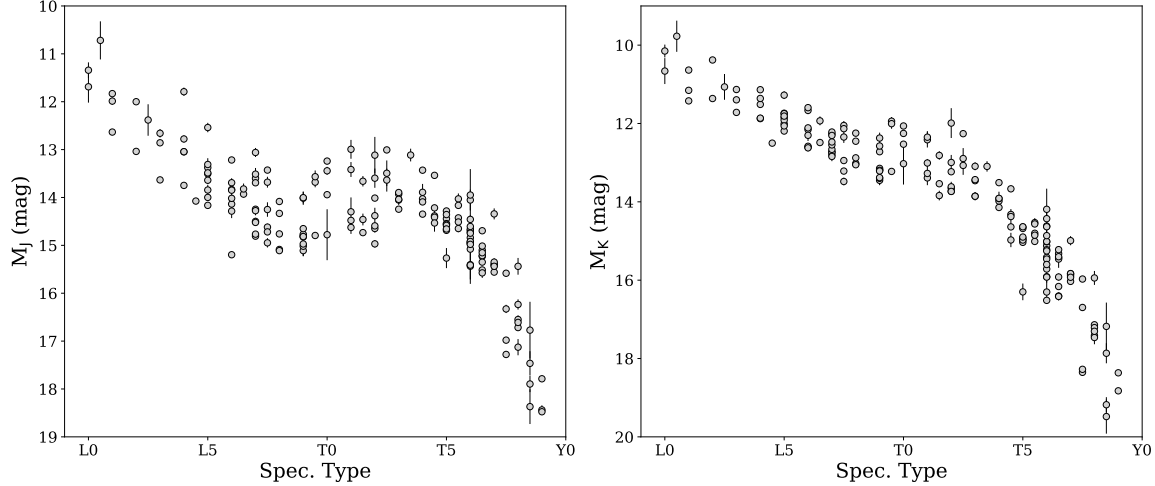


Figure 9. Absolute J -band (left) and absolute K -band (right) magnitudes as a function of spectral type for the sample presented in this work. Near-infrared spectral types from Table 1 are used for both panels except in cases where no near-infrared spectral type exists, then optical types are used.

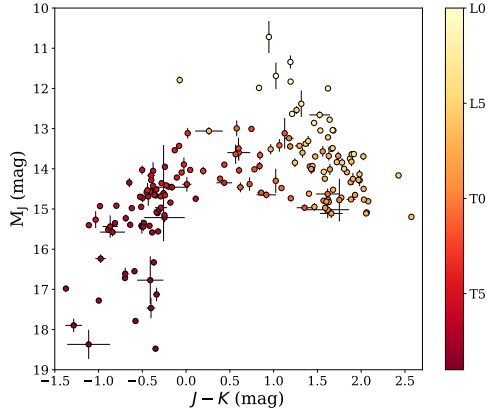


Figure 10. Absolute J -band magnitude as a function of $J - K$ color for the sample presented in this work. Near-infrared spectral types from Table 1 are used for both panels except in cases where no near-infrared spectral type exists, then optical types are used. Symbols are colored by spectral type.

point out where our new results may help in resolving some issues, these are brief comments and we acknowledge that we have not included all useful references to previous relevant work.

13.1. Binaries

We first review objects in this study that are binaries or suspected binaries. This includes resolved binaries, spectral binaries, and objects which might be binary due to their positions in spectral type vs. absolute magnitude diagrams.

13.1.1. Resolved Binaries

We note that for the objects in this subsection, although resolved with larger aperture ground-based telescopes or HST, separations are typically a small fraction of an arcsecond, well within the $\sim 1.1''$ FWHM of a typical frame taken with ASTROCAM on the 1.55-m telescope at NOFS. Thus, while these binaries likely had some affect on the final astrometric quality, we find no systematic effects.

J031100.13+164815.6: Early spectral typing of this object classified it as an L8 at both optical (Kirkpatrick et al. 2000) and near-infrared (Reid et al. 2001) wavelengths. It was later typed as L9 using optical and near-infrared spectra by Geballe et al. (2002), while Schneider et al. (2014) adopted a near-infrared spectral type of L9.5, and Manjavacas et al. (2019) determined a near-infrared type of T2. It was resolved as an approximately equal brightness binary with a separation of 204.3 ± 0.4 mas in Stumpf et al. (2010), who also estimated a distance of 25 ± 4 pc for the pair. A π_{abs} of 36.9 ± 3.4 mas was presented in Smart et al. (2013) which is consistent with our result of π_{abs} of 35.89 ± 1.73 mas.

J042348.22-041402.0: Cruz et al. (2003) noted a discrepancy between optical and near-infrared spectral types for this object (also discussed in Burgasser et al. 2003e). Vrba et al. (2004) and Knapp et al. (2004) also noted the discrepant optical/infrared types and suggest binarity or youth could be an explanation. Burgasser et al. (2005b) is devoted to this object, where HST data were used to resolve this as an L6+T2 binary with a separation of $0''.16$. Burgasser et al. (2010) used spectral decomposition to find types $L7.5 \pm 0.3$ and $T2.0 \pm 0.2$. Dupuy & Liu (2012) derived spectral component types of $L6.5 \pm 1$ and $T2 \pm 0.5$. Dupuy & Liu (2017) monitored

this binary with *HST* and found a period of 12.30 ± 0.06 years and a total mass of $83 \pm 3 M_{\text{Jup}}$.

J070036.80+315718.2: This object was found to be a binary by [Reid et al. \(2006\)](#) using *HST* images, who estimate a spectral type of L6 for the secondary and a separation of $\sim 0''.2$. [Dupuy & Liu \(2012\)](#) used spectral decomposition to estimate types of $\text{L3} \pm 1$ and $\text{L6.5} \pm 1.5$. [Dupuy & Liu \(2017\)](#) measured a full orbit for the pair (23.9 ± 0.5 years) and suggested that the secondary (2M0700+3157B) is itself an unresolved binary, because they find that it is more massive than the L3 primary.

J085035.75+105715.3: [Reid et al. \(2001\)](#) resolved this object as a $0''.16$ binary in *HST* imaging and suggested the fainter companion is a very late L or early T dwarf. [Konopacky et al. \(2010\)](#) found an orbital period of 24^{+69}_{-6} years. [Faherty et al. \(2011\)](#) found this to be a hierarchical system containing a young ($\lesssim 1.5$ Gyr) M5+M6 primary (NLTT 20346). [Burgasser et al. \(2011a\)](#) determined L6+L7 component types but suggested that this may be a triple system. [Dupuy & Liu \(2012\)](#) determined component types of $\text{L6.5} \pm 1$ and $\text{L8.5} \pm 1$. However, [Dupuy & Liu \(2012\)](#) suggested that companionship with the M+M pair NLTT 20346 is a chance alignment, based on their updated astrometry, and find that there is no need to invoke additional multiplicity to either of the L components. Based on Gaia results for NLTT 20346AB and the astrometry from this work (which is consistent with [Dupuy & Liu \(2012, 2017\)](#)), this is likely a chance alignment. [Dupuy & Liu \(2017\)](#) give an orbital period of 48^{+7}_{-6} years (though state that the solution is poorly constrained), while also measuring a low total mass for the system, suggesting that it may be young.

J091534.04+042204.8: This object was discovered by [Reid et al. \(2006\)](#) as 2MASS J09153413+0422045, who resolved this as a $0''.73$ separation candidate binary from *HST* images. With flux ratios close to equal they gave optical spectral types of L7 to both components. [Reid et al. \(2006\)](#) also state that this object was independently identified as a binary by M. Liu (private communication). Several authors have provided updated spectral typing with similar results: [Reid et al. \(2008\)](#) gave component types of L6: and L6:, [Liu et al. \(2010\)](#) gave component types of $\text{L6} \pm 1$ and $\text{L7}^{+3}_{-1.5}$, and [Bardalez Gagliuffi et al. \(2019\)](#) gave component types of L6 and L6.

J092615.40+584717.6: [Burgasser et al. \(2006b\)](#) found that this source was slightly elongated in *HST* images ($a = 0''.07$) and suggested component spectral types of T4+T4 based on their approximately equal brightness. Several authors have provided updated spectral typing giving similar results: [Liu et al. \(2010\)](#) gave component types of $\text{T4.5} \pm 0.5$ and $\text{T3}^{+2.5}_{-4.0}$, [Geißler et al. \(2011\)](#) esti-

mate component types of T3–T4+T6 based on spectral template fitting, [Dupuy & Liu \(2012\)](#) find component types of $\text{T3.5} \pm 1$ and $\text{T5} \pm 1$, and [Bardalez Gagliuffi et al. \(2015\)](#) found component types of $\text{T4} \pm 0.1$ and $\text{T5.3} \pm 0.7$. A poorly constrained orbit was given in [Dupuy & Liu \(2017\)](#), who found a period of $12.9^{+1.3}_{-1.9}$ years.

J102109.51–030421.1: This object was identified by [Burgasser et al. \(2006b\)](#) as a binary from *HST* images with component types of T1 and T5 based on spectral decomposition and a separation of $0''.17$ (one of the first flux-reversal binaries, maybe the first). [Burgasser et al. \(2010\)](#) found component types of $\text{T1.0} \pm 0.4$ and $\text{T5.5} \pm 0.7$, while [Dupuy & Liu \(2012\)](#) found component types of $\text{T0} \pm 1$ and $\text{T5} \pm 0.5$ and suggested, based on color-magnitude diagram positions, that the A component of this system may in fact be an unresolved binary. [Dupuy & Liu \(2017\)](#) provided a poorly constrained orbit with a period of 86^{+13}_{-17} years.

J121757.13+162635.1: [Liu et al. \(2012\)](#) resolved this object as an $\sim 0''.76$ binary and estimated component spectral types of $\text{T9} \pm 0.5$ and $\text{Y0} \pm 0.5$. [Leggett et al. \(2014\)](#) presented resolved spectroscopy of each component and found spectral types of T8.5 and Y0–Y0.5. [Zhang et al. \(2019\)](#) suggested an sdT9 spectral type for the primary.

J122554.84–273958.5: This object was resolved by [Burgasser et al. \(2003c\)](#) as a $0''.28$ binary with spectral component types of T6 and T8. [Dupuy & Liu \(2012\)](#) determined similar spectral component types of $\text{T5.5} \pm 0.5$ and $\text{T8} \pm 0.5$.

J151114.38+060739.4: [Burgasser et al. \(2010\)](#) found this object to be a strong spectral binary candidate with component types of $\text{L5.5} \pm 0.8$ and $\text{T5} \pm 0.4$. It was resolved in Keck/NIRC2 images by [Bardalez Gagliuffi et al. \(2015\)](#) with a separation of 108 ± 11 mas, who determined similar spectral component types of $\text{L5} \pm 1$ and $\text{T5} \pm 0.5$.

J155301.80+153239.5: The first published mention of this object being a binary came from [Knapp et al. \(2004\)](#) who listed it as 2MASS J1553+1532AB, citing A. Burgasser (private communication). [Burgasser et al. \(2006a\)](#) suggested this object as an alternate T7 standard, although mentioning it as an approximately equal magnitude binary citing Burgasser in prep. [Burgasser et al. \(2006b\)](#) resolved this object as a $0''.35$ binary in both *HST* and Keck/NIRC images, estimating component spectral types of T6.5 and T7. [Dupuy & Liu \(2012\)](#) found similar component types of $\text{T6.5} \pm 0.5$ and $\text{T7.5} \pm 0.5$. See also §13.3 for evidence that this object may be young, as a member of the Carina-Near Moving Group.

J172811.54+394859.0: This object was resolved as a binary in *HST* images by [Gizis et al. \(2003\)](#) and [Bouy et al. \(2003\)](#) with a separation of ~ 130 mas. Orbital parameters were determined by [Konopacky et al. \(2010\)](#), who found an orbital period of 31.3 ± 12.7 yrs. [Burgasser et al. \(2011a\)](#) presented a detailed investigation of *HST* data and found component spectral types of L5 and L6.5, with the primary component having thick condensate clouds to account for its colors and low luminosity on CMDs. [Dupuy & Liu \(2012\)](#) found component types of $L5 \pm 1$ and $L7 \pm 1$ and also noted that the primary is unusually red. [Dupuy & Liu \(2017\)](#) calculated orbital parameters including a period of $40.8^{+1.6}_{-1.2}$ years.

J210115.58+175656.0: This object was found to be a binary in *HST* images by [Bouy et al. \(2003\)](#) and [Gizis et al. \(2003\)](#) with a separation of ~ 235 mas, with [Gizis et al. \(2003\)](#) estimating the secondary having a spectral type of L8 or later. [Liu et al. \(2010\)](#) estimated component spectral types of $L7.5 \pm 0.5$ and $T1^{+2}_{-2.5}$, while [Dupuy & Liu \(2012\)](#) found component spectral types of $L7 \pm 1$ and $L8 \pm 1$.

The absolute magnitudes of these resolved binaries compared to the rest of the sample in this work are shown on Figures 11 and 12.

13.1.2. Spectral Binaries

In this section we give brief summaries of previous work on spectrally-detected binaries, along with our own estimations of binary likelihood based on template-fitting.

J003259.67+141037.2: This object was classified as L9 by [Schneider et al. \(2014\)](#) based on near-infrared spectra. It was suggested as a visual spectroscopic binary by [Bardalez Gagliuffi et al. \(2015\)](#) with component types $L6.2 \pm 0.7$ and $T2.4 \pm 1.9$.

J011912.41+240331.7: [Chiu et al. \(2006\)](#) classified this object as a T2 based on near-infrared spectra. It was suggested as an unresolved binary with spectral types $T0 \pm 0.7$ and $T4 \pm 0.4$ by [Burgasser et al. \(2010\)](#). We note that this object, with an absolute *J*-band magnitude of ~ 14.4 and an absolute *K*-band magnitude of ~ 13.7 , does not appear overluminous in either of the panels of Figure 11.

J023618.06+004852.1: This object was classified as an L9 from visual spectra by [Scholz et al. \(2009\)](#) and as an L6.5 from near-infrared spectra by [Geballe et al. \(2002\)](#). It was selected as a strong spectral binary candidate by [Bardalez Gagliuffi et al. \(2014\)](#), with individual components of $L5.0 \pm 0.6$ and $T1.9 \pm 1.1$.

J075840.07+324718.8: [Pineda et al. \(2016\)](#) classified this object as a T3 based on visual spectra while [Knapp et al. \(2004\)](#) classified it as a T2 based on near-infrared

spectra. It was identified as a weak near-infrared spectroscopic binary candidate in [Burgasser et al. \(2010\)](#) with individual components of L7.5 and T4. [Bardalez Gagliuffi et al. \(2015\)](#) selected it as a visual spectral binary with components of T2.3 and T2.2.

J090900.31+652525.8: This object was classified as a T1.5 based on near-infrared spectra by [Chiu et al. \(2006\)](#). It was labeled as a weak spectroscopic binary candidate based on near-infrared spectra by [Burgasser et al. \(2010\)](#), with component types of T1.5 and T2.5. We note that this object, with an absolute *J*-band magnitude of ~ 14.5 and an absolute *K*-band magnitude of ~ 13.8 , does not appear overluminous in either of the panels of Figure 11.

J094908.49-154548.3: This object was discovered as 2MASS J09490860-1545485 in [Tinney et al. \(2005\)](#), who found a near-infrared type of T1. It was found to be a weak spectroscopic binary candidate in [Burgasser et al. \(2010\)](#), who found component types of T2 and $T1.5 \pm 1$.

J103931.32+325623.7: This object was classified as a T1 based on near-infrared spectra by [Chiu et al. \(2006\)](#). It was identified as a strong binary candidate based on near-infrared spectra by [Burgasser et al. \(2010\)](#), with component types of $L7 \pm 0.2$ and $T4 \pm 0.2$.

J110611.58+275414.1: [Looper et al. \(2007\)](#) discovered this object and classified it as a T2.5 based on near-infrared spectra. It is a strong binary candidate based on near-infrared spectra by [Burgasser et al. \(2010\)](#), who found component types of $T0 \pm 0.2$ and $T4.5 \pm 0.2$.

J120746.66+024426.8: Discovered as SDSS J120747.17+024424.8 in [Hawley et al. \(2002\)](#) with an optical spectral type of L8. Suggested as a weak binary candidate in [Burgasser et al. \(2010\)](#) with component types of $L6.5 \pm 0.7$ and $T2.5 \pm 0.5$.

J131141.74+362925.2: This object was found by [Kirkpatrick et al. \(2011\)](#) to have a near-infrared spectral type of L5 pec (blue) and who suggested its peculiar spectroscopic features may be indicative of unresolved binarity, with component types of $L3.5 \pm 0.7$ and $T2 \pm 0.5$. [Bardalez Gagliuffi et al. \(2014\)](#) also identified it as a probable binary based on near-infrared spectra, with component types of $L4.8 \pm 0.6$ and $T4.1 \pm 2.7$.

J140255.70+080053.4: [Kellogg et al. \(2015\)](#) found this object to have a near infrared type of T2 pec, but also suggested it is a binary with L8+T5 components.

J143945.64+304218.7: [Chiu et al. \(2006\)](#) classified this object as a T2.5 from near-infrared spectra. It was deemed a strong binary candidate based on near-infrared spectra by [Burgasser et al. \(2010\)](#) with component types of $T1 \pm 0.2$ and $T5 \pm 0.6$.

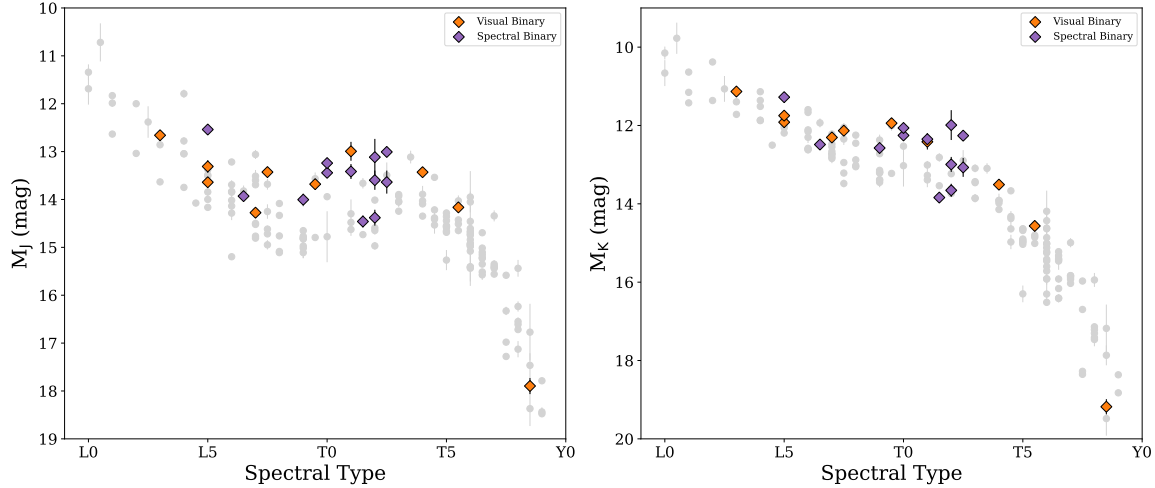


Figure 11. Same as 9 but with the positions of visual and spectral binaries highlighted.

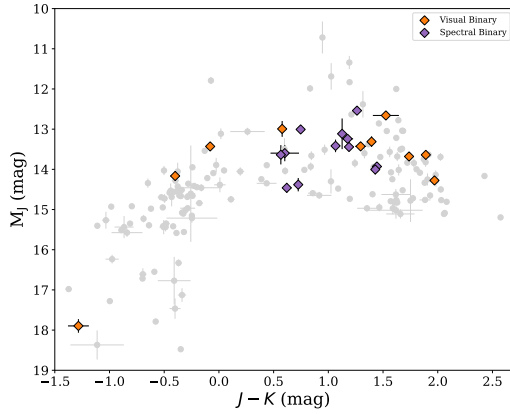


Figure 12. Same as 10 but with the positions of visual and spectral binaries highlighted.

J171145.73+223204.2: This object was discovered by Burgasser et al. (2010) who gave it a near-infrared type of L9, but suggested it to be a strong binary candidate with component types of $L5 \pm 0.4$ and $T5.5 \pm 1.2$. Bardalez Gagliuffi et al. (2014) found component types of $L1.5 \pm 0.6$ and $T2.5 \pm 1.0$ based on near-infrared spectra. Bardalez Gagliuffi et al. (2015) later suggested component types of $L5.5 \pm 0.5$ and $T5.3 \pm 1.0$ and showed that this system is not resolved in Keck/NIRC2 images. Manjavacas et al. (2019) found component types of L6 and T3 based on *HST* imaging.

J183058.60+454258.2: This object was originally classified as an L9 by Kirkpatrick et al. (2011). However, it was also mentioned in Best et al. (2015) to show signs of methane absorption and meet several of the criteria outlined in Burgasser et al. (2010) for binarity.

J212702.63+761756.8: Kirkpatrick et al. (2010) discovered this object and measured optical and near-infrared spectral types of L7 and T0 pec, respectively,

suggesting that this is an L+T binary with component types of L7 and T3.5. Bardalez Gagliuffi et al. (2014) gave component types of $L8.5 \pm 1.0$ and $T4.5 \pm 2.0$, based on near-infrared spectra.

As a check on the above binarity indications, we use the binary template fitting procedure outlined in Bravo et al. (2023), available spectra from the Spex Prism Archive (Burgasser & Splat Development Team 2017), and the parallax distance determinations of this paper to make an estimate of whether the objects are strong, marginal, or poor binary candidates based on comparison of fits to binary or single-object templates.

We confirm these objects as strong spectral binary candidates: J103931.32+325623.7 (L7+T4), J110611.58+275414.1 (T1+T3), J131141.74+362925.2 (L4+T2), J140255.70+080053.4 (L8+T3), J171145.73+223204.2 (L6+T7), and J120746.66+024426.8 (T0+T1).

These objects are marginally better fit by a binary template than a single template ($2 \leq \Delta\chi^2 \leq 3$): J011912.41+240331.7 (T2+T8), J023618.06+004852.1 (L5+T1), J090900.31+652525.8 (T1+T3), and J094908.49-154548.3 (T1+T4).

We find that these objects do not have binary fits that are significantly better than single object fits: J003259.67+141037.2 (L9), J075840.07+324718.8 (T2), J143945.64+304218.7 (T3), and J183058.60+454258.2 (L9).

The absolute magnitudes of spectral binaries compared to the rest of the sample in this work are shown on Figures 11 and 12.

13.1.3. *Binary Objects Which may Have Been Missed*

Despite best efforts to find binary brown dwarfs by high spatial resolution imaging and spectral de-

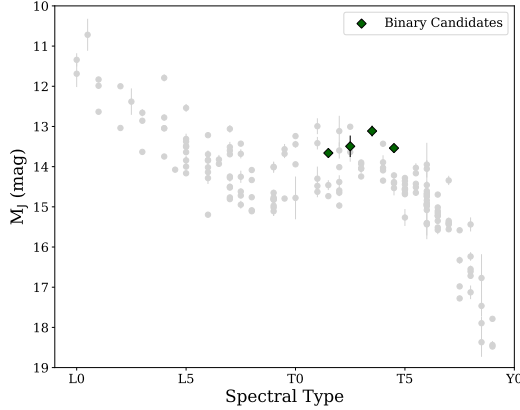


Figure 13. Absolute J -band magnitudes as a function of spectral type with the positions of potential binary objects highlighted.

convolution, it is likely that there remain some number of undiscovered binary objects, including those in this study. A difficult class for binary discovery would be those for which the components have very nearly equal spectral types, remain unresolved due to close orbits and/or distance, but for which a combination of low masses and orbital parameters give little indication of velocity spectral line broadening. Due to having similar spectral types, such objects might still be revealed by being roughly a factor of two (≈ 0.75 mag) brighter in absolute magnitude than single objects of similar spectral type. This brightness difference can still be difficult to detect without accurate parallaxes and photometry and due to the width and steepness of the general cooling curve as seen in absolute magnitude versus spectral type diagrams. Fortunately, the “J-band bump” produces a flat region from late-L to mid-T spectral types in the M_J versus spectral type diagram. Inspection of the left panel of Figure 11 shows a clear locus of known non-subdwarf binaries roughly a factor of two above the single object locus for this spectral range. We note that there are several other objects in the binary locus which are not currently-known binaries. While not a proof of binarity we list these objects for further scrutiny: J055919.85–140454.8, J104828.96+091940.9, J132407.64+190625.5, and J175023.78+422238.6 and plot them in Figure 13. We note that J055919.85–140454.8 has previously been mentioned as being overluminous in Dahn et al. (2002) and Burgasser (2007).

13.2. Wide Companions

In this section we discuss brown dwarfs included in this work that have previously been suggested as being widely separated companions to stars. In several cases

we parenthetically add the phrase “Astrometry is consistent”, which refers to a general consistency of the brown dwarf proper motions and parallaxes determined in this work to those of the Gaia DR3 data for the putative companion star, although a rigorous comparison has not been carried out. For two objects we provide somewhat more extended discussions due to their circumstances.

J001502.52+295928.7: This object was suggested as a possible wide (~ 5070 AU) companion to NLTT 730 in Deacon et al. (2014). (Astrometry is consistent.)

J064626.92+793454.5: This object was discovered as HD 46588 B in Loutrel et al. (2011) with a near-infrared spectral type of $L9\pm 1$ and a separation of $\sim 80''$. (Astrometry is consistent.)

J091534.04+042204.8AB: We present the possibility that J091534.04+042204.8AB is a wide ($\sim 660''$) companion to HD 79555AB, which is itself a K4 spectroscopic binary. See §13.1.1 for a discussion of the discovery and binary properties of J091534.04+042204.8AB. We first consider the Gaia astrometry for both objects, but we note the difficulties found for Gaia proper motions for resolved binaries, including J091534.04+042204.8AB, which we discuss in §10.2. Gaia astrometry for HD 79555 has $\pi=55.9338\pm 0.1607$ mas, $\mu_\alpha = -75.445\pm 0.161$ mas/yr, $\mu_\delta = 19.604\pm 0.182$ mas/yr which is largely consistent with its astrometry for J091534.04+042204.8AB of $\pi=56.6678\pm 0.9493$ mas, $\mu_\alpha = -113.180\pm 1.004$ mas/yr, $\mu_\delta = 21.278\pm 0.890$ mas/yr. While the parallaxes and μ_δ ’s are consistent, the μ_α ’s are similar, but statistically significantly different. This may not be surprising considering the binary nature of both objects and noting that HD 79555AB itself has an elevated RUWE value of 5.021. However, we note that the proper motion derived for HD 79555AB from Høg et al. (2000) ($\mu_\alpha = -114.4\pm 1.3$ mas/yr, $\mu_\delta = 26.8\pm 1.3$ mas/yr) agrees much better with the value for J091534.04+042204.8AB we find in this paper ($\mu_\alpha = -112.27\pm 0.28$ mas/yr, $\mu_\delta = 25.89\pm 0.31$ mas/yr), which strongly suggests these objects are wide companions and would be the first time these objects have been associated. The putative primary has been suggested to be part of the Castor Moving Group (Anosova & Orlov 1991) in Maldonado et al. (2010) with a young age determination confirmed in Brandt et al. (2014), thus making this a new benchmark system if physical association can be confirmed. J091534.04+042204.8AB is assigned an INT-G gravity classification in Bouy et al. (2022), so the ages of the components are generally consistent. However, this object was rejected as a low-gravity candidate from visual inspection in Bardalez Gagliuffi et al. (2019). The separation is 11,845 AU at the distance of HD 79555 from Gaia.

J095105.35+355800.1: This object is noted as a wide separation (13''.3) companion to LP 261-75 (M:) in [Burgasser et al. \(2005a\)](#). The system is listed as young (100-200 Myr) with a primary spectral type of M4.5 in [Zhang et al. \(2020\)](#). (Astrometry is consistent.)

J112254.33+255020.2: [Kirkpatrick et al. \(2011\)](#) discovered this object as WISEPC J112254.73+255021.5 with a near-infrared spectral type of T6. They further noted that it is near the M5 star LHS 302, with a similar distance estimate and proper motion. (Astrometry is consistent.)

J152322.78+301453.4: [McLean et al. \(2000\)](#) first published this object as 2MASSW J152322.6+301456 with a near-infrared spectral type of L8/L9. [Kirkpatrick et al. \(2000\)](#) gave an optical spectral type of L8 and note that this object is also known as Gl 584C. [Kirkpatrick et al. \(2001\)](#) confirmed the wide companionship of this source to the G+G dwarf primary Gliese 584AB. (Astrometry is consistent.)

J175805.45+463318.2: [Faherty et al. \(2010\)](#) suggested this object as a companion to G 204-39 (M3) with a separation of 198'', suggesting it is young and metal-rich. (Astrometry is consistent.)

J235122.32+301054.1: We note the possibility that this object is a wide ($\sim 930''$) companion to BD+29 5007. Gaia astrometry for BD+29 5007 ($\pi=42.2919\pm0.0166$ mas, $\mu_\alpha = 255.381\pm0.018$ mas/yr, $\mu_\delta = 10.628\pm0.011$ mas/yr) is consistent with its astrometry for the putative companion from this work ($\pi=40.79\pm2.06$ mas, $\mu_\alpha = 254.86\pm1.27$ mas/yr, $\mu_\delta = 6.89\pm1.48$ mas/yr). This would be the first time that these objects have been associated. The separation is 22,103 AU at the distance of BD+29 5007. (Astrometry is consistent.)

13.3. Young Objects

The astrometry for every object in this study was input into BANYAN Σ ([Gagné et al. 2018b](#)) to look for kinematic matches to known moving groups. Objects with BANYAN Σ probabilities greater than 80% are considered for further discussion below, where we review previous evidence for youth.

J004521.80+163444.0: This object has a 98.4% probability from BANYAN Σ of belonging to the Argus association ([Torres et al. 2008; Zuckerman 2019](#)). [Schmidt et al. \(2007\)](#) measured an H α equivalent width for this object of -10.06 Å. [Reid et al. \(2008\)](#) provide an optical spectral type of (L2), the parenthesis indicating signs of low gravity and measure an H α equivalent width of -14 Å. [Cruz et al. \(2009\)](#) provide optical and near-infrared types of L2 β and L2 γ , respectively, and give an H α equivalent width of -13.1 ± 2.2 Å. [Allers & Liu \(2013\)](#) give this object a VL-G gravity classification. [Gagné et al. \(2014\)](#) suggest that this object is a high-probability member of the Argus association. [Zapatero Osorio et al. \(2014\)](#) detect lithium in this object's spectrum. Using updated parallax and radial velocity information, [Gagné et al. \(2015b\)](#) reaffirm membership in the Argus association. [Faherty et al. \(2016\)](#) measure $\pi_{\text{abs}} = 62.5\pm3.7$ mas, measured a new radial velocity, adopt a spectral type of L0 β , give a gravity score of INT-G, and suggest that this object is a bona fide member of Argus. [Liu et al. \(2016\)](#) find $\pi_{\text{abs}} = 65.9\pm1.3$ mas and also conclude Argus membership. This object was proposed as the low-gravity L1 spectral standard in [Piscarreta et al. \(2024\)](#).

J005911.15-011401.4: This object has a 96.6% probability from BANYAN Σ of belonging to the Carina-Near Moving Group ([Zuckerman et al. 2006](#)) and has no mention of youth elsewhere in the literature. A young age for this source is unlikely considering the T8.5 spectral type of this object ([Cushing et al. 2011](#)).

J020743.00+000056.1: This object has a 98.4% probability from BANYAN Σ of belonging to the Argus association ([Torres et al. 2008; Zuckerman 2019](#)). This object has been known to have odd colors in [Marley et al. \(2002\)](#), and was suggested to be metal-rich in [Marocco et al. \(2010\)](#). [Zhang et al. \(2021\)](#) also suggest Argus membership for this object, but was ultimately ruled-out as member. Youth is not evident by its normal T4.5 spectral type ([Geballe et al. 2002](#)).

J023618.06+004852.1: This object has a 98.2% probability from BANYAN Σ of belonging to the AB Doradus Moving Group ([Zuckerman et al. 2004](#)). It is suggested as a possible member of the Pleiades Moving Group in [Casewell et al. \(2008\)](#) and listed as an AB Dor member in [Hurt et al. \(2024\)](#). It is discussed as being a spectral binary candidate in §13.1.2.

J035523.53+113336.7: This object has a 99.7% probability from BANYAN Σ of belonging to the AB Doradus Moving Group ([Zuckerman et al. 2004](#)). [Reid et al. \(2008\)](#) give an optical spectral type of L5 and note the presence of lithium in this object's spectrum and its exceptionally red $J - K$ color. It was given an L5 γ spectral type by [Cruz et al. \(2009\)](#) who suggest it may be a planetary mass field object. [Faherty et al. \(2013\)](#) discussed this object extensively and propose it to be a member of the AB Dor association. Likewise, [Liu et al. \(2013\)](#) suggest AB Dor membership. [Allers & Liu \(2013\)](#) classify this object as L3 VL-G in the near-infrared. It is considered a bona fide AB Dor member by [Gagné et al. \(2014\)](#), [Faherty et al. \(2016\)](#), and [Liu et al. \(2016\)](#).

J062720.06-111429.6: This object has a 99.1% probability from BANYAN Σ of belonging to the AB Do-

radius Moving Group (Zuckerman et al. 2004) and is also listed as candidate AB Dor member by Zhang et al. (2021). The available near-infrared spectral type of T6 by Kirkpatrick et al. (2011) was not noted to have any indications of youth.

J075840.07+324718.8: This object has a 88.3% probability from BANYAN Σ of belonging to the Carina-Near Moving Group (Zuckerman et al. 2006) and was also noted as high-probability Carina-Near member by Ashraf et al. (2022). It was suggested as having low-gravity and being young (0.04-0.4 Gyr) by Stephens et al. (2009). Strong brightness variations were seen by Radigan et al. (2014), who found a period of 4.9 ± 0.2 hrs.

J081957.98–033529.3: This object has a 74.9% probability from BANYAN Σ of belonging to the β Pictoris Moving Group (Zuckerman et al. 2001). However, this probability increases to 85% when its radial velocity, measured by Hsu et al. (2021), is included. It is also listed as a candidate β Pictoris Moving Group member in Zhang et al. (2021) and has been shown to have significant photometric variability (Liu et al. 2024).

J101014.45–040650.0: This object has a 97.0% probability from BANYAN Σ of belonging to the Carina-Near Moving Group (Zuckerman et al. 2006) and is also considered a Carina-Near Moving Group member by Sanghi et al. (2023) and Hurt et al. (2024). Large amplitude variability was noted by Wilson et al. (2014) and confirmed by Radigan (2014). It has also been used as the L6 near-infrared standard (Kirkpatrick et al. 2010; Cruz et al. 2018) (see §13.5).

J111009.77+011608.7: This object has a 98.8% probability from BANYAN Σ of belonging to the AB Dor radius Moving Group (Zuckerman et al. 2004). Knapp et al. (2004) found a spectral type of T5.5 and suggested that this object may be young and have a planetary mass based on evidence of low surface gravity in its spectrum. Stephens et al. (2009) presented a *Spitzer* IRS mid-IR spectrum and noted this object as very red. Gagné et al. (2015a) measured a radial velocity of 7.5 ± 3.8 km s $^{-1}$ and firmly establish that this object is a planetary mass member of the AB Dor association. This object was proposed as the T5 low-gravity spectral standard in Piscarreta et al. (2024).

J132434.67+635827.1: This object has a 98.2% probability from BANYAN Σ of belonging to the AB Dor radius Moving Group (Zuckerman et al. 2004). Discovered as 2MASS J13243559+6358284 by Looper et al. (2007) who gave it a near-infrared spectral type of T2:pec due to being noticeably redder than the T2 standard. Looper et al. (2007) further suggested binarity or youth may be the cause of this object's unusual spec-

trum. This object was labeled as a red photometric outlier in Faherty et al. (2009). Yang et al. (2016) also found significant variability with *Spitzer* monitoring. Significant banding was inferred by Apai et al. (2017). Gagné et al. (2018a) measured $\pi = 78.7 \pm 9.0$ mas and $RV = -23.7^{+0.4}_{-0.2}$ and deduced that this object is a young, planetary-mass T dwarf in the AB Dor association.

J155301.80+153239.5: This object has a 92.8% probability from BANYAN Σ of belonging to the Carina-Near Moving Group (Zuckerman et al. 2006). It is also considered a Carina-Near candidate member by Zhang et al. (2021), with kinematics confirmed by Hsu et al. (2021). It is a resolved binary in Keck AO images from Dupuy & Liu (2012) who determined T6.5+T7.5 components. (see §13.1.1).

J162413.95+002915.6: This object has a 98.3% probability from BANYAN Σ of belonging to the Carina-Near Moving Group (Zuckerman et al. 2006). It is also suggested as a Carina-Near Moving Group candidate by Zhang et al. (2021), although ruled out as Carina-Near moving group member by Hsu et al. (2021).

J213927.29+022024.7: This object has a 81.5% probability from BANYAN Σ of belonging to the Carina-Near Moving Group (Zuckerman et al. 2006) and is also considered to be a Carina-Near Moving Group member by Zhang et al. (2021). It is found to be a variable object in several studies, including Radigan et al. (2012) who found large-amplitude variations ($\sim 26\%$ in J -band) with a period of 7.721 ± 0.005 hr and note this object is single based on *HST* imaging. Apai et al. (2013) presented time-resolved *HST* spectroscopy again confirming the variability and finding a period of 7.83 ± 0.1 hr, while Vos et al. (2023) found evidence of patchy high-altitude fosterite clouds in this object's atmosphere.

J224431.96+204339.1: This object has a 99.7% probability from BANYAN Σ of belonging to the AB Dor radius Moving Group (Zuckerman et al. 2004). Dahn et al. (2002) note this object's very red $J - K$ color, while McLean et al. (2003) presented a near-infrared spectrum and noted this object's unusual red color, a peaked H -band, and weak potassium lines and suggest low-gravity or low metallicity. Kirkpatrick et al. (2008) discussed at length why this object looks normal in the optical but unusual in the infrared. Allers & Liu (2013) type this object as L6 VL-G in the near-infrared. Gagné et al. (2014) found that this object is a strong candidate member of AB Dor. It is given a near-infrared type of L6–L8 γ in Gagné et al. (2015b) and was considered to be a likely AB Dor member in Faherty et al. (2016), albeit with no RV or parallax data. Liu et al. (2016) measured a π_{abs} of 58.7 ± 1.0 mas which strengthened the case for

AB Dor membership. [Vos et al. \(2018\)](#) measured an RV of $-16^{+0.8}_{-0.9}$ km s $^{-1}$, confirming AB Dor membership, and found *Spitzer* variability with a period of 11 ± 2 hr.

The absolute magnitudes of the young objects identified in this work are shown in Figures 14 and 15.

13.4. Subdwarfs

In this section we give brief summaries of the known and suspected subdwarfs which were part of this study. We also list parenthetically the values of V_{\tan} we determined for each object.

J004121.65+354712.5: Discovered as 2MASS J00412179+3547133 by [Burgasser et al. \(2004\)](#) who typed it as sdL? because it exhibited spectral features similar to the L1 near-infrared standard, but also showed stronger FeH absorption, weaker CO absorption, and a bluer spectral slope. [Zhang et al. \(2017b\)](#) provide an optical spectrum and classify this object as sdL0.5. ($V_{\tan} = 64.98\pm11.14$ km s $^{-1}$)

J044853.70–193543.6: Discovered as WISEPA J044853.29–193548.5 by [Kirkpatrick et al. \(2011\)](#), who gave a near-infrared spectral type of T5 pec because of enhanced Y band flux and suppressed K band flux in its spectrum. [Kirkpatrick et al. \(2011\)](#) speculate that it may be metal-poor. It is included in the list of metal-poor T dwarfs in [Zhang et al. \(2019\)](#) and classified as an sdT5 in [Burgasser et al. \(2025\)](#). ($V_{\tan} = 103.61\pm9.99$ km s $^{-1}$)

J052536.18+673951.5: Discovered as WISEPA J052536.33+673952.3 by [Kirkpatrick et al. \(2011\)](#), who determined a near-infrared type of T6 pec and suggested low metallicity. It is also included in the list of metal-poor T dwarfs in [Zhang et al. \(2019\)](#). ($V_{\tan} = 31.08\pm3.92$ km s $^{-1}$)

J053312.61+824617.2: Discovered by [Burgasser et al. \(2003e\)](#) as 2MASS J05325346+8246465, they classified it as the first known L-type subdwarf, based on both optical and near-infrared spectra; although no exact spectral type was given, late-L was suggested. [Burgasser et al. \(2007\)](#) later classified this object as sdL7. It is typed as esdL7 in [Zhang et al. \(2013\)](#) and as an esdL8 standard in [Burgasser et al. \(2025\)](#). ($V_{\tan} = 321.85\pm10.57$ km s $^{-1}$)

J061407.41+391233.2: Discovered as WISEPA J061407.49+391236.4 by [Kirkpatrick et al. \(2011\)](#) who found a near-infrared spectral type of T6. Suggested to be a T subdwarf in [Zhang et al. \(2019\)](#). ($V_{\tan} = 50.17\pm1.40$ km s $^{-1}$).

J093735.98+293120.8: Discovered as 2MASSI J0937347+293142 by [Burgasser et al. \(2002\)](#) who noted this object as a peculiar T dwarf with very blue near-infrared colors (the bluest T dwarf at that time), pos-

sibly suggestive of low-metallicity and give a spectral type T6p. [Burgasser et al. \(2003a\)](#) presented an optical spectrum, finding a type of T7 and a very red slope, suggesting that this object may be a metal-poor halo/thick disk brown dwarf. A π_{abs} of 162.84 ± 3.88 was presented in [Vrba et al. \(2004\)](#) and noted as subluminous in all near-infrared bands. A *Spitzer* IRS spectrum was presented in [Cushing et al. \(2006\)](#) who again suggested low-metallicity and/or high $\log g$. [Burgasser et al. \(2025\)](#) take this object as an sdT6 standard. ($V_{\tan} = 46.06\pm0.34$ km s $^{-1}$)

J093936.13–244844.3: Discovered as 2MASS J09393548–2448279 by [Tinney et al. \(2005\)](#) who gave it an initial spectral type of T8 and noted its blue near-infrared color. An optical spectral type of T8 is given by [Pineda et al. \(2016\)](#). It was suggested as having low metallicity by [Leggett et al. \(2007\)](#). [Burgasser et al. \(2008\)](#) argue that model fits require a highly inflated radius, in conflict with brown dwarf models, and suggest that this source is an unresolved equal-mass binary with low-metallicity ($[\text{M}/\text{H}] \approx -0.3$). Used in retrieval analysis of [Line et al. \(2017\)](#), who also find significant low-metallicity. [Zhang et al. \(2019\)](#) suggest an sdT7.5 spectral type while [Burgasser et al. \(2025\)](#) consider it to be an d/sdT8 standard. ($V_{\tan} = 30.77\pm0.21$ km s $^{-1}$)

J111447.51–261830.0: Discovered as 2MASS J11145133–2618235 by [Tinney et al. \(2005\)](#) who classified it as T7.5 \pm 0.5 from near-infrared spectra, estimated a distance of 7 pc (possibly the coldest brown dwarf known at that time), and noted it as having a large space velocity. [Burgasser et al. \(2006a\)](#) suggested this object may have subsolar metallicity while [Leggett et al. \(2007\)](#) suggest that value is $[\text{m}/\text{H}] \approx -0.3$. Used in retrieval analysis of [Line et al. \(2017\)](#) who derive a near-solar metallicity. An optical spectral type of T8 is given by [Pineda et al. \(2016\)](#). ($V_{\tan} = 77.83\pm0.76$ km s $^{-1}$)

J115821.40+043446.3: Discovered as SDSS J115820.75+043501.7 by [Zhang et al. \(2009\)](#). It was spectral-typed by [Kirkpatrick et al. \(2010\)](#) as sdL7 in both the near-infrared and the optical based on enhanced abundances of TiO, FeH, and CrH and a blue near-infrared spectrum. It was suggested as an sdL7 standard by [Greco et al. \(2019\)](#) and adopted as a d/sdL8 standard by [Burgasser et al. \(2025\)](#). ($V_{\tan} = 119.64\pm7.02$ km s $^{-1}$)

J143535.75–004348.6: Discovered as SDSS J143535.72–004347.0 by [Hawley et al. \(2002\)](#) who classified it as an L3 based on optical spectra, while [\(Knapp et al. 2004\)](#) provided an L2.5 classification from near-infrared spectra. It has been suggested as metal-poor

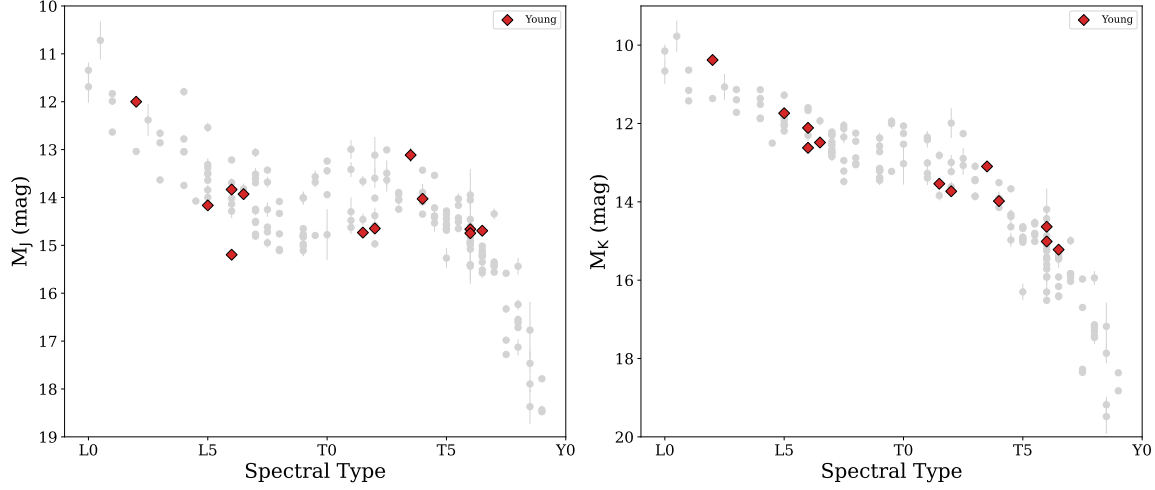


Figure 14. Same as 9 but with the positions of young objects highlighted.

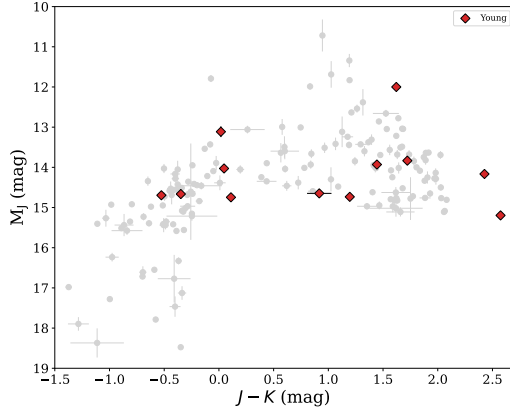


Figure 15. Same as 10 but with the positions of young objects highlighted.

by [Lodieu et al. \(2017\)](#) based on various color indices. ($V_{\tan} = 30.22 \pm 4.45 \text{ km s}^{-1}$)

J162618.23+392523.4: Discovered as 2MASS J16262034+3925190 by [Burgasser \(2004\)](#) and determined to be a high-proper motion, halo, low-metallicity L dwarf based on a near-infrared spectrum (the 2nd known L subdwarf). An optical spectrum presented by [Gizis & Harvin \(2006\)](#) indicated this object to be a mid-L subdwarf. [Burgasser et al. \(2007\)](#) suggested an sdL4 classification based on its near-infrared spectrum, while [Zhang et al. \(2013\)](#) gave an optical spectral type of esdL4 (referencing a Zhang et al. 2013 conference proceeding). It is classified as usdL4 by [Zhang et al. \(2017b\)](#) and determined to be part of the “halo transition zone” in [Zhang et al. \(2017a\)](#). [Dahn et al. \(2017\)](#) find $\pi_{\text{abs}} = 31.08 \pm 0.55 \text{ mas}$ and found residuals possibly indicative of a binary system. [Gonzales et al. \(2018\)](#) provided $8.0 \mu\text{m}$ *Spitzer* photometry and derived numerous physical parameters based on this object’s SED.

It is listed as the sdL4 optical/near-infrared standard in [Greco et al. \(2019\)](#). ($V_{\tan} = 113.63 \pm 3.96 \text{ km s}^{-1}$)

J175609.98+281516.4: Discovered as 2MASS J17561080+2815238 by [Kirkpatrick et al. \(2010\)](#) who also determined optical and near-infrared spectral types of sdL1 and L1 (pec), respectively. [Greco et al. \(2019\)](#) suggest this object to be an optical/near-infrared sdL1 standard. We note that the relatively high value of V_{\tan} is consistent with the subdwarf nature of this object. ($V_{\tan} = 113.63 \pm 3.96 \text{ km s}^{-1}$)

The absolute magnitudes of the subdwarfs included in this parallax program are shown in Figures 16 and 17.

13.5. Brown Dwarf Spectral Standards

Several L- and T-type optical and near-infrared standards were observed as part of this program. While some of these have been mentioned in the previous section, here we give a complete list of the objects which are considered standards and for which we provide parallax and proper motion results. We note that, for twelve of the twenty standards listed below, the parallax results in this work are the most precise yet measured.

The near-infrared L dwarf standards from [Kirkpatrick et al. \(2010\)](#) include J150653.09+132105.8 (L3), J101014.45–040650.0 (L6), J010332.40+193536.5 (L7), and J163229.48+190439.6 (L8). J101014.45–040650.0 and J163229.48+190439.6 are also the L6 and L8 optical standards, respectively ([Kirkpatrick 2005](#); [Geifler et al. 2011](#)). J010332.40+193536.5 was later typed as L6 β ([Faherty et al. 2012](#)) and has been considered a possible member of the Argus association ([Torres et al. 2008](#); [Zuckerman 2019](#)) by [Gagné et al. \(2014, 2015b\)](#). (We also note that J010332.40+193536.5 did not meet our BANYAN Σ criterion for association with any moving group and thus was left out of §13.3.) [Gagné](#)

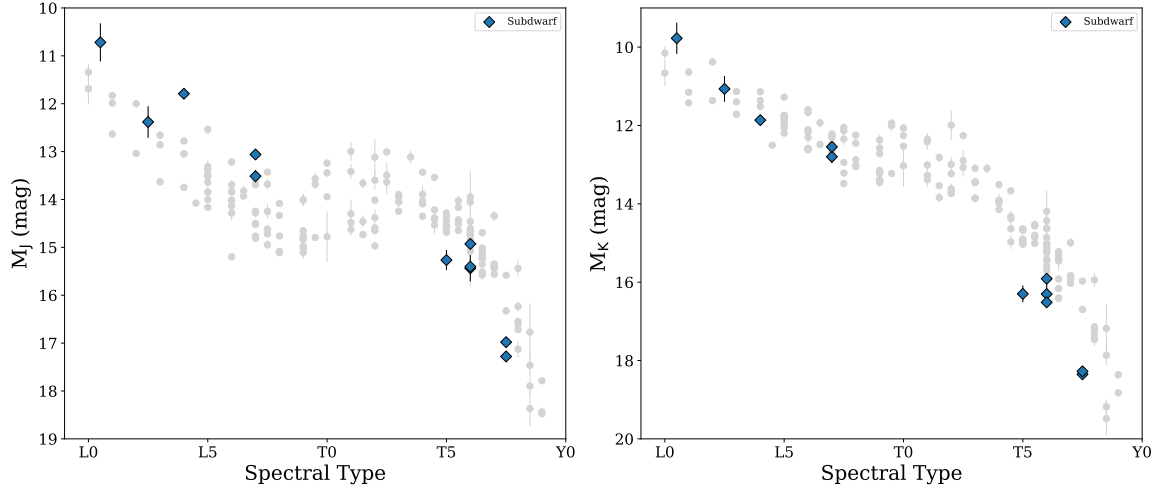


Figure 16. Same as 9 but with the positions of subdwarfs highlighted.

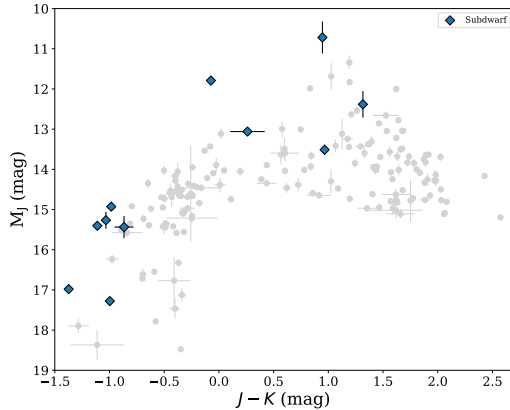


Figure 17. Same as 10 but with the positions of subdwarfs highlighted.

et al. (2015c) described this object as a red brown dwarf with no clear signs of low gravity, and retype it as L6 pec. Cruz et al. (2018) no longer consider this object a near-infrared standard, and instead proposed J082518.97+211546.1 as the L7.5 near-infrared standard, which is included in this program.

The T dwarf near-infrared standards are given in Burgasser et al. (2006a), most of which are included in this parallax program, including J120746.66+024426.8 (T0), J083717.18−000020.8 (T1), J125453.41−012245.6 (T2), J225418.98+312353.0 (T4), J150319.71+252528.3 (T5), J162413.95+002915.6 (T6), J072719.22+170950.1 (T7), and J041522.17−093457.1 (T8). The T9 near-infrared standard J072226.89−054027.5 (Lucas et al. 2010; Cushing et al. 2011) was also included in our program.

Several subdwarf standards were also included as part of this program. The near-infrared subdwarf standards from Greco et al. (2019) include J175609.98+281516.4 (sdL1),

J162618.23+392523.4 (sdL4), and J115821.40+043446.3 (sdL7). J115821.40+043446.3 was later updated to be the d/sdL8 standard in Burgasser et al. (2025). We note that Greco et al. (2019) consider J175609.98+281516.4 to also be an optical sdL1 standard. Other subdwarf standards from Burgasser et al. (2025) include J053312.61+824617.2 (esdL8), J093735.98+293120.8 (sdT6), and J093936.13−244844.3 (d/sdT8).

14. SUMMARY

We have measured parallaxes and proper motions with high accuracy for a vast majority of the 173 L- and T-type dwarfs and subdwarfs in this study with median accuracies of $\sigma(\pi_{abs}) = 1.51$ mas and $\sigma(\mu_{abs}) = 1.02$ mas yr^{-1} , with target object median distances of ≈ 18 pc and median reference frame distances of ≈ 1 kpc. These results provide the first parallaxes and proper motions for 16 objects and the current highest precision parallaxes and proper motions for an additional 106 objects. Comparison of our results with 40 objects with parallaxes and proper motions in Gaia DR3 showed no systematic differences, confirmed our quoted precisions, and allowed for an investigation of resolved binarity on astrometric results. We also provide a uniform set of J , H , K_S photometry in the UKIRT/MKO system for all objects in our study. Although quality parallax and proper motion determinations are important for all brown dwarfs, we further investigate several brown dwarf populations included in our sample. While for all binary objects in the study we provide new absolute magnitudes, for the spectral binary subset we also include new spectral template fitting to help determine binarity. For wide companion candidates our proper motions results are used for confirmation. Proper motions are also used for confirmation of potential young objects with stel-

lar moving groups. Several subdwarfs are discussed in some detail. Finally, our parallaxes and new photometry provide reliable near-infrared absolute magnitudes for several brown dwarf spectral standards.

15. APPENDIX A

We present in Table 7 additional JHK photometry obtained with ASTROCAM at the 1.55-m telescope, primarily of Series 1 objects. The observations, obtained in the early 2000's, are on the CIT photometric system using the standards of [Guetter et al. \(2003\)](#). Column (1) gives the CatWISE object names, column (2) the J

band magnitudes and associated error bars, columns (3) and (4) the $(J - H)$ and $(J - K)$ colors and associated error bars, respectively, and column (5) the number of independent nights of observation. The results are given in terms of J magnitude and $(J - H)$ and $(J - K)$ colors, as that was the fashion in which the data were reduced. This photometry is presented for purposes of completeness only and is not used in any of the science discussions in this paper, as our subsequent UKIRT JHK photometry presented in this paper supersedes in accuracy and uniformity this earlier photometry.

Table 7. New JHK Photometry in the CIT System

Name (CatWISE)	$J \pm \sigma(J)$ (mag)	$(J - H) \pm \sigma(J - H)$ (mag)	$(J - K) \pm \sigma(J - K)$ (mag)	Nights (Number)
(1)	(2)	(3)	(4)	(5)
J003030.38-145033.8	16.51 ± 0.03	1.18 ± 0.02	2.01 ± 0.03	5
J003259.67+141037.2	16.65 ± 0.03	0.98 ± 0.03	1.60 ± 0.03	5
J010753.11+004157.7	15.75 ± 0.03	1.25 ± 0.03	2.05 ± 0.07	1
J015142.59+124428.7	16.30 ± 0.02	0.80 ± 0.02	1.00 ± 0.03	4
J020743.00+000056.1	16.73 ± 0.02	-0.06 ± 0.03	-0.08 ± 0.04	4
J024313.38-245332.8	15.08 ± 0.03	-0.34 ± 0.02	-0.12 ± 0.03	4
J031100.13+164815.6	15.90 ± 0.06	0.96 ± 0.04	1.61 ± 0.03	2
J032842.66+230204.1	16.51 ± 0.02	0.98 ± 0.02	1.49 ± 0.02	4
J041522.17-093457.1	15.19 ± 0.02	-0.55 ± 0.02	-0.45 ± 0.06	5
J042348.22-041402.0	14.26 ± 0.03	0.82 ± 0.02	1.32 ± 0.02	2
J051609.20-044553.3	15.49 ± 0.03	-0.32 ± 0.02	-0.19 ± 0.03	4
J053312.61+824617.2	15.02 ± 0.03	0.13 ± 0.02	0.11 ± 0.02	3
J053952.16-005856.5	13.88 ± 0.05	0.83 ± 0.03	1.40 ± 0.03	1
J055919.85-140454.8	13.55 ± 0.02	-0.12 ± 0.02	-0.21 ± 0.03	2
J072719.22+170950.1	15.10 ± 0.03	-0.56 ± 0.05	-0.31 ± 0.03	3
J075547.93+221212.8	15.39 ± 0.04	-0.33 ± 0.02	-0.39 ± 0.05	4
J083006.91+482838.3	15.27 ± 0.02	0.90 ± 0.02	1.47 ± 0.02	2
J083717.18-000020.8	17.03 ± 0.02	0.67 ± 0.02	1.05 ± 0.03	3
J092615.40+584717.6	15.41 ± 0.02	-0.03 ± 0.03	-0.05 ± 0.04	4
J093735.98+293120.8	14.28 ± 0.02	-0.47 ± 0.02	-1.03 ± 0.02	2
J093936.13-244844.3	15.60 ± 0.02	-0.55 ± 0.02	-1.30 ± 0.04	3
J095105.35+355800.1	17.13 ± 0.05	1.14 ± 0.02	1.89 ± 0.03	2
J102109.51-030421.1	15.94 ± 0.02	0.29 ± 0.02	0.49 ± 0.03	2
J104751.75+212414.7	15.37 ± 0.02	-0.49 ± 0.02	-0.80 ± 0.03	4
J111009.77+011608.7	16.11 ± 0.04	-0.17 ± 0.03	0.06 ± 0.04	3
J111447.51-261830.0	15.59 ± 0.02	-0.56 ± 0.02	-1.04 ± 0.04	4
J121709.86-031111.8	15.42 ± 0.02	-0.56 ± 0.03	-0.31 ± 0.03	2
J122554.84-273958.5	14.83 ± 0.02	-0.38 ± 0.03	-0.39 ± 0.02	2
J123737.03+652607.2	15.59 ± 0.02	-0.52 ± 0.02	-0.99 ± 0.04	3
J125453.41-012245.6	14.71 ± 0.04	0.59 ± 0.03	0.75 ± 0.05	1
J134645.89-003152.2	15.53 ± 0.03	-0.47 ± 0.02	-0.27 ± 0.03	4
J143517.22-004612.9	16.45 ± 0.04	0.66 ± 0.03	1.12 ± 0.04	4
J143535.75-004348.6	16.52 ± 0.03	0.81 ± 0.03	1.30 ± 0.03	4
J144600.78+002450.9	15.57 ± 0.02	1.02 ± 0.04	1.63 ± 0.06	2
J150319.71+252528.3	13.51 ± 0.03	-0.36 ± 0.03	-0.44 ± 0.03	3

Table 7 *continued*

Table 7 (*continued*)

Name (CatWISE)	$J \pm \sigma(J)$ (mag)	$(J - H) \pm \sigma(J - H)$ (mag)	$(J - K) \pm \sigma(J - K)$ (mag)	Nights (Number)
(1)	(2)	(3)	(4)	(5)
J152322.78+301453.4	16.11 \pm 0.04	1.07 \pm 0.02	1.72 \pm 0.02	3
J155301.80+153239.5	15.34 \pm 0.02	-0.51 \pm 0.02	-0.44 \pm 0.02	2
J162413.95+002915.6	15.07 \pm 0.02	-0.42 \pm 0.03	-0.57 \pm 0.05	4
J163229.48+190439.6	15.73 \pm 0.03	1.10 \pm 0.02	1.77 \pm 0.04	2
J171145.73+223204.2	16.72 \pm 0.04	0.82 \pm 0.02	1.40 \pm 0.04	5
J172811.54+394859.0	15.79 \pm 0.03	1.11 \pm 0.03	1.88 \pm 0.03	2
J175023.78+422238.6	16.13 \pm 0.03	0.59 \pm 0.02	0.77 \pm 0.02	3
J175033.14+175905.4	16.12 \pm 0.05	0.22 \pm 0.03	0.05 \pm 0.03	3
J175805.45+463318.2	15.80 \pm 0.04	-0.44 \pm 0.02	-0.21 \pm 0.02	4
J184108.67+311728.6	15.94 \pm 0.02	1.01 \pm 0.04	1.59 \pm 0.02	5
J190106.23+471820.5	15.47 \pm 0.02	-0.21 \pm 0.02	-0.31 \pm 0.02	7
J210115.58+175656.0	16.87 \pm 0.04	1.19 \pm 0.04	1.91 \pm 0.06	3
J212414.06+010003.8	15.72 \pm 0.03	-0.24 \pm 0.02	-0.21 \pm 0.04	4
J222444.39-015908.2	13.96 \pm 0.03	1.14 \pm 0.06	1.91 \pm 0.05	2
J224253.65+254256.2	14.64 \pm 0.02	1.00 \pm 0.02	1.68 \pm 0.02	3
J224431.96+204339.1	16.40 \pm 0.03	1.39 \pm 0.03	2.42 \pm 0.03	4
J225418.98+312353.0	14.95 \pm 0.02	0.05 \pm 0.02	-0.03 \pm 0.03	5
J225529.03-003436.4	15.57 \pm 0.02	0.77 \pm 0.02	1.21 \pm 0.02	3
J233910.67+135212.9	15.74 \pm 0.03	-0.28 \pm 0.03	-0.30 \pm 0.04	2
J235654.19-155322.9	15.44 \pm 0.02	-0.28 \pm 0.03	-0.17 \pm 0.03	2

16. ACKNOWLEDGEMENTS

FJV would like to thank C.C. Dahn, apart from his direct contributions to this paper, for his many personal discussions over the years on how to correctly do ground-based astrometry and optical photometry. FJV would also like to acknowledge D.G. Monet for developing the software, used in this and previous USNO/NOFS astrometry, which included the tools necessary for detailed analyses of the astrometric data.

This work has made use of data from the European Space Agency (ESA) mission Gaia (<https://www.cosmos.esa.int/gaia>), processed by the Gaia Data Processing and Analysis Consortium (DPAC, <https://www.cosmos.esa.int/web/gaia/dpac/consortium>). Funding for the DPAC has been provided by national institutions, in particular the institutions participating in the Gaia Multilateral Agreement.

This publication makes use of data products from the Two Micron All Sky Survey, which is a joint project of the University of Massachusetts and the Infrared Processing and Analysis Center/California Institute of Technology, funded by the National Aeronautics and Space Administration and the National Science Foundation.

This publication makes use of data products from the Wide-field Infrared Survey Explorer, which is a joint project of the University of California, Los Angeles, and the Jet Propulsion Laboratory/California Institute of Technology, funded by the National Aeronautics and Space Administration. This publication also makes use of data products from NEOWISE, which is a project of the Jet Propulsion Laboratory/California Institute of Technology, funded by the Planetary Science Division of the National Aeronautics and Space Administration.

This publication makes use of data products from the UKIRT Hemisphere Survey, which is a joint project of the United States Naval Observatory, the University of Hawaii Institute for Astronomy, the Cambridge University Cambridge Astronomy Survey Unit, and the University of Edinburgh Wide-Field Astronomy Unit (WFAU). The WFAU gratefully acknowledges support for this work from the Science and Technology Facilities Council (STFC) through ST/T002956/1 and previous grants.

This work has benefited from The UltracoolSheet at <http://bit.ly/UltracoolSheet>, maintained by Will Best, Trent Dupuy, Michael Liu, Aniket Sanghi, Rob Siverd, and Zhoujian Zhang, and developed from compilations by [Dupuy & Liu \(2012\)](#); [Dupuy & Kraus \(2013\)](#); [Deacon et al. \(2014\)](#); [Liu et al. \(2016\)](#); [Best et al. \(2018, 2021\)](#); [Sanghi et al. \(2023\)](#); [Schneider et al. \(2023\)](#).

REFERENCES

Aberasturi, M., Solano, E., & Martín, E. L. 2011, *A&A*, 534, L7, doi: [10.1051/0004-6361/201117822](https://doi.org/10.1051/0004-6361/201117822)

Albert, L., Artigau, É., Delorme, P., et al. 2011, *AJ*, 141, 203, doi: [10.1088/0004-6256/141/6/203](https://doi.org/10.1088/0004-6256/141/6/203)

Allers, K. N., & Liu, M. C. 2013, *ApJ*, 772, 79, doi: [10.1088/0004-637X/772/2/79](https://doi.org/10.1088/0004-637X/772/2/79)

Anosova, J. P., & Orlov, V. V. 1991, *A&A*, 252, 123

Apai, D., Radigan, J., Buenzli, E., et al. 2013, *ApJ*, 768, 121, doi: [10.1088/0004-637X/768/2/121](https://doi.org/10.1088/0004-637X/768/2/121)

Apai, D., Karalidi, T., Marley, M. S., et al. 2017, *Science*, 357, 683, doi: [10.1126/science.aam9848](https://doi.org/10.1126/science.aam9848)

Ashraf, A., Bardalez Gagliuffi, D. C., Manjavacas, E., et al. 2022, *ApJ*, 934, 178, doi: [10.3847/1538-4357/ac7aab](https://doi.org/10.3847/1538-4357/ac7aab)

Bardalez Gagliuffi, D. C., Gelino, C. R., & Burgasser, A. J. 2015, *AJ*, 150, 163, doi: [10.1088/0004-6256/150/5/163](https://doi.org/10.1088/0004-6256/150/5/163)

Bardalez Gagliuffi, D. C., Burgasser, A. J., Gelino, C. R., et al. 2014, *ApJ*, 794, 143, doi: [10.1088/0004-637X/794/2/143](https://doi.org/10.1088/0004-637X/794/2/143)

Bardalez Gagliuffi, D. C., Burgasser, A. J., Schmidt, S. J., et al. 2019, *ApJ*, 883, 205, doi: [10.3847/1538-4357/ab253d](https://doi.org/10.3847/1538-4357/ab253d)

Best, W. M. J., Liu, M. C., Magnier, E. A., & Dupuy, T. J. 2021, *AJ*, 161, 42, doi: [10.3847/1538-3881/abc893](https://doi.org/10.3847/1538-3881/abc893)

Best, W. M. J., Liu, M. C., Magnier, E. A., et al. 2015, *ApJ*, 814, 118, doi: [10.1088/0004-637X/814/2/118](https://doi.org/10.1088/0004-637X/814/2/118)

Best, W. M. J., Magnier, E. A., Liu, M. C., et al. 2018, *ApJS*, 234, 1, doi: [10.3847/1538-4365/aa9982](https://doi.org/10.3847/1538-4365/aa9982)

Bouy, H., Brandner, W., Martín, E. L., et al. 2003, *AJ*, 126, 1526, doi: [10.1086/377343](https://doi.org/10.1086/377343)

Bouy, H., Tamura, M., Barrado, D., et al. 2022, *A&A*, 664, A111, doi: [10.1051/0004-6361/202243850](https://doi.org/10.1051/0004-6361/202243850)

Brandt, T. D., Kuzuhara, M., McElwain, M. W., et al. 2014, *ApJ*, 786, 1, doi: [10.1088/0004-637X/786/1/1](https://doi.org/10.1088/0004-637X/786/1/1)

Bravo, A., Schneider, A. C., Bardalez Gagliuffi, D., et al. 2023, *AJ*, 166, 226, doi: [10.3847/1538-3881/acffc1](https://doi.org/10.3847/1538-3881/acffc1)

Burgasser, A. J. 2004, *ApJL*, 614, L73, doi: [10.1086/425418](https://doi.org/10.1086/425418)

—. 2007, *ApJ*, 659, 655, doi: [10.1086/511027](https://doi.org/10.1086/511027)

Burgasser, A. J., Bardalez-Gagliuffi, D. C., & Gizis, J. E. 2011a, *AJ*, 141, 70, doi: [10.1088/0004-6256/141/3/70](https://doi.org/10.1088/0004-6256/141/3/70)

Burgasser, A. J., Cruz, K. L., Cushing, M., et al. 2010, *ApJ*, 710, 1142, doi: [10.1088/0004-637X/710/2/1142](https://doi.org/10.1088/0004-637X/710/2/1142)

Burgasser, A. J., Cruz, K. L., & Kirkpatrick, J. D. 2007, *ApJ*, 657, 494, doi: [10.1086/510148](https://doi.org/10.1086/510148)

Burgasser, A. J., Geballe, T. R., Leggett, S. K., Kirkpatrick, J. D., & Golimowski, D. A. 2006a, *ApJ*, 637, 1067, doi: [10.1086/498563](https://doi.org/10.1086/498563)

Burgasser, A. J., Kirkpatrick, J. D., Cruz, K. L., et al. 2006b, *ApJS*, 166, 585, doi: [10.1086/506327](https://doi.org/10.1086/506327)

Burgasser, A. J., Kirkpatrick, J. D., Liebert, J., & Burrows, A. 2003a, *ApJ*, 594, 510, doi: [10.1086/376756](https://doi.org/10.1086/376756)

Burgasser, A. J., Kirkpatrick, J. D., & Lowrance, P. J. 2005a, *AJ*, 129, 2849, doi: [10.1086/430218](https://doi.org/10.1086/430218)

Burgasser, A. J., Kirkpatrick, J. D., McElwain, M. W., et al. 2003b, *AJ*, 125, 850, doi: [10.1086/345975](https://doi.org/10.1086/345975)

Burgasser, A. J., Kirkpatrick, J. D., Reid, I. N., et al. 2003c, *ApJ*, 586, 512, doi: [10.1086/346263](https://doi.org/10.1086/346263)

Burgasser, A. J., McElwain, M. W., & Kirkpatrick, J. D. 2003d, *AJ*, 126, 2487, doi: [10.1086/378608](https://doi.org/10.1086/378608)

Burgasser, A. J., McElwain, M. W., Kirkpatrick, J. D., et al. 2004, *AJ*, 127, 2856, doi: [10.1086/383549](https://doi.org/10.1086/383549)

Burgasser, A. J., Reid, I. N., Leggett, S. K., et al. 2005b, *ApJL*, 634, L177, doi: [10.1086/498866](https://doi.org/10.1086/498866)

Burgasser, A. J., & Splat Development Team. 2017, in *Astronomical Society of India Conference Series*, Vol. 14, *Astronomical Society of India Conference Series*, 7–12, doi: [10.48550/arXiv.1707.00062](https://doi.org/10.48550/arXiv.1707.00062)

Burgasser, A. J., Tinney, C. G., Cushing, M. C., et al. 2008, *ApJL*, 689, L53, doi: [10.1086/595747](https://doi.org/10.1086/595747)

Burgasser, A. J., Kirkpatrick, J. D., Brown, M. E., et al. 1999, *ApJL*, 522, L65, doi: [10.1086/312221](https://doi.org/10.1086/312221)

Burgasser, A. J., Wilson, J. C., Kirkpatrick, J. D., et al. 2000, *AJ*, 120, 1100, doi: [10.1086/301475](https://doi.org/10.1086/301475)

Burgasser, A. J., Kirkpatrick, J. D., Brown, M. E., et al. 2002, *ApJ*, 564, 421, doi: [10.1086/324033](https://doi.org/10.1086/324033)

Burgasser, A. J., Kirkpatrick, J. D., Burrows, A., et al. 2003e, *ApJ*, 592, 1186, doi: [10.1086/375813](https://doi.org/10.1086/375813)

Burgasser, A. J., Cushing, M. C., Kirkpatrick, J. D., et al. 2011b, *ApJ*, 735, 116, doi: [10.1088/0004-637X/735/2/116](https://doi.org/10.1088/0004-637X/735/2/116)

Burgasser, A. J., Schneider, A. C., Meisner, A. M., et al. 2025, *ApJ*, 982, 79, doi: [10.3847/1538-4357/adb39f](https://doi.org/10.3847/1538-4357/adb39f)

Burningham, B., Pinfield, D. J., Leggett, S. K., et al. 2008, *MNRAS*, 391, 320, doi: [10.1111/j.1365-2966.2008.13885.x](https://doi.org/10.1111/j.1365-2966.2008.13885.x)

Burningham, B., Pinfield, D. J., Lucas, P. W., et al. 2010, *MNRAS*, 406, 1885, doi: [10.1111/j.1365-2966.2010.16800.x](https://doi.org/10.1111/j.1365-2966.2010.16800.x)

Casali, M., Adamson, A., Alves de Oliveira, C., et al. 2007, *A&A*, 467, 777, doi: [10.1051/0004-6361:20066514](https://doi.org/10.1051/0004-6361:20066514)

Casewell, S. L., Jameson, R. F., & Burleigh, M. R. 2008, *MNRAS*, 390, 1517, doi: [10.1111/j.1365-2966.2008.13855.x](https://doi.org/10.1111/j.1365-2966.2008.13855.x)

Castro, P. J., & Gizis, J. E. 2012, *ApJ*, 746, 3, doi: [10.1088/0004-637X/746/1/3](https://doi.org/10.1088/0004-637X/746/1/3)

Castro, P. J., Gizis, J. E., Harris, H. C., et al. 2013, *ApJ*, 776, 126, doi: [10.1088/0004-637X/776/2/126](https://doi.org/10.1088/0004-637X/776/2/126)

Castro-Ginard, A., Penoyre, Z., Casey, A. R., et al. 2024, *A&A*, 688, A1, doi: [10.1051/0004-6361/202450172](https://doi.org/10.1051/0004-6361/202450172)

Chambers, K. C., Magnier, E. A., Metcalfe, N., et al. 2016, arXiv e-prints, arXiv:1612.05560, doi: [10.48550/arXiv.1612.05560](https://doi.org/10.48550/arXiv.1612.05560)

Chiu, K., Fan, X., Leggett, S. K., et al. 2006, AJ, 131, 2722, doi: [10.1086/501431](https://doi.org/10.1086/501431)

Cruz, K. L., Kirkpatrick, J. D., & Burgasser, A. J. 2009, AJ, 137, 3345, doi: [10.1088/0004-6256/137/2/3345](https://doi.org/10.1088/0004-6256/137/2/3345)

Cruz, K. L., Núñez, A., Burgasser, A. J., et al. 2018, AJ, 155, 34, doi: [10.3847/1538-3881/aa9d8a](https://doi.org/10.3847/1538-3881/aa9d8a)

Cruz, K. L., Reid, I. N., Liebert, J., Kirkpatrick, J. D., & Lowrance, P. J. 2003, AJ, 126, 2421, doi: [10.1086/378607](https://doi.org/10.1086/378607)

Cruz, K. L., Reid, I. N., Kirkpatrick, J. D., et al. 2007, AJ, 133, 439, doi: [10.1086/510132](https://doi.org/10.1086/510132)

Cushing, M. C., Roellig, T. L., Marley, M. S., et al. 2006, ApJ, 648, 614, doi: [10.1086/505637](https://doi.org/10.1086/505637)

Cushing, M. C., Kirkpatrick, J. D., Gelino, C. R., et al. 2011, ApJ, 743, 50, doi: [10.1088/0004-637X/743/1/50](https://doi.org/10.1088/0004-637X/743/1/50)

Dahn, C. C., Harrington, R. S., Kallarakal, V. V., et al. 1988, AJ, 95, 237, doi: [10.1086/114633](https://doi.org/10.1086/114633)

Dahn, C. C., Harris, H. C., Vrba, F. J., et al. 2002, AJ, 124, 1170, doi: [10.1086/341646](https://doi.org/10.1086/341646)

Dahn, C. C., Harris, H. C., Subasavage, J. P., et al. 2017, AJ, 154, 147, doi: [10.3847/1538-3881/aa880b](https://doi.org/10.3847/1538-3881/aa880b)

Deacon, N. R., Liu, M. C., Magnier, E. A., et al. 2011, AJ, 142, 77, doi: [10.1088/0004-6256/142/3/77](https://doi.org/10.1088/0004-6256/142/3/77)

—. 2014, ApJ, 792, 119, doi: [10.1088/0004-637X/792/2/119](https://doi.org/10.1088/0004-637X/792/2/119)

Delorme, P., Delfosse, X., Albert, L., et al. 2008, A&A, 482, 961, doi: [10.1051/0004-6361:20079317](https://doi.org/10.1051/0004-6361:20079317)

Dupuy, T. J., & Kraus, A. L. 2013, Science, 341, 1492, doi: [10.1126/science.1241917](https://doi.org/10.1126/science.1241917)

Dupuy, T. J., & Liu, M. C. 2012, ApJS, 201, 19, doi: [10.1088/0067-0049/201/2/19](https://doi.org/10.1088/0067-0049/201/2/19)

—. 2017, ApJS, 231, 15, doi: [10.3847/1538-4365/aa5e4c](https://doi.org/10.3847/1538-4365/aa5e4c)

Dye, S., Lawrence, A., Read, M. A., et al. 2018, MNRAS, 473, 5113, doi: [10.1093/mnras/stx2622](https://doi.org/10.1093/mnras/stx2622)

Fabricius, C., Luri, X., Arenou, F., et al. 2021, A&A, 649, A5, doi: [10.1051/0004-6361/202039834](https://doi.org/10.1051/0004-6361/202039834)

Faherty, J. K., Burgasser, A. J., Bochanski, J. J., et al. 2011, AJ, 141, 71, doi: [10.1088/0004-6256/141/3/71](https://doi.org/10.1088/0004-6256/141/3/71)

Faherty, J. K., Burgasser, A. J., Cruz, K. L., et al. 2009, AJ, 137, 1, doi: [10.1088/0004-6256/137/1/1](https://doi.org/10.1088/0004-6256/137/1/1)

Faherty, J. K., Burgasser, A. J., West, A. A., et al. 2010, AJ, 139, 176, doi: [10.1088/0004-6256/139/1/176](https://doi.org/10.1088/0004-6256/139/1/176)

Faherty, J. K., Rice, E. L., Cruz, K. L., Mamajek, E. E., & Núñez, A. 2013, AJ, 145, 2, doi: [10.1088/0004-6256/145/1/2](https://doi.org/10.1088/0004-6256/145/1/2)

Faherty, J. K., Burgasser, A. J., Walter, F. M., et al. 2012, ApJ, 752, 56, doi: [10.1088/0004-637X/752/1/56](https://doi.org/10.1088/0004-637X/752/1/56)

Faherty, J. K., Riedel, A. R., Cruz, K. L., et al. 2016, ApJS, 225, 10, doi: [10.3847/0067-0049/225/1/10](https://doi.org/10.3847/0067-0049/225/1/10)

Fan, X., Knapp, G. R., Strauss, M. A., et al. 2000, AJ, 119, 928, doi: [10.1086/301224](https://doi.org/10.1086/301224)

Fan, X., Narayanan, V. K., Lupton, R. H., et al. 2001, AJ, 122, 2833, doi: [10.1086/324111](https://doi.org/10.1086/324111)

Fischer, J., Vrba, F. J., Toomey, D. W., et al. 2003, in Society of Photo-Optical Instrumentation Engineers (SPIE) Conference Series, Vol. 4841, Instrument Design and Performance for Optical/Infrared Ground-based Telescopes, ed. M. Iye & A. F. M. Moorwood, 564–577, doi: [10.1117/12.461033](https://doi.org/10.1117/12.461033)

Fowler, A. M., Gatley, I., McIntyre, P., Vrba, F. J., & Hoffman, A. W. 1996, in Society of Photo-Optical Instrumentation Engineers (SPIE) Conference Series, Vol. 2816, Infrared Detectors for Remote Sensing: Physics, Materials, and Devices, ed. R. E. Longshore & J. W. Baars, 150–160, doi: [10.1117/12.255162](https://doi.org/10.1117/12.255162)

Gagné, J., Allers, K. N., Theissen, C. A., et al. 2018a, ApJL, 854, L27, doi: [10.3847/2041-8213/aaacf](https://doi.org/10.3847/2041-8213/aaacf)

Gagné, J., Burgasser, A. J., Faherty, J. K., et al. 2015a, ApJL, 808, L20, doi: [10.1088/2041-8205/808/1/L20](https://doi.org/10.1088/2041-8205/808/1/L20)

Gagné, J., Lafrenière, D., Doyon, R., Malo, L., & Artigau, É. 2014, ApJ, 783, 121, doi: [10.1088/0004-637X/783/2/121](https://doi.org/10.1088/0004-637X/783/2/121)

—. 2015b, ApJ, 798, 73, doi: [10.1088/0004-637X/798/2/73](https://doi.org/10.1088/0004-637X/798/2/73)

Gagné, J., Faherty, J. K., Cruz, K. L., et al. 2015c, ApJS, 219, 33, doi: [10.1088/0067-0049/219/2/33](https://doi.org/10.1088/0067-0049/219/2/33)

Gagné, J., Mamajek, E. E., Malo, L., et al. 2018b, ApJ, 856, 23, doi: [10.3847/1538-4357/aaae09](https://doi.org/10.3847/1538-4357/aaae09)

Gaia Collaboration, Brown, A. G. A., Vallenari, A., et al. 2016, A&A, 595, A2, doi: [10.1051/0004-6361/201629512](https://doi.org/10.1051/0004-6361/201629512)

Gaia Collaboration, Vallenari, A., Brown, A. G. A., et al. 2023, A&A, 674, A1, doi: [10.1051/0004-6361/202243940](https://doi.org/10.1051/0004-6361/202243940)

Geballe, T. R., Knapp, G. R., Leggett, S. K., et al. 2002, ApJ, 564, 466, doi: [10.1086/324078](https://doi.org/10.1086/324078)

Geißler, K., Metchev, S., Kirkpatrick, J. D., Berriman, G. B., &Looper, D. 2011, ApJ, 732, 56, doi: [10.1088/0004-637X/732/1/56](https://doi.org/10.1088/0004-637X/732/1/56)

Gelino, C. R., Kirkpatrick, J. D., Cushing, M. C., et al. 2011, AJ, 142, 57, doi: [10.1088/0004-6256/142/2/57](https://doi.org/10.1088/0004-6256/142/2/57)

Gizis, J. E., Burgasser, A. J., Faherty, J. K., Castro, P. J., & Shara, M. M. 2011a, AJ, 142, 171, doi: [10.1088/0004-6256/142/5/171](https://doi.org/10.1088/0004-6256/142/5/171)

Gizis, J. E., Burgasser, A. J., & Vrba, F. J. 2015, AJ, 150, 179, doi: [10.1088/0004-6256/150/6/179](https://doi.org/10.1088/0004-6256/150/6/179)

Gizis, J. E., & Harvin, J. 2006, AJ, 132, 2372, doi: [10.1086/508514](https://doi.org/10.1086/508514)

Gizis, J. E., Monet, D. G., Reid, I. N., et al. 2000, AJ, 120, 1085, doi: [10.1086/301456](https://doi.org/10.1086/301456)

Gizis, J. E., Reid, I. N., Knapp, G. R., et al. 2003, AJ, 125, 3302, doi: [10.1086/374991](https://doi.org/10.1086/374991)

Gizis, J. E., Troup, N. W., & Burgasser, A. J. 2011b, *ApJL*, 736, L34, doi: [10.1088/2041-8205/736/2/L34](https://doi.org/10.1088/2041-8205/736/2/L34)

Gonzales, E. C., Faherty, J. K., Gagné, J., Artigau, É., & Bardalez Gagliuffi, D. 2018, *ApJ*, 864, 100, doi: [10.3847/1538-4357/aad3c7](https://doi.org/10.3847/1538-4357/aad3c7)

Greco, J. J., Schneider, A. C., Cushing, M. C., Kirkpatrick, J. D., & Burgasser, A. J. 2019, *AJ*, 158, 182, doi: [10.3847/1538-3881/ab3ebe](https://doi.org/10.3847/1538-3881/ab3ebe)

Guetter, H. H., Vrba, F. J., Henden, A. A., & Luginbuhl, C. B. 2003, *AJ*, 125, 3344, doi: [10.1086/375305](https://doi.org/10.1086/375305)

Harris, H. C., & Vrba, F. J. 1992, *PASP*, 104, 140, doi: [10.1086/132969](https://doi.org/10.1086/132969)

Hawley, S. L., Covey, K. R., Knapp, G. R., et al. 2002, *AJ*, 123, 3409, doi: [10.1086/340697](https://doi.org/10.1086/340697)

Hodgkin, S. T., Irwin, M. J., Hewett, P. C., & Warren, S. J. 2009, *MNRAS*, 394, 675, doi: [10.1111/j.1365-2966.2008.14387.x](https://doi.org/10.1111/j.1365-2966.2008.14387.x)

Høg, E., Fabricius, C., Makarov, V. V., et al. 2000, *A&A*, 355, L27

Hsu, C.-C., Burgasser, A. J., Theissen, C. A., et al. 2021, *ApJS*, 257, 45, doi: [10.3847/1538-4365/ac1c7d](https://doi.org/10.3847/1538-4365/ac1c7d)

Hurt, S. A., Liu, M. C., Zhang, Z., et al. 2024, *ApJ*, 961, 121, doi: [10.3847/1538-4357/ad0b12](https://doi.org/10.3847/1538-4357/ad0b12)

Jameson, R. F., Casewell, S. L., Bannister, N. P., et al. 2008, *MNRAS*, 384, 1399, doi: [10.1111/j.1365-2966.2007.12637.x](https://doi.org/10.1111/j.1365-2966.2007.12637.x)

Kellogg, K., Metchev, S., Geißler, K., et al. 2015, *AJ*, 150, 182, doi: [10.1088/0004-6256/150/6/182](https://doi.org/10.1088/0004-6256/150/6/182)

Kirkpatrick, J. D. 2005, *ARA&A*, 43, 195, doi: [10.1146/annurev.astro.42.053102.134017](https://doi.org/10.1146/annurev.astro.42.053102.134017)

Kirkpatrick, J. D., Dahn, C. C., Monet, D. G., et al. 2001, *AJ*, 121, 3235, doi: [10.1086/321085](https://doi.org/10.1086/321085)

Kirkpatrick, J. D., Reid, I. N., Liebert, J., et al. 1999, *ApJ*, 519, 802, doi: [10.1086/307414](https://doi.org/10.1086/307414)

—. 2000, *AJ*, 120, 447, doi: [10.1086/301427](https://doi.org/10.1086/301427)

Kirkpatrick, J. D., Cruz, K. L., Barman, T. S., et al. 2008, *ApJ*, 689, 1295, doi: [10.1086/592768](https://doi.org/10.1086/592768)

Kirkpatrick, J. D.,Looper, D. L., Burgasser, A. J., et al. 2010, *ApJS*, 190, 100, doi: [10.1088/0067-0049/190/1/100](https://doi.org/10.1088/0067-0049/190/1/100)

Kirkpatrick, J. D., Cushing, M. C., Gelino, C. R., et al. 2011, *ApJS*, 197, 19, doi: [10.1088/0067-0049/197/2/19](https://doi.org/10.1088/0067-0049/197/2/19)

Kirkpatrick, J. D., Martin, E. C., Smart, R. L., et al. 2019, *ApJS*, 240, 19, doi: [10.3847/1538-4365/aaf6af](https://doi.org/10.3847/1538-4365/aaf6af)

Kirkpatrick, J. D., Marocco, F., Caselden, D., et al. 2021, *ApJL*, 915, L6, doi: [10.3847/2041-8213/ac0437](https://doi.org/10.3847/2041-8213/ac0437)

Knapp, G. R., Leggett, S. K., Fan, X., et al. 2004, *AJ*, 127, 3553, doi: [10.1086/420707](https://doi.org/10.1086/420707)

Konopacky, Q. M., Ghez, A. M., Barman, T. S., et al. 2010, *ApJ*, 711, 1087, doi: [10.1088/0004-637X/711/2/1087](https://doi.org/10.1088/0004-637X/711/2/1087)

Lawrence, A., Warren, S. J., Almaini, O., et al. 2007, *MNRAS*, 379, 1599, doi: [10.1111/j.1365-2966.2007.12040.x](https://doi.org/10.1111/j.1365-2966.2007.12040.x)

Leggett, S. K., Liu, M. C., Dupuy, T. J., et al. 2014, *ApJ*, 780, 62, doi: [10.1088/0004-637X/780/1/62](https://doi.org/10.1088/0004-637X/780/1/62)

Leggett, S. K., Marley, M. S., Freedman, R., et al. 2007, *ApJ*, 667, 537, doi: [10.1086/519948](https://doi.org/10.1086/519948)

Leggett, S. K., Tremblin, P., Esplin, T. L., Luhman, K. L., & Morley, C. V. 2017, *ApJ*, 842, 118, doi: [10.3847/1538-4357/aa6fb5](https://doi.org/10.3847/1538-4357/aa6fb5)

Leggett, S. K., Geballe, T. R., Fan, X., et al. 2000, *ApJL*, 536, L35, doi: [10.1086/312728](https://doi.org/10.1086/312728)

Leggett, S. K., Golimowski, D. A., Fan, X., et al. 2002, *ApJ*, 564, 452, doi: [10.1086/324037](https://doi.org/10.1086/324037)

Leggett, S. K., Birmingham, B., Saumon, D., et al. 2010, *ApJ*, 710, 1627, doi: [10.1088/0004-637X/710/2/1627](https://doi.org/10.1088/0004-637X/710/2/1627)

Leggett, S. K., Dupuy, T. J., Morley, C. V., et al. 2019, *ApJ*, 882, 117, doi: [10.3847/1538-4357/ab3393](https://doi.org/10.3847/1538-4357/ab3393)

Line, M. R., Marley, M. S., Liu, M. C., et al. 2017, *ApJ*, 848, 83, doi: [10.3847/1538-4357/aa7ff0](https://doi.org/10.3847/1538-4357/aa7ff0)

Liu, M. C., Dupuy, T. J., & Allers, K. N. 2013, *Astronomische Nachrichten*, 334, 85, doi: [10.1002/asna.201211783](https://doi.org/10.1002/asna.201211783)

—. 2016, *ApJ*, 833, 96, doi: [10.3847/1538-4357/833/1/96](https://doi.org/10.3847/1538-4357/833/1/96)

Liu, M. C., Dupuy, T. J., Bowler, B. P., Leggett, S. K., & Best, W. M. J. 2012, *ApJ*, 758, 57, doi: [10.1088/0004-637X/758/1/57](https://doi.org/10.1088/0004-637X/758/1/57)

Liu, M. C., Dupuy, T. J., & Leggett, S. K. 2010, *ApJ*, 722, 311, doi: [10.1088/0004-637X/722/1/311](https://doi.org/10.1088/0004-637X/722/1/311)

Liu, M. C., Deacon, N. R., Magnier, E. A., et al. 2011, *ApJL*, 740, L32, doi: [10.1088/2041-8205/740/2/L32](https://doi.org/10.1088/2041-8205/740/2/L32)

Liu, P., Biller, B. A., Vos, J. M., et al. 2024, *MNRAS*, 527, 6624, doi: [10.1093/mnras/stad3502](https://doi.org/10.1093/mnras/stad3502)

Lodie, N., Espinoza Contreras, M., Zapatero Osorio, M. R., et al. 2017, *A&A*, 598, A92, doi: [10.1051/0004-6361/201629410](https://doi.org/10.1051/0004-6361/201629410)

Looper, D. L., Gelino, C. R., Burgasser, A. J., & Kirkpatrick, J. D. 2008a, *ApJ*, 685, 1183, doi: [10.1086/590382](https://doi.org/10.1086/590382)

Looper, D. L., Kirkpatrick, J. D., & Burgasser, A. J. 2007, *AJ*, 134, 1162, doi: [10.1086/520645](https://doi.org/10.1086/520645)

Looper, D. L., Kirkpatrick, J. D., Cutri, R. M., et al. 2008b, *ApJ*, 686, 528, doi: [10.1086/591025](https://doi.org/10.1086/591025)

Loutrel, N. P., Luhman, K. L., Lowrance, P. J., & Bochanski, J. J. 2011, *ApJ*, 739, 81, doi: [10.1088/0004-637X/739/2/81](https://doi.org/10.1088/0004-637X/739/2/81)

Lucas, P. W., Tinney, C. G., Birmingham, B., et al. 2010, *MNRAS*, 408, L56, doi: [10.1111/j.1745-3933.2010.00927.x](https://doi.org/10.1111/j.1745-3933.2010.00927.x)

Luginbuhl, C. B., Henden, A. A., Vrba, F. J., & Guetter, H. H. 1998, in Society of Photo-Optical Instrumentation Engineers (SPIE) Conference Series, Vol. 3354, Infrared Astronomical Instrumentation, ed. A. M. Fowler, 240–246, doi: [10.1117/12.317305](https://doi.org/10.1117/12.317305)

Luyten, W. J. 1976, Univ. Minnesota, 0

Maldonado, J., Martínez-Arnáiz, R. M., Eiroa, C., Montes, D., & Montesinos, B. 2010, *A&A*, 521, A12, doi: [10.1051/0004-6361/201014948](https://doi.org/10.1051/0004-6361/201014948)

Manjavacas, E., Goldman, B., Reffert, S., & Henning, T. 2013, *A&A*, 560, A52, doi: [10.1051/0004-6361/201321720](https://doi.org/10.1051/0004-6361/201321720)

Manjavacas, E., Apai, D., Zhou, Y., et al. 2019, *AJ*, 157, 101, doi: [10.3847/1538-3881/aaf88f](https://doi.org/10.3847/1538-3881/aaf88f)

Marley, M. S., Seager, S., Saumon, D., et al. 2002, *ApJ*, 568, 335, doi: [10.1086/338800](https://doi.org/10.1086/338800)

Marocco, F., Smart, R. L., Jones, H. R. A., et al. 2010, *A&A*, 524, A38, doi: [10.1051/0004-6361/201015394](https://doi.org/10.1051/0004-6361/201015394)

Marocco, F., Andrei, A. H., Smart, R. L., et al. 2013, *AJ*, 146, 161, doi: [10.1088/0004-6256/146/6/161](https://doi.org/10.1088/0004-6256/146/6/161)

Marocco, F., Jones, H. R. A., Day-Jones, A. C., et al. 2015, *MNRAS*, 449, 3651, doi: [10.1093/mnras/stv530](https://doi.org/10.1093/mnras/stv530)

Marocco, F., Eisenhardt, P. R. M., Fowler, J. W., et al. 2021, *ApJS*, 253, 8, doi: [10.3847/1538-4365/abd805](https://doi.org/10.3847/1538-4365/abd805)

Martin, E. C., Kirkpatrick, J. D., Beichman, C. A., et al. 2018, *ApJ*, 867, 109, doi: [10.3847/1538-4357/aaelaf](https://doi.org/10.3847/1538-4357/aaelaf)

McLean, I. S., McGovern, M. R., Burgasser, A. J., et al. 2003, *ApJ*, 596, 561, doi: [10.1086/377636](https://doi.org/10.1086/377636)

McLean, I. S., Prato, L., Kim, S. S., et al. 2001, *ApJL*, 561, L115, doi: [10.1086/324380](https://doi.org/10.1086/324380)

McLean, I. S., Wilcox, M. K., Becklin, E. E., et al. 2000, *ApJL*, 533, L45, doi: [10.1086/312600](https://doi.org/10.1086/312600)

McMahon, R. G., Banerji, M., Gonzalez, E., et al. 2013, *The Messenger*, 154, 35

Metchev, S. A., Kirkpatrick, J. D., Beriman, G. B., &Looper, D. 2008, *ApJ*, 676, 1281, doi: [10.1086/524721](https://doi.org/10.1086/524721)

Monet, D. G., & Dahn, C. C. 1983, *AJ*, 88, 1489, doi: [10.1086/113438](https://doi.org/10.1086/113438)

Monet, D. G., Dahn, C. C., Vrba, F. J., et al. 1992, *AJ*, 103, 638, doi: [10.1086/116091](https://doi.org/10.1086/116091)

Pineda, J. S., Hallinan, G., Kirkpatrick, J. D., et al. 2016, *ApJ*, 826, 73, doi: [10.3847/0004-637X/826/1/73](https://doi.org/10.3847/0004-637X/826/1/73)

Piscarreta, L., Mužić, K., Almendros-Abad, V., & Scholz, A. 2024, *A&A*, 686, A37, doi: [10.1051/0004-6361/202347327](https://doi.org/10.1051/0004-6361/202347327)

Radigan, J. 2014, *ApJ*, 797, 120, doi: [10.1088/0004-637X/797/2/120](https://doi.org/10.1088/0004-637X/797/2/120)

Radigan, J., Jayawardhana, R., Lafrenière, D., et al. 2012, *ApJ*, 750, 105, doi: [10.1088/0004-637X/750/2/105](https://doi.org/10.1088/0004-637X/750/2/105)

—. 2013, *ApJ*, 778, 36, doi: [10.1088/0004-637X/778/1/36](https://doi.org/10.1088/0004-637X/778/1/36)

Radigan, J., Lafrenière, D., Jayawardhana, R., & Artigau, E. 2014, *ApJ*, 793, 75, doi: [10.1088/0004-637X/793/2/75](https://doi.org/10.1088/0004-637X/793/2/75)

Reid, I. N., Cruz, K. L., Kirkpatrick, J. D., et al. 2008, *AJ*, 136, 1290, doi: [10.1088/0004-6256/136/3/1290](https://doi.org/10.1088/0004-6256/136/3/1290)

Reid, I. N., Gizis, J. E., Kirkpatrick, J. D., & Koerner, D. W. 2001, *AJ*, 121, 489, doi: [10.1086/318023](https://doi.org/10.1086/318023)

Reid, I. N., Lewitus, E., Allen, P. R., Cruz, K. L., & Burgasser, A. J. 2006, *AJ*, 132, 891, doi: [10.1086/505626](https://doi.org/10.1086/505626)

Reylé, C., Delorme, P., Willott, C. J., et al. 2010, *A&A*, 522, A112, doi: [10.1051/0004-6361/200913234](https://doi.org/10.1051/0004-6361/200913234)

Sahlmann, J., Lazorenko, P. F., Ségransan, D., et al. 2014, *A&A*, 565, A20, doi: [10.1051/0004-6361/201323208](https://doi.org/10.1051/0004-6361/201323208)

Salim, S., Lépine, S., Rich, R. M., & Shara, M. M. 2003, *ApJL*, 586, L149, doi: [10.1086/374794](https://doi.org/10.1086/374794)

Sanghi, A., Liu, M. C., Best, W. M. J., et al. 2023, *ApJ*, 959, 63, doi: [10.3847/1538-4357/acff66](https://doi.org/10.3847/1538-4357/acff66)

Schmidt, S. J., Cruz, K. L., Bongiorno, B. J., Liebert, J., & Reid, I. N. 2007, *AJ*, 133, 2258, doi: [10.1086/512158](https://doi.org/10.1086/512158)

Schmidt, S. J., West, A. A., Hawley, S. L., & Pineda, J. S. 2010, *AJ*, 139, 1808, doi: [10.1088/0004-6256/139/5/1808](https://doi.org/10.1088/0004-6256/139/5/1808)

Schneider, A. C., Cushing, M. C., Kirkpatrick, J. D., et al. 2014, *AJ*, 147, 34, doi: [10.1088/0004-6256/147/2/34](https://doi.org/10.1088/0004-6256/147/2/34)

Schneider, A. C., Munn, J. A., Vrba, F. J., et al. 2023, *AJ*, 166, 103, doi: [10.3847/1538-3881/ace9bf](https://doi.org/10.3847/1538-3881/ace9bf)

Schneider, A. C., Vrba, F. J., Bruursema, J., et al. 2025, *AJ*, 170, 86, doi: [10.3847/1538-3881/ade43c](https://doi.org/10.3847/1538-3881/ade43c)

Schneider, D. P., Knapp, G. R., Hawley, S. L., et al. 2002, *AJ*, 123, 458, doi: [10.1086/338095](https://doi.org/10.1086/338095)

Scholz, R. D. 2010, *A&A*, 515, A92, doi: [10.1051/0004-6361/201014264](https://doi.org/10.1051/0004-6361/201014264)

Scholz, R. D., Bihain, G., Schnurr, O., & Storm, J. 2011, *A&A*, 532, L5, doi: [10.1051/0004-6361/201117297](https://doi.org/10.1051/0004-6361/201117297)

Scholz, R. D., Storm, J., Knapp, G. R., & Zinnecker, H. 2009, *A&A*, 494, 949, doi: [10.1051/0004-6361:200811053](https://doi.org/10.1051/0004-6361:200811053)

Simons, D. A., & Tokunaga, A. 2002, *PASP*, 114, 169, doi: [10.1086/338544](https://doi.org/10.1086/338544)

Skrutskie, M. F., Cutri, R. M., Stiening, R., et al. 2006, *AJ*, 131, 1163, doi: [10.1086/498708](https://doi.org/10.1086/498708)

Smart, R. L., Tinney, C. G., Bucciarelli, B., et al. 2013, *MNRAS*, 433, 2054, doi: [10.1093/mnras/stt876](https://doi.org/10.1093/mnras/stt876)

Smart, R. L., Bucciarelli, B., Jones, H. R. A., et al. 2018, *MNRAS*, 481, 3548, doi: [10.1093/mnras/sty2520](https://doi.org/10.1093/mnras/sty2520)

Stephens, D. C., Leggett, S. K., Cushing, M. C., et al. 2009, *ApJ*, 702, 154, doi: [10.1088/0004-637X/702/1/154](https://doi.org/10.1088/0004-637X/702/1/154)

Strand, K. A. 1964, *Science*, 144, 1299, doi: [10.1126/science.144.3624.1299](https://doi.org/10.1126/science.144.3624.1299)

Strauss, M. A., Fan, X., Gunn, J. E., et al. 1999, *ApJL*, 522, L61, doi: [10.1086/312218](https://doi.org/10.1086/312218)

Stumpf, M. B., Brandner, W., Bouy, H., Henning, T., & Hippler, S. 2010, *A&A*, 516, A37, doi: [10.1051/0004-6361/200913711](https://doi.org/10.1051/0004-6361/200913711)

Sutherland, W., Emerson, J., Dalton, G., et al. 2015, *A&A*, 575, A25, doi: [10.1051/0004-6361/201424973](https://doi.org/10.1051/0004-6361/201424973)

Theissen, C. A. 2018, *ApJ*, 862, 173, doi: [10.3847/1538-4357/aaccfa](https://doi.org/10.3847/1538-4357/aaccfa)

Thompson, M. A., Kirkpatrick, J. D., Mace, G. N., et al. 2013, *PASP*, 125, 809, doi: [10.1086/671426](https://doi.org/10.1086/671426)

Thorstensen, J. R., & Kirkpatrick, J. D. 2003, *PASP*, 115, 1207, doi: [10.1086/378080](https://doi.org/10.1086/378080)

Tinney, C. G., Burgasser, A. J., & Kirkpatrick, J. D. 2003, *AJ*, 126, 975, doi: [10.1086/376481](https://doi.org/10.1086/376481)

Tinney, C. G., Burgasser, A. J., Kirkpatrick, J. D., & McElwain, M. W. 2005, *AJ*, 130, 2326, doi: [10.1086/491734](https://doi.org/10.1086/491734)

Torres, C. A. O., Quast, G. R., Melo, C. H. F., & Sterzik, M. F. 2008, in *Handbook of Star Forming Regions*, Volume II, ed. B. Reipurth, Vol. 5, 757, doi: [10.48550/arXiv.0808.3362](https://doi.org/10.48550/arXiv.0808.3362)

Vos, J. M., Allers, K. N., Biller, B. A., et al. 2018, *MNRAS*, 474, 1041, doi: [10.1093/mnras/stx2752](https://doi.org/10.1093/mnras/stx2752)

Vos, J. M., Birmingham, B., Faherty, J. K., et al. 2023, *ApJ*, 944, 138, doi: [10.3847/1538-4357/acab58](https://doi.org/10.3847/1538-4357/acab58)

Vrba, F. J., Henden, A. A., Luginbuhl, C. B., Guetter, H. H., & Monet, D. G. 2000, in *American Astronomical Society Meeting Abstracts*, Vol. 196, American Astronomical Society Meeting Abstracts #196, 03.08

Vrba, F. J., Henden, A. A., Luginbuhl, C. B., et al. 2004, *AJ*, 127, 2948, doi: [10.1086/383554](https://doi.org/10.1086/383554)

Wilson, J. C., Miller, N. A., Gizis, J. E., et al. 2003, in *IAU Symposium*, Vol. 211, Brown Dwarfs, ed. E. Martín, 197

Wilson, P. A., Rajan, A., & Patience, J. 2014, *A&A*, 566, A111, doi: [10.1051/0004-6361/201322995](https://doi.org/10.1051/0004-6361/201322995)

Wright, E. L., Eisenhardt, P. R. M., Mainzer, A. K., et al. 2010, *AJ*, 140, 1868, doi: [10.1088/0004-6256/140/6/1868](https://doi.org/10.1088/0004-6256/140/6/1868)

Yang, H., Apai, D., Marley, M. S., et al. 2016, *ApJ*, 826, 8, doi: [10.3847/0004-637X/826/1/8](https://doi.org/10.3847/0004-637X/826/1/8)

York, D. G., Adelman, J., Anderson, Jr., J. E., et al. 2000, *AJ*, 120, 1579, doi: [10.1086/301513](https://doi.org/10.1086/301513)

Zapatero Osorio, M. R., Béjar, V. J. S., Miles-Páez, P. A., et al. 2014, *A&A*, 568, A6, doi: [10.1051/0004-6361/201321340](https://doi.org/10.1051/0004-6361/201321340)

Zhang, Z., Liu, M. C., Best, W. M. J., Dupuy, T. J., & Siverd, R. J. 2021, *ApJ*, 911, 7, doi: [10.3847/1538-4357/abe3fa](https://doi.org/10.3847/1538-4357/abe3fa)

Zhang, Z., Liu, M. C., Hermes, J. J., et al. 2020, *ApJ*, 891, 171, doi: [10.3847/1538-4357/ab765c](https://doi.org/10.3847/1538-4357/ab765c)

Zhang, Z. H., Burgasser, A. J., Gálvez-Ortiz, M. C., et al. 2019, *MNRAS*, 486, 1260, doi: [10.1093/mnras/stz777](https://doi.org/10.1093/mnras/stz777)

Zhang, Z. H., Homeier, D., Pinfield, D. J., et al. 2017a, *MNRAS*, 468, 261, doi: [10.1093/mnras/stx350](https://doi.org/10.1093/mnras/stx350)

Zhang, Z. H., Pokorny, R. S., Jones, H. R. A., et al. 2009, *A&A*, 497, 619, doi: [10.1051/0004-6361/200810314](https://doi.org/10.1051/0004-6361/200810314)

Zhang, Z. H., Pinfield, D. J., Birmingham, B., et al. 2013, *MNRAS*, 434, 1005, doi: [10.1093/mnras/stt1030](https://doi.org/10.1093/mnras/stt1030)

Zhang, Z. H., Pinfield, D. J., Gálvez-Ortiz, M. C., et al. 2017b, *MNRAS*, 464, 3040, doi: [10.1093/mnras/stw2438](https://doi.org/10.1093/mnras/stw2438)

Zuckerman, B. 2019, *ApJ*, 870, 27, doi: [10.3847/1538-4357/aaee66](https://doi.org/10.3847/1538-4357/aaee66)

Zuckerman, B., Bessell, M. S., Song, I., & Kim, S. 2006, *ApJL*, 649, L115, doi: [10.1086/508060](https://doi.org/10.1086/508060)

Zuckerman, B., Song, I., & Bessell, M. S. 2004, *ApJL*, 613, L65, doi: [10.1086/425036](https://doi.org/10.1086/425036)

Zuckerman, B., Song, I., Bessell, M. S., & Webb, R. A. 2001, *ApJL*, 562, L87, doi: [10.1086/337968](https://doi.org/10.1086/337968)